TECHNISCHE UNIVERSITÄT MÜNCHEN

Wissenschaftszentrum Weihenstephan für Ernährung, Landnutzung und Umwelt

Lehrstuhl für Molekulare Ernährungsmedizin

Molecular functions in brown adipose tissue and their physiological significance in the context of systemic glucose homeostasis in mice

Stefanie Maurer

Vollständiger Abdruck der von der Fakultät Wissenschaftszentrum Weihenstephan für Ernährung, Landnutzung und Umwelt der Technischen Universität München zur Erlangung des akademischen Grades eines

Doktors der Naturwissenschaften

genehmigten Dissertation.

Vorsitzender:	Univ.-Prof. Dr. Michael Schemann
Prüfer der Dissertation:	1. Univ.-Prof. Dr. Martin Klingenspor
	2. Univ.-Prof. Dr. Hannelore Daniel

Die Dissertation wurde am 29.02.2016 bei der Technischen Universität München eingereicht und durch die Fakultät Wissenschaftszentrum Weihenstephan für Ernährung, Landnutzung und Umwelt am 10.06.2016 angenommen.

TABLE OF CONTENT

ABBREVIATIONS

129S6	129S6/SvEvTac
AA	arachidonic acid
ADP	adenosine diphosphate
ALA	α-linolenic acid
ANOVA	analysis of variance
ANT	adenine nucleotide translocase
ATP	adenosine triphosphate
AUC	area under the curve
BAT	brown adipose tissue
BHT	butylated hydroxytoluene
BL6J	C57BL/6J
BMI	body mass index
BMR	basal metabolic rate
bp	base pairs
brite	brown-in-white, referring to brown-like adipocytes in WAT
cAMP	cyclic adenosine monophosphate
CCO	cytochrome *c* oxidase
cDNA	complementary DNA
Cidea	cell death-inducing DNA fragmentation factor, alpha subunit-like effector A
CL	CL-316243
CNS	central nervous system
COX	cyclooxygenase
Cox4i2	CCO subunit 4 isoform 2
Cox6a2	CCO subunit 6a isoform 2
Cox7a1	CCO subunit 7a isoform 1
Cox7a2	CCO subunit 7a isoform 2
CYP450	cytochrome P450
Δp	proton motive force
DGLA	dihomo-γ-linolenic acid
DHA	docosahexaenoic acid
DIO	diet-induced obesity
DIT	diet-induced thermogenesis
DNA	desoxyribonucleic acid
Eef2	eukaryotic translation elongation factor 2
EP4	PGE_2 receptor subtype 4
EPA	eicosapentaenoic acid
gDNA	genomic DNA
GDP	guanosine diphosphate
GLA	γ-linolenic acid
Glut	facilitated glucose transporter
Gtf2b	general transcription factor 2b
gWAT	visceral gonadal WAT

HET	heterozygous
HFD	high-fat diet
HP	heat production
HSL	hormone sensitive lipase
Hsp90	heat shock protein 90 alpha (cytosolic), class B member 1
iBAT	interscapular BAT
IFD	intermediate-fat diet
IL-4	interleukin 4
IMS	intermembrane space
IP	PGI_2 receptor
iSST	interscapular skin surface temperature
ITT	insulin tolerance test
iWAT	subcutaneous inguinal WAT
KO	knockout
LA	linoleic acid
LFCD	low-fat control diet
LOX	lipoxygenase
MR	metabolic rate
mRNA	messenger RNA
Myf5	myogenic factor 5
NE	norepinephrine
NE_{max}	maximal NE-stimulated
ns	not significant
NST	non-shivering thermogenesis
oGTT	oral glucose tolerance test
p38 MAPK	p38 mitogen-activated protein kinases
PCR	polymerase chain reaction
PKA	protein kinase A
PPAR	peroxisome proliferator-activated receptor
qRT-PCR	quantitative real-time PCR
RER	respiratory exchange ratio
RM ANOVA	repeated measures ANOVA
RNA	ribonucleic acid
SDS-PAGE	sodium dodecyl sulfate polyacrylamide gel electrophoresis
SPF	specified pathogen free
T2D	type 2 diabetes mellitus
Tbp	TATA box binding protein
TRP	transient receptor potential ion channel
Ucp	uncoupling protein
vs.	versus
WAT	white adipose tissue
WT	wildtype

Formal and trivial names of common oxylipin abbreviations are listed in Table 10 and Table 11.

ABSTRACT

Brown adipose tissue is a specialized, mammalian organ providing adaptive heat production for the maintenance of normothermia. In addition to the primary metabolization of fatty acids, this non-shivering thermogenesis is supported by the uptake of glucose from the systemic blood circulation. The activation of brown adipose tissue in mice and humans results in increased glucose uptake, which is linked to enhanced energy expenditure. This effect may be complemented by the abundance of brite adipocytes (brown-in-white), which constitute an additional, inducible pool of cells present in white adipose tissue capable of providing non-shivering thermogenesis. The recruitment of additional capacity for non-shivering thermogenesis in humans may contribute to an increase in energy expenditure concomitant with a beneficial effect on glucose homeostasis.

To further investigate such relationship, different mouse models were characterized with respect to their capacity for non-shivering thermogenesis. Using a knockout mouse model, the cold-induced expression of the protein Cox7a1 in brown adipose tissue was identified to be dispensable for the recruitment of non-shivering thermogenesis. In a polygenic approach, the inbred mouse strain 129S6/SvEvTac was found to exhibit a higher capacity for non-shivering thermogenesis compared to C57BL/6J inbred mice.

Cyclooxygenase represents a key enzyme in the recruitment of brite cells. In order to elucidate the efficacy of a nutritional intervention for recruitment of brite cells, mice of both inbred strains were subjected to a feeding experiment characterized by the modulation of substrate availability for cyclooxygenase. Different fatty acid metabolites were identified as possible regulators of brite cell abundance. The further characterization of their individual potential in the recruitment of brite cells is promising.

The capacity for non-shivering thermogenesis is determined by environmental temperature and genetic factors, and may be further influenced by the dietary fatty acid composition. To investigate whether these factors affect systemic glucose homeostasis in the context of non-shivering thermogenesis, glucose tolerance was assessed under obesogenic and non-obesogenic conditions. Glucose tolerance of 129S6/SvEvTac and C57BL/6J mice was comparable when mice of both strains were fed a control diet in thermoneutral environment. An elevation of the dietary fat content did not influence glucose tolerance in 129S6/SvEvTac mice but resulted in an impairment of glucose tolerance in C57BL/6J mice. This impairment was more pronounced in uncoupling protein 1-deficient mice, which are characterized by impaired non-shivering thermogenesis, and independent from insulin sensitivity. Collectively, these data corroborate a significant contribution of brown adipose tissue-derived non-shivering thermogenesis to the regulation of systemic glucose homeostasis. Brown adipose tissue may thus serve as effective target in the prevention or treatment of diabetes in humans.

ZUSAMMENFASSUNG

Das Braune Fettgewebe ist es spezialisiertes Gewebe zur Wärmeproduktion, das vor allem bei Kleinsäugern zur Aufrechterhaltung der normalen Körpertemperatur beiträgt. Über die hauptsächliche Verstoffwechselung von Fettsäuren hinaus wird diese zitterfreie Thermogenese durch die Aufnahme von Glukose aus der Blutzirkulation unterstützt. Eine Aktivierung des Braunen Fettgewebes führt sowohl bei der Maus als auch beim Mensch zur verstärkten Glukoseaufnahme und ist mit einem Anstieg des Energieverbrauchs verbunden. Brite-Zellen (englisch: brown-in-white), die eine zusätzliche, induzierbare Zellpopulation im Weißen Fettgewebe mit Fähigkeit zur zitterfreien Thermogenese darstellen, könnten diesen Effekt verstärken. Die Rekrutierung zusätzlicher Kapazität zur zitterfreien Thermogenese könnte den Energieverbrauch eines Menschen erhöhen und die Glukosetoleranz günstig beeinflussen.

Um einen solchen Zusammenhang im Tiermodell näher zu untersuchen, wurden verschiedene Mausmodelle hinsichtlich ihrer Kapazität zur zitterfreien Thermogenese charakterisiert. Mit Hilfe eines entsprechenden Knockoutmodells konnte gezeigt werden, dass die kälteinduzierte Expression des Proteins Cox7a1 im Braunen Fettgewebe keinen Einfluss auf die Rekrutierung der zitterfreien Thermogenese hat. In einem polygenen Ansatz konnte ermittelt werden, dass Mäuse des Inzuchtstammes 129S6/SvEvTac gegenüber C57BL/6J Mäusen über eine bessere Fähigkeit zur zitterfreien Wärmebildung verfügen.

Die Cyclooxygenase stellt ein Schlüsselenzym in der Rekrutierung von Brite-Zellen dar. Im Rahmen eines Fütterungsexperiments mit Mäusen beider Inzuchtstämme wurde die Substratverfügbarkeit für dieses Enzym beeinflusst, um die Wirksamkeit einer Ernährungsintervention zur Rekrutierung von Brite-Zellen zu prüfen. Es konnten verschiedene Fettsäuremetabolite mit möglichem Potential zur Erhöhung der Abundanz von Brite-Zellen identifiziert werden, deren weitere Charakterisierung vielversprechend ist.

Die Kapazität zur zitterfreien Thermogenese wird durch die Umgebungstemperatur, genetische Faktoren und darüber hinaus möglicherweise durch die Fettsäurekomposition der Diät beeinflusst. Es wurde untersucht, ob diese Faktoren die Glukosehomöostase im Kontext der Kapazität zur zitterfreien Wärmebildung beeinflussen. Hierfür wurden Diäten mit unterschiedlichem Fettgehalt gefüttert. Die Glukosetoleranz von 129S6/SvEvTac und C57BL/6J Mäusen war vergleichbar wenn diese eine Kontrolldiät in thermoneutraler Umgebung erhielten. Ein Anstieg des Fettgehalts der Diät hatte keinen Einfluss auf die Glukosetoleranz von 129S6/SvEvTac Mäusen, führte jedoch zu einer Verschlechterung bei C57BL/6J Mäusen. Diese Verschlechterung war bei Entkopplerprotein 1-defizienten Mäusen, deren Fähigkeit zur zitterfreien Thermogenese beeinträchtigt ist, stärker ausgeprägt und darüber hinaus unabhängig von der Insulinsensitivität. Insgesamt untermauern diese Ergebnisse einen signifikanten Beitrag der Braunfett-Thermogenese zur Regulation der systemischen Glukosehomöostase. Das Braune Fettgewebe könnte demnach als wirksames Ziel der Prävention und Therapie von humanem Diabetes dienen.

1 INTRODUCTION

1.1 The adipose organ – white, brite and brown

Energy balance is determined by energy intake and energy expenditure. The existence of adipose tissue is pivotal for this relation. Excess energy derived from food is stored in adipose tissue depots mainly in the form of triglycerides, which can be mobilized in times of fasting and starvation to fuel energy consuming processes throughout the body. This energy turnover constitutes the primary function of white adipose tissue (WAT), which represents the major share of the mammalian adipose organ. Its excessive storage capacity prevents ectopic fat deposition and thus lipotoxicity in response to energetic surplus [1]. WAT occurs in different locations mainly as dermal, subcutaneous and visceral depots. In rodents such as mice, depots in the cervical and inguinal region as well as the mesenteric, perigonadal and retroperitoneal region represent the major sites for subcutaneous and visceral WAT, respectively [2].

Similarly to WAT, brown adipose tissue (BAT) is capable of storing energy as fat, which is, however, mobilized to fuel the endogenous cellular energy demand. The primary function of BAT is entirely opposite to that of WAT since stored energy is dissipated for the purpose of heat production as adaptive mechanism to maintain core body temperature in a cold environment. Occurence of BAT in animals was first described more than 450 years ago [3] and its function and properties have been extensively studied since the 1960s, particularly in rodents (for a review, see [4]). These possess significant amounts of visceral and subcutaneous BAT in the mediastinic and perirenal region as well as the cervical, axillary, subscapular and interscapular region, respectively [2]. The anatomical arrangement of all BAT depots mimics a thoracic heating jacket below the fur [5]. The interscapular depot represents the largest among all murine depots. Drainage of this tissue by a large blood vessel, the Sulzer's vein, allows the transfer of locally produced heat to the blood circulation and thus ensures heat distribution throughout the body [6].

Apart from adipocyte precursor cells, endothelial cells, immune cells or cells of the connective tissue, mature brown and white adipocytes represent the major fraction residing in BAT and WAT, respectively (Figure 1). Both cell types are capable of storing fat in cytosolic lipid vacuoles (lipid droplets), but their morphological appearance differs according to the physiological functions of the two tissues. White adipocytes are up to 160 µm in diameter, although the size depends on species, nutritional status and depot [7]. They are spherical in shape and characterized by unilocular appearance, exhibiting a single lipid droplet per cell that occupies most of the intracellular volume thus reducing the portion of the cytosolic compartment and squeezing the nucleus into a peripheral position [2]. In contrast, brown adipocytes are only up to 50 µm in diameter [7]. They are characterized by a central nucleus and multilocular appearance, storing fat within multiple small lipid droplets [2] with an increased interphase between lipid and cytosolic lipases. The latter may facilitate lipolysis for a rapid supply of fuel for thermogenesis [8].

In addition to classical brown and white adipocytes, a novel type of adipocyte was found to occur in the adipose organ of rodents [9]. These cells are present in WAT although they

resemble the morphology and molecular features of brown adipocytes and are therefore referred to as 'brite' (brown-in-white) [10] or 'beige' [11] adipocytes (Figure 1). The abundance of brite cells in murine WAT is not an overall phenomenon but depends on multiple factors such as age, strain or pretreatment of the animal, for instance. Subcutaneous depots, such as the inguinal depot, have a higher propensity for the expression of brite adipocytes than visceral depots [12].

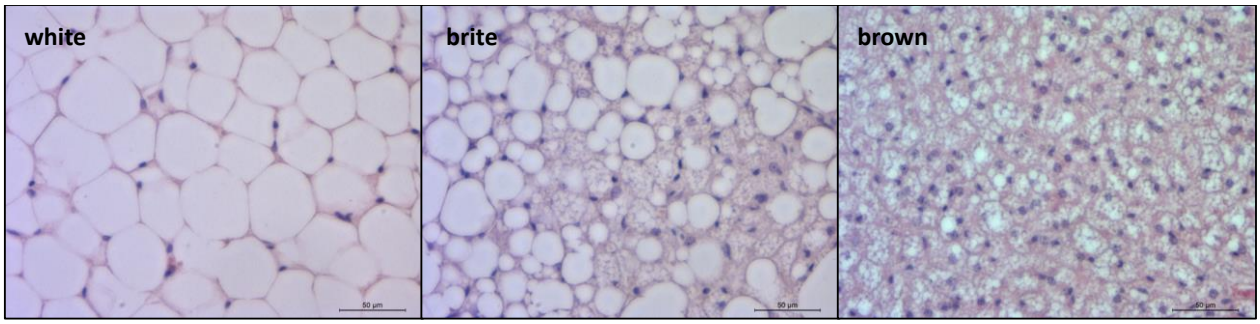

Figure 1: Sections from WAT and BAT illustrating white, brite and brown adipocyte morphology. Nuclei are colored blue (hematoxylin) and cytosolic compunds are stained red (eosin).

An increase in the abundance of brite adipocytes is named 'browning of WAT', which may arise either from a committed population of brite preadipocytes present in WAT [13] or from interconversion of mature, fully differentiated white adipocytes ('transdifferentiation') [14-17]. Additionally, brite adipocytes may be present at a basal state camouflaged as white-like adipocytes, which turn into multilocular cells upon proper stimulation bearing the potential to become re-camouflaged when stimulation ceases [18]. The primary function of brite adipocytes as well as their developmental origin are still a matter of debate. Based on their similar morphology (Figure 1), their responsiveness to thermogenic stimuli [9, 19] and their ability to produce heat [20, 21], brite adipocytes may contribute to thermogenesis similar to brown adipocytes in BAT. In contrast to white adipocytes, brown adipocytes are derived from a myogenic factor 5 (Myf5) positive precursor and thus developmentally related to skeletal muscle cells [22]. Brite adipocytes were found to originate from both Myf5-positive and Myf5-negative precursors within different sites of the adipose organ [22-24] along with a subpopulation arising from a smooth muscle-like origin [25]. Thus, brite cells are a novel type of adipocytes characterized by heterogenous ontogeny with a functional relation to brown adiocytes.

1.2 Non-shivering thermogenesis

In endothermic animals, body temperature is kept fairly constant independent of environmental conditions by means of physiological mechanisms that provide heat production or changes in heat loss. Such regulation is required when the ambient temperature is below or above the thermoneutral zone, which is defined as the range of ambient temperatures at which the metabolic rate is basal [26]. The thermoneutral zone varies between species. It is around 30°C in naked humans [27] and laboratory mice [26]. Prevalent habitation at room temperature

(20°C-23°C) obligatory demands adaptive heat production in mice, whereas humans generally protect themselves from heat loss by clothing. Adaptive heat production is achieved by shivering and non-shivering thermogenesis (NST).

Shivering is an involuntary process, characterized by repeated contractions of skeletal muscle fueled by hydrolysis of adenosine triphosphate (ATP) without physical work. The energy turnover results in the dissipation of heat. Shivering occurs when NST, which is mediated by BAT, is not sufficient to fully compensate heat loss [28]. In small mammals, the activation of NST is essential to survive in cold environment.

1.2.1 Temperature sensation and central control of BAT activity

The activity of BAT as physiological response to ambient temperature is under control of the central nervous system (CNS). Temperature sensation is translated by cutaneous thermoreceptors that belong to the superfamily of transient receptor potential (TRP) ion channels. TRP subfamily M member 8 mediates sensation of innocuous cold [29-31]. In the current model of CNS-mediated BAT activation (Figure 2) [32], the thermal information detected by TRP receptors is transmitted in an afferent pathway from the skin to the hypothalamic preoptic area. Efferent signaling is dependent on cold or warm thermosensation. In cold environment, the preoptic area coordinates the excitation of a sympathetic pathway that activates BAT [33, 34], which is densely innervated by unmyelinated sympathetic nerve fibers [35, 36].

1.2.2 Sympathetic activation of brown adipocytes

The postganglionic effect of sympathetic signaling is conferred by interaction of norepinephrine (NE) with adrenergic receptors of BAT. All three types of G-protein coupled β-adrenoreceptors (β_1, β_2 and β_3) are expressed in brown adipocytes. The β_3-subtype is almost exclusively expressed in WAT and BAT and is most likely responsible for the activation of thermogenesis [37-39]. Upon ligand binding (Figure 2), adrenergic signaling in brown adipocytes involves activation of adenylyl cyclase that increases intracellular levels of cyclic adenosine monophosphate (cAMP) [40]. This second messenger activates protein kinase A (PKA), which disseminates the thermogenic signal. Lipid droplet associated proteins as well as cytosolic lipases are PKA-targets, culminating in disinhibition of lipolysis and breakdown of stored triglycerides [41]. Moreover, adrenergically stimulated lipolysis is supported by PKA-independent pathways [42, 43]. Free fatty acids are shuttled into mitochondria where they have a dual function [44]: they either undergo β-oxidation to serve as fuel for thermogenesis, or serve as direct activator of NST. The latter mechanism is provoked by interaction with the mitochondrial uncoupling protein 1 (Ucp1) [45], which is the causative [46] and indispensable [47] component of NST in mammals.

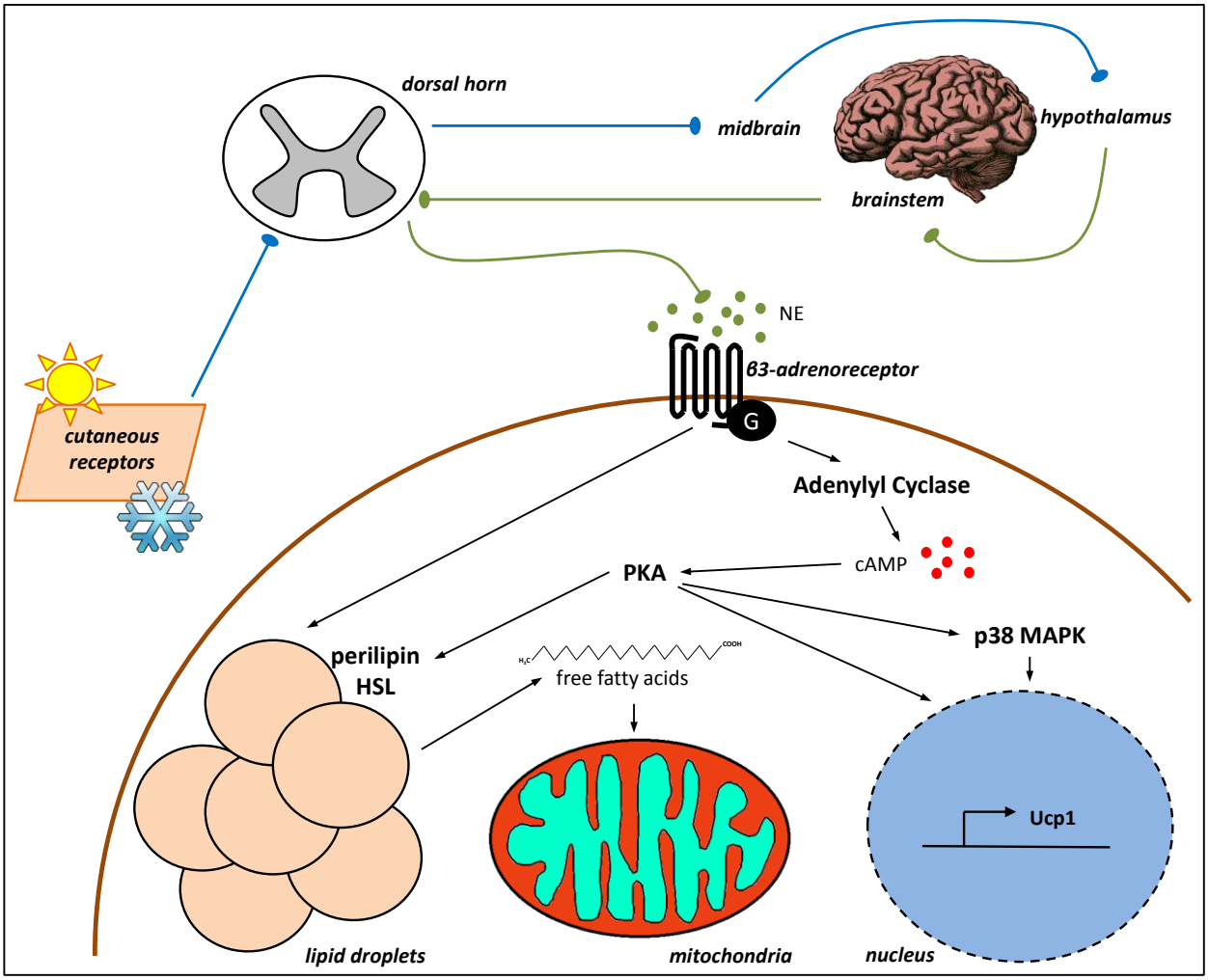

Figure 2: Central and cellular signaling pathways in the control of BAT activity. Temperature sensation and CNS-mediated signaling involves afferent (blue) and efferent (green) neuronal pathways, resulting in the release of norepinephrine (NE) and subsequent activation of the G-Protein coupled β_3-adrenoreceptor. Adrenergic signaling in brown adipocytes involves lipolysis from lipid droplets, activation and fueling of mitochondrial thermogenesis and nuclear transcription of the uncoupling protein 1 (Ucp1) gene. HSL=hormone sensitive lipase; PKA=protein kinase A; cAMP=cyclic adenosine monophosphate; p38 MAPK= p38 mitogen-activated protein kinases.

Transcription of the Ucp1 gene is rapidly initiated after cold-exposure [48-50] and driven by PKA and p38 mitogen-activated protein kinases (p38 MAPK) [51]. These enzymes phosphorylate several transcription factors such as PPAR gamma coactivator 1α, which binds to a peroxisome proliferator-activated receptor (PPAR) within the promoter region of the Ucp1 gene. The cold-induced effect on Ucp1 transcription can be mimicked by PPARα and PPARγ agonist treatment, both of which are major regulators for Ucp1 gene expression in mature and undifferentiated adipocytes, respectively [52]. Ucp1 is exclusively expressed in brown and brite adipocytes, although minor expression has also been reported for thymocytes [53].

1.2.3 Mechanism of heat production in BAT

Ucp1 represents the heat producing entity of brown adipocytes. Ucp1 is a mitochondrial protein and its abundance in brown adipocytes results from a very high quantity of mitochondria with dense cristae [2]. This protein was initially described as ‘GDP-binding

protein' or 'thermogenin' [28], due to its ability to bind purine nucleotides and to mediate NST, respectively. Ucp1 is a 32 kDa protein of the mitochondrial inner membrane. Although its structure has not yet been elucidated, the protein is predicted to have 6 membrane spanning domains [54, 55]. The human and the murine orthologues share almost 80% identity within the 307 amino acid-protein, which is encoded by the 6-exon nuclear gene. Ucp1 has two paralogues [56-59], Ucp2 and Ucp3, which are 56.3% and 53.9% identical with the murine Ucp1 peptide, respectively. The first is expressed in multiple tissues, whereas the latter occurs mainly in BAT and skeletal muscle. Ucp2 and Ucp3 do not confer NST [47, 60-63].

Its denomination as 'uncoupling protein' directly refers to the cellular function of Ucp1 that is to uncouple mitochondrial respiration from ATP production. According to the chemiosmotic theory [64, 65], ATP synthesis is in all types of cells driven by the electrochemical proton gradient across the mitochondrial inner membrane. This intermediate is referred to as proton motive force (Δp) that consists of the mitochondrial membrane potential and a pH-gradient as result of the forced, unequal distribution of protons between the mitochondrial matrix and the mitochondrial intermembrane space (IMS). The conserved energy that is derived from the metabolization of macronutrients is represented by Δp. This metabolization involves β-oxidation and/or citric acid cycle. These reactions serve as electron donors for the four complexes of the respiratory chain. In a stepwise process, electrons are passed on from donor to acceptor molecules involving the membrane-associated mobile carrier proteins ubiquinone and cytochrome *c*. The energy difference resulting from a steady decrease in negative redox potential along the chain is used by Complex I, III and IV for the translocation of protons into the IMS to generate Δp (Figure 3).

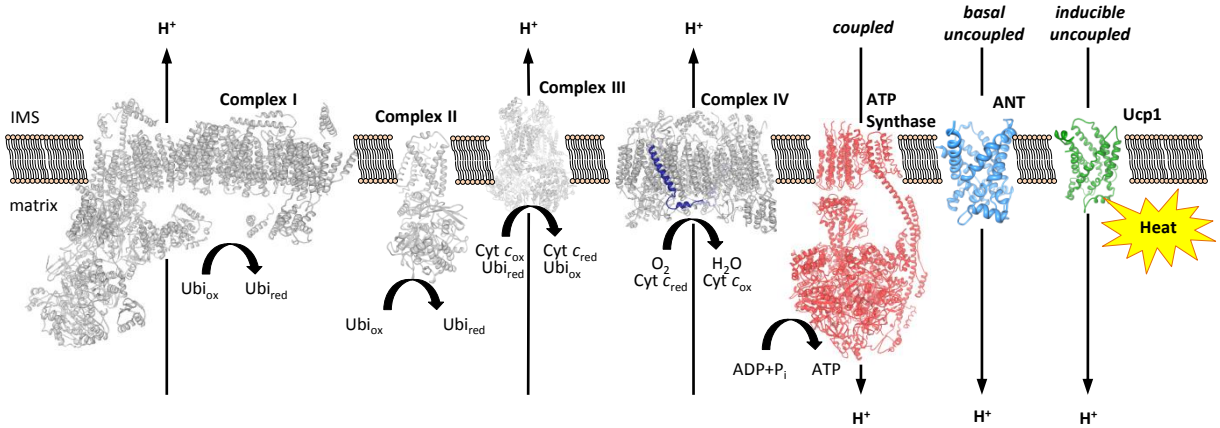

Figure 3: Mitochondrial coupled and uncoupled respiration. In a serial reaction, electrons obtained from the metabolization of macronutrients are passed through the complexes of the respiratory chain catalyzed by the mobile carrier molecules ubiquinone (Ubi) and cytochrome *c* (Cyt *c*) occurring in oxidized (ox) and reduced (red) form, finally resulting in the reduction of oxygen to water. Consequently, protons are translocated into the mitochondrial intermembrane space (IMS) by Complex I, III and IV, thus generating a proton gradient across the membrane. This intermediate is used to drive ATP synthesis or heat production via the basal (exemplarily depicted by the adenine nucleotide translocase (ANT)) and inducible proton leak thereby uncoupling respiration from ATP production. Depicted structures (obtained from http://www.rcsb.org) are Complex I from bovine heart (PDB-ID 4UQ8, [66]), Complex II from porcine heart (PDB-ID 1ZOY, [67]), Complex III from bovine heart (PDB-ID 1BGY, [68]), Complex IV from bovine heart with subunit 7a highlighted in dark blue (PDB-ID 2OCC, [69]), bovine ATP synthase (PDB-ID 5ARA, [70]), ANT from bovine heart (PDB-ID 1OKC, [71]) and murine Ucp2 (PDB-ID 2LCK, [55]).

The final and rate-limiting step within this chain is catalyzed by Complex IV [72-74], which oxidizes cytochrome *c* and thereby reduces oxygen to water, reflecting mitochondrial respiration. In all cell types throughout the body, ATP synthesis is driven by re-translocation of protons into the mitochondrial matrix thus depleting Δp (Figure 3). This process is referred to as 'coupled respiration' and controlled by the availability of adenosine diphosphate (ADP) [75, 76]. This oxidative phosphorylation, however, only plays a minor role in brown adipocytes where Ucp1 bypasses Δp for the purpose of heat production, which constitutes the basis of 'uncoupled respiration' (Figure 3) [77]. In fact, the abundance of ATP synthase in BAT is low [78, 79], whereas Ucp1 accounts for up to 7.7% of total mitochondrial protein in cold-acclimated brown adipocytes [80] emphasizing the fundamental importance of uncoupled vs. coupled respiration for the specialized function of BAT. Incomplete coupling of respiration and ATP synthesis is named 'proton leak' and in its basal form (Figure 3) is a common characteristic of all cell types throughout the body [81]. However, only brown adipocytes dissipate a vast portion of the proton motive force by inducible leak respiration due to the presence of Ucp1 [44]. The activity of Ucp1 is controlled by the opposing effects of inhibitory purine nucleotides and activating fatty acids. Guanosine di- and triphosphate as well as ADP and ATP are capable of binding to Ucp1 [82-84], which may cause full inhibition of proton conductance [85, 86]. Fatty acids released during cold-induced lipolysis can overcome this inhibition to activate Ucp1 by a yet unresolved mechanism [87].

1.3 BAT in humans

Uncoupled respiration in BAT provids NST, which is the primary source for adaptive heat production in small mammals that possess substantial amounts of this thermogenic tissue. In contrast, the significant occurrence of BAT in humans was in the past believed to be restricted to infants and to decline with age [88], leading to the dogma that BAT function is insignificant for adult humans [89]. This view has recently been revised by the use of an imaging technique (Figure 4), demonstrating not only the presence of human BAT but also its metabolic activity due to its ability to take up glucose from the bloodstream [90-93]. In humans, the estimated mass of active BAT amounts only a few dozen grams [91, 94-96] and is thus much less abundant than WAT. BAT depots are located in different regions of the neck, shoulder and thorax (Figure 4). The supraclavicular depot, an anterior subcutaneous depot, is generally considered as most active. Infants, but not adult humans, possess a depot that corresponds to rodent interscapular BAT. This depot resembles the morphology of rodent brown adipocytes [97], whereas depots in adults are discussed to consist of both brown and brite adipocytes [97-102]. Browning of WAT, as it occurs in rodents, has so far only been reported in response to tumor-associated [103] and trauma-induced [104] adrenergic stimulation, leaving the plasticity of human WAT largely unexplored.

The activity of BAT is high in lean, lower in overweight and almost absent in morbidly obese subjects (Figure 4) [91-93, 105]. Increased body mass index (BMI) may be either cause or consequence of reduced BAT activity. In fact, a mechanism referred to as 'diet-induced

thermogenesis' involves BAT as regulator of body mass development dissipating excess energy from food in the absence of any thermoregulatory requirement [106]. At least in rodents, the absence of BAT function may result in obesity via such mechanism [107, 108]. In contrast, catecholamine resistance of adipose tissues [109, 110] as well as increased insulation of obese subjects [111] may be causative for reduced BAT activity.

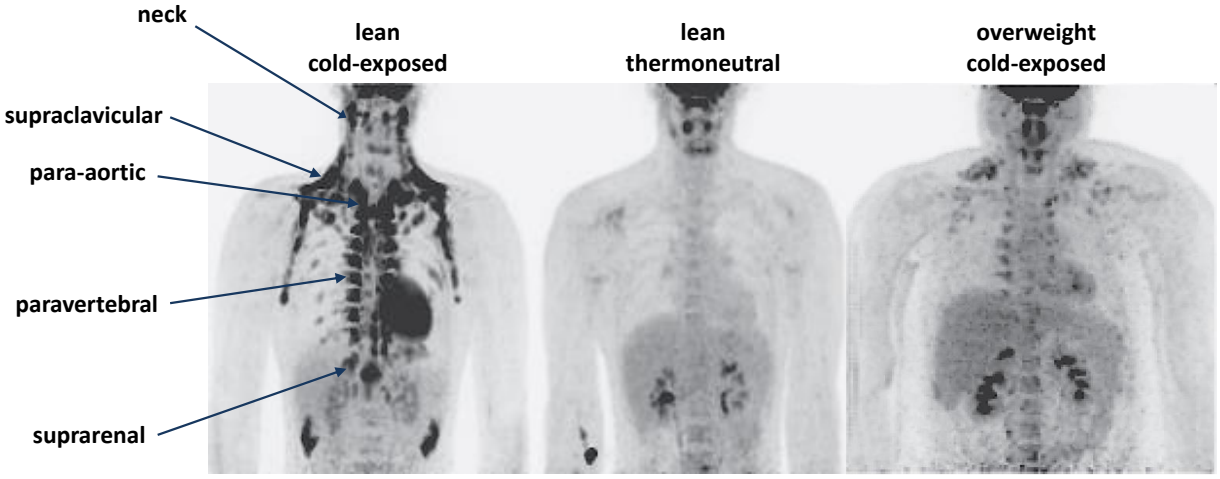

Figure 4: Location and activity of BAT in humans. Combined positron emission tomography/computed tomography-images show distribution of a glucose tracer (dark areas) in a lean and an obese subject 1 hour after administration and thus 2 hours after constant exposure to cold (16°C) or thermoneutral (22°C) conditions. Arrows indicate sites of intense glucose tracer-uptake reflecting BAT (figures modified from [92]; nomenclature of depots according to [89]).

Human BAT is most potently activatable by cold-exposure [92, 95, 112, 113] and β_3-adrenergic agonist treatment [114]. This activation is reflected in increased glucose uptake into BAT (Figure 4) and associated with an increase in energy expenditure. As little as 63 g of activated BAT is estimated to dissipate the energy of around 4 kg of adipose tissue per year [90].
Fatty acids are the primary substrate to fuel BAT-mediated thermogenesis [115]. Glucose uptake into rodent [116, 117] and human [113] BAT is, however, considerably upregulated in response to cold. This regulation may constitute enhanced whole body glucose disposal in cold-exposed humans [113]. Moreover, rodent models of transplanted BAT and brite fat exhibit improved glucose tolerance and attenuated body mass gain [118, 119], suggesting a beneficial metabolic effect of brown and brite adipocyte abundance. Altogether these findings shed light on BAT and brite fat as novel targets in the prevention and therapy of obesity and diabetes.

1.4 Obesity and diabetes – prevalence, pathophysiology and current treatment options

Long-term disequilibrium of energy balance results in a dysregulation of body mass known as underweight and overweight. Besides the role of genetic factors, the latter is caused by continuous storage of excess energy from food with concomitant reduction of energy expenditure and is thus the simple result of a convenient lifestyle. Overweight (BMI ≥ 25 kg/m^2) and obesity (BMI ≥ 30 kg/m^2) have reached global epidemic extents during the last decades since the number of affected people has more than doubled from 1980 to 2013 [120].

Meanwhile more people die from overweight than from underweight [121]. The prevalence of overweight and obesity in 2013 was amounted to affect more than half of the adult European population with peak prevalences moving to younger ages [120]. Overweight and obesity are associated with the burden of multiple comorbidities including different types of cancer and cardiovascular disease, and a profound risk for type II diabetes mellitus (T2D) [122-124].

In non-diabetic subjects, blood glucose levels are regulated in an autonomous manner by adjusted secretion of insulin. A rise in systemic blood glucose levels in response to food intake causes glucose uptake into pancreatic β-cells with subsequent glucose oxidation to drive the ATP-dependent mechanism of insulin release. The effect of insulin is mediated via interaction with its receptor, initiating a signaling cascade that inhibits hepatic glucose production and leads to the translocation of insulin-sensitive glucose transporters that confer glucose uptake into target tissues and thus reduction of blood glucose levels. This system is dysregulated in type II diabetic subjects. The transition from normoglycemia towards T2D is characterized by reduced insulin sensitivity, hyperinsulinemia and progressive pancreatic β-cell failure. This relative lack of insulin causes hyperglycemia and the inability to autonomously regulate blood glucose levels [125].

The etiology of T2D is related to the pathologic expansion of adipose tissue mass. Both insulin sensitivity and β-cell function are significantly influenced by chronically increased plasma levels of free fatty acids during obesity causing lipotoxic effects. Increased fatty acid influx into β-cells is associated with β-cell dysfunction and decline in cell number [126]. Ectopic fat deposition in liver and muscle targets components of the insulin signaling pathway thereby promoting insulin resistance, which is further affected by chronic adipose tissue inflammation [127, 128]. Moreover, visceral fat deposition is hypothesized to support a drainage mechanism, thus facilitating delivery of fatty acids and inflammatory cytokines into the liver via the portal vein promoting hepatic insulin resistance and disinhibition of hepatic glucose output [129].

T2D constitutes by far the most prevalent among the different diabetic diseases [130] and is globally among the top leading causes for disabilities and deaths [131, 132]. State-of-the-art T2D treatment includes lifestyle intervention (dietetic treatment, physical activity) and pharmacotherapy aiming at body weight reduction, normoglycemia and an improvement of insulin sensitivity to avoid complications and sequelae that constitute T2D mortality [133]. However, bariatric surgery as sole substantial alternative is not only far more successful than conventional treatment strategies in the long-term [134], but also highly effective regarding weight loss, remission and resolution of T2D in obese patients [135]. Although considered as useful also in non-morbidly obese (BMI ≥ 30 kg/m^2) T2D subjects [136], the procedure involves the common risks, complications and strains of a surgery. Up to more than 80% of all T2D subjects are overweight or obese [137-139] and around 60% of all T2D cases may be prevented if the affected subjects had normal body weight [140]. Far more than 300 million people worldwide are predicted to suffer from T2D by 2030 [132, 141], emphasizing the need for preventive and curative treatment strategies.

1.5 Modulation of BAT activity and abundance

The use of BAT and brite fat as anti-obesity and anti-diabetes target is based on different mechanisms: activation of existing depots, expansion of thermogenic tissue with brown adipocyte character (recruitment) as well as the long-term maintenance of tissue activation. Given the low abundance of BAT in humans, recruitment of additional BAT capacity appears crucial, but was so far only reported in response to intermittent cold-exposure [142-145]. Pharmacological or nutritional compounds are favorable with regard to a widespread application. In order to achieve this, it is necessary to (1) deepen the current understanding about the molecular machinery that drives NST, (2) identify indispensable components in this machinery that underlie the recruitment and activation of brown and brite adipocytes and (3) manipulate key elements of characterized pathways.

1.5.1 Identification of molecular components with crucial function in the recruitment of NST

Heat production is a mitochondrial process. Increased thermogenic capacity in response to prolonged cold-exposure results from mitochondrial biogenesis [28] and qualitative changes of the BAT mitochondrial proteome [146]. This versatility constitutes the exceptional oxidative capacity of BAT to confer NST via uncoupled respiration. This key functional difference to WAT is underscored by expression levels of multiple subunits of respiratory chain complexes and Ucp1, which are more abundant in BAT compared to WAT (Figure 5).

The expression of subunit isoforms is a unique property of Complex IV with respect to respiratory chain complexes [147]. Mammalian Complex IV, named cytochrome *c* oxidase (CCO), is a dimeric enzyme [148] comprising 13 subunits per monomer [149, 150]. The mitochondrial encoded subunits 1, 2 and 3 confer the catalytic activity of CCO, whereas the residual 10 nuclear encoded subunits are suggested to have regulatory functions affecting CCO activity [150]. At least five of these subunits are expressed as different isoforms [151-156], three of which as ‘heart-type’ and ‘liver-type’ isoforms, constituting one important level in the regulation of tissue-specific CCO activity. One of these is subunit 7a (Cox7a). This subunit is located in the periphery of CCO (compare Figure 3), comprises a hydrophobic C-terminal transmembrane region [148, 157] and may be involved in the maturation of the holoenzyme during a late stage of CCO assembly [158]. Cox7a1 and Cox7a2 represent the heart and liver-type isoforms, respectively. These paralogues proteins are encoded by separate genes, share about 65% sequence identity within the mature peptides and are of nearly identical molecular weight. Cox7a2 is ubiquitously expressed whereas Cox7a1 is abundantly present in heart and skeletal muscle, accounting for 60% and 50% of total Cox7a transcript abundance in adult mice, respectively [159]. Due to its high abundance, ablation of Cox7a1 in mice results in reduced CCO activity in heart and skeletal muscle [160, 161], both of which are tissues of high oxidative capacity like BAT. Both Cox7a1 and Cox7a2 are expressed in BAT (Figure 5). Cox7a1 is not detected in WAT, whereas Cox7a2 appears to be more abundant in WAT than in BAT. Interestingly, Cox7a1 but not Cox7a2 is a cold-responsive protein of BAT, which is, similar to

Ucp1, upregulated several-fold when heat production is acutely (4 days at 4°C) or chronically (24 days at 4°C) stimulated (Figure 5). Moreover, Cox7a1 is one of several brown adipocyte marker genes widely used to substantiate the presence of brite adipocytes based on its consistent upregulation in cold-activated WAT and BAT [162, 163].

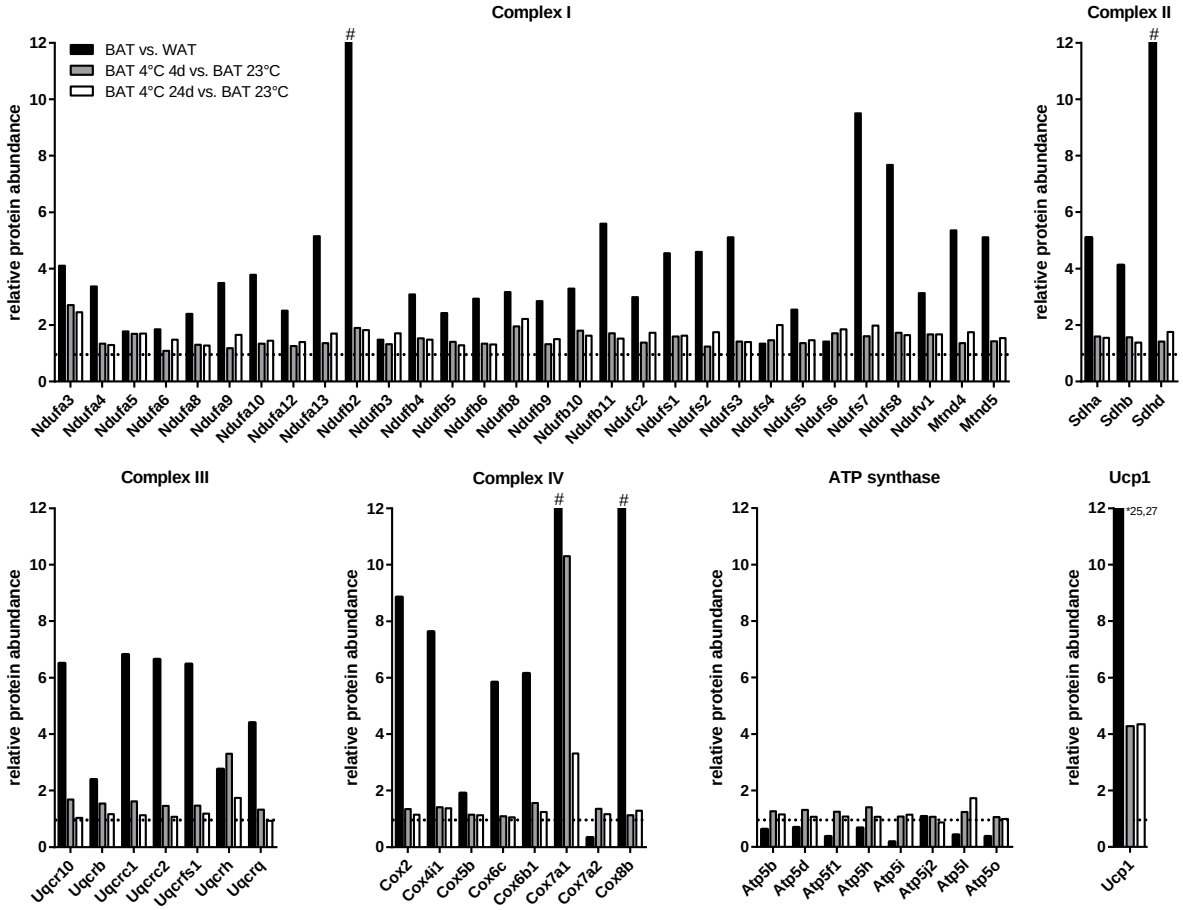

Figure 5: Abundance of proteins in murine BAT and WAT associated with respiratory chain complexes. Mice were housed at room temperature (23°C) or cold-exposed (4°C) for 4 days and 24 days, respectively. BAT and WAT were dissected and subjected to liquid chromatography/mass spectrometry analysis for quantification of mitochondrial proteins. Relative protein abundance is indicated (1) in BAT vs. WAT at 23°C and (2) in BAT at 4°C vs. BAT at 23°C. Depicted proteins were selected based on their identification in both measurements. # indicates proteins that were exclusively detected in BAT but not WAT. * indicates actual protein abundance of Ucp1 in BAT vs. WAT since y-axis was set to 12. Depicted data are publicly available and were extracted from supplementary material provided by [146]. The figure is presented in identical form in [164].

Altogether, these findings suggest a central function for Cox7a1 for the thermogenic property of brown and brite adipocytes: Cox7a1 may replace Cox7a2 during cold-acclimation, thus increasing CCO activity in response to Ucp1-mediated uncoupling to adaptively elevate the capacity for NST. Characterization of BAT function in Cox7a1-ablated mice will help to define the so far unknown functional role for this protein in the molecular thermogenic machinery of brown and brite adipocytes.

1.5.2 Dietary manipulation of key pathways in the recruitment of brite adipocytes

Thermogenic stimulation induces Ucp1 expression, lipolysis and mitochondrial biogenesis in brown and brite adipocytes, although intracellular signal transduction is not mediated in identical manner in both cells types. In fact, the cyclooxygenase (COX) enzyme has been identified as a key regulator in recruitment of brite but not brown adipocytes [165, 166]. This enzyme is ubiquitously expressed occurring as constitutive isoform COX-1 and inducible isoform COX-2. Besides lipoxygenase (LOX) and the cytochrome P450 (CYP450) enzymes, the formation of oxylipins functionally involves COX. Oxylipins are oxygenated metabolites referred to as eicosanoids and docosanoids that originate from the metabolization of polyunsatured fatty acids [167]. Eicosanoids are further subcategorized into prostaglandins, leukotriens, lipoxins, thromboxanes and others, dependent on their particular biosynthesis pathway (compare Table 10). There are n6 and n3-derived oxylipins to be distinguished (Figure 6) that are derived from the metabolism of arachidonic acid (AA) or eicosapentaenoic acid (EPA) and docosahexaenoic acid (DHA), respectively.

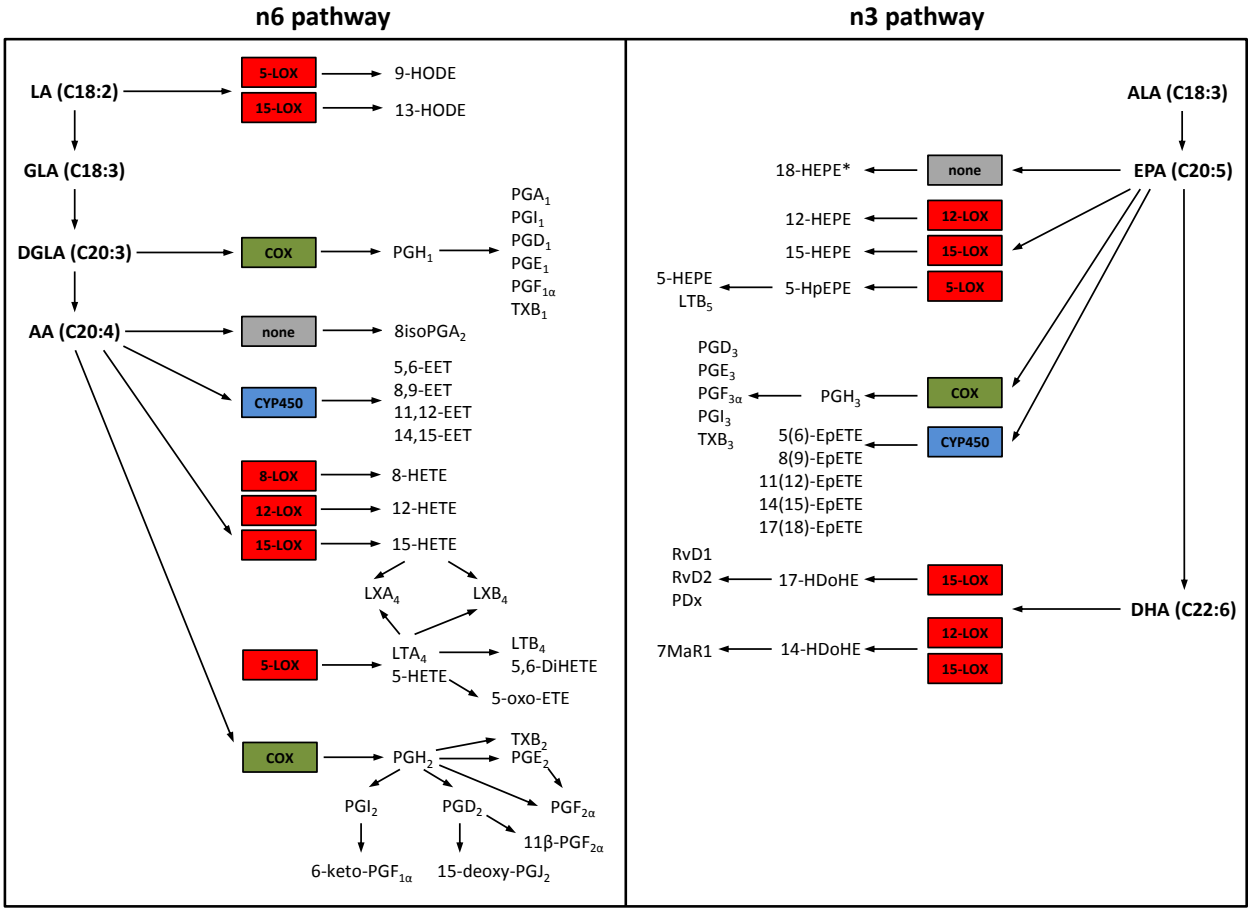

Figure 6: Biosynthesis of n6 and n3 fatty acids and their metabolism to selected oxylipins. Schematic draw according to [168-171]. Biosynthesis of 5,6-DiHETE and 8isoPGA$_2$ were appended [172, 173]. Compare Table 10 and Table 11 for classification and nomenclature of metabolites (not listed in tables: HpEPE=hydroperoxy-EPA; EpETE=epoxy eicosatetraenoic acid). Oxylipin precursor fatty acids (LA=linoleic acid; GLA=γ-linolenic acid; DGLA=dihomo-γ-linolenic acid; AA=arachidonic acid; ALA=α-linolenic acid; EPA=eicosapentaenoic acid; DHA=docosahexaenoic acid) are indicated with chain length and number of double bonds. Enzymes involved in oxylipin formation (COX=cyclooxygenase; LOX=lipoxygenase; CYP450=cytochrome P450 enzymes) are highlighted in green, red and blue. Synthesis of oxylipins via non-enzymatic oxygenation is indicated in grey. *18-HEPE is indicated to be formed from a non-enzymatic pathway [168] but may also involve COX-2 and CYP450 [170].

Cold-exposure and β_3-adrenergic stimulation both result in an upregulation of COX in murine WAT. Concomitant Ucp1 expression is prevented in COX-2 ablated mice and in mice treated with COX inhibitors, whereas enhanced browning is observed in COX-2 overexpressing mice even in the absence of an exogenous stimulus [165, 166]. This effect has been associated with endogenous secretion of prostaglandin E_2 (PGE_2) [165, 166] and prostaglandin I_2 (PGI_2) [165] from mature adipocytes, both of which are AA-derived COX-metabolites (Figure 6) proposed to trigger brite recruitment from precursor cells via interaction with their specific cell surface receptors [165]. Their browning potential was recently investigated in more detail. PGE_2 is suggested to drive brite adipogenesis in PPARγ-dependent manner [174, 175]. Differentiation of primary progenitor cells from murine WAT in the presence of PGI_2 leads to strong induction of thermogenic and oxidative gene expression pathways that is synergized by NE and preceded by early cell cycle activation and cytoskeleton changes [176]. The action of PGI_2 is mediated by the PGI_2 receptor (IP) [165], whereas the effect of PGE_2 is ascribed to the EP4 receptor, which is one of four PGE_2-receptor subtypes [166]. Both IP and EP4 receptor activation involves cAMP formation and PKA-mediated signal transduction [177], which are crucial components of the β_3-adrenergic signaling pathway in brown adipocytes (compare Figure 2). Increased synthesis of endogenous IP and EP4 receptor ligands from AA may thus beneficially affect brite adipocyte abundance.

Cellular AA, EPA and DHA either originate from ingestion or from endogenous synthesis on the basis of essential fatty acids (Figure 6). They are stored as phospholipids to become available as substrate upon liberation by phospholipase A_2. An increase in EPA and DHA ingestion elevates the amount of these fatty acids stored as phospholipids in adipose tissue [178]. Increased availability of EPA reduces AA oxygenation by COX [179, 180]. Thus, oxylipin formation constitutes a process manipulable by dietary fatty acid composition. Administration of diets with different ratios of dietary n6 versus n3 fatty acids may help to increase the COX-mediated production of AA-derived oxylipins with proposed browning effect (PGE_2 and PGI_2) and to identify further candidate compounds synthesized from other pathways (Figure 6).

1.6 Objective of the present work

The present thesis originated from the European collaborative project ‘DIABAT’ (recruitment and activation of brown adipocytes as preventive and curative therapy for type 2 diabetes). This project aimed to expand basic knowledge on the function, regulation and physiology of brown and brite adipocytes to distinctly develop, implement and validate BAT-centered therapies against obesity and T2D in human subjects. The results in mice here described will therefore contribute and support this objective in a translational context.

Human BAT-centered intervention strategies against obesity and T2D must aim at the activation of existing BAT depots and the recruitment of additional capacity. To achieve this, it is necessary to identify the essential components that drive thermogenesis in brown and brite adipocytes. The CCO subunit isoform Cox7a1, a cold-responsive protein of BAT, seemed to be a promising candidate. High abundance of Cox7a1 in heart and skeletal muscle contributes to the

high oxidative capacity of these tissues. This functional relationship has so far not been addressed in cold-activated BAT. Thus, Cox7a1-ablated mice were characterized on the molecular, cellular and organismic level to elucidate the function of this protein for NST.

NST is a highly energy consuming process that is supported by glucose uptake into BAT from the bloodstream. This glucose uptake is dependent on abundance and activity of the tissue. The thermogenic capacity and function of BAT thus renders this tissue a sink for circulating glucose hypothesized to influence blood glucose clearance in mice and men. This thesis therefore aimed to investigate the relationship between NST capacity and glucose tolerance in more detail. For that purpose, two different inbred mouse strains, 129S6/SvEvTac and C57BL/6J, were characterized with respect to their NST capacity. The capacity for NST in mice may be influenced by the abundance of brite adipocytes possibly affecting blood glucose clearance. Mice of both inbred strains were fed with diets differing in the dietary fatty acid composition to manipulate oxylipin production in WAT in order to investigate the efficacy of a nutritional intervention approach in WAT browning. These mouse models were further challenged means of environmental temperature and dietary fat content to elucidate the role of NST capacity in the regulation of systemic glucose tolerance. Finally, glucose homeostasis was investigated in Ucp1-ablated mice with negligible NST capacity to validate effects observed in inbred mice.

2 MATERIAL AND METHODS

2.1 Mouse lines

In total, four different mouse lines were employed bred on the background of C57BL/6J (BL6J) and 129S6/SvEvTac (129S6) inbred strains. All mice were bred within the specified pathogen free (SPF) facility located at the Kleintierforschungszentrum Weihenstephan. Offspring of all mouse lines used was weaned at three weeks of age. If necessary, genotyping was performed using tail tips (≤ 1 mm of distal tail end) or ear punches obtained at weaning. All mice were housed inside the SPF facility in individual ventilated cages (501 cm^2) at room temperature (23°C ± 1°C), 55% relative humidity and 12/12 hour light/dark cycle (5:00 am/pm CET) with *ad libitum* access to standard rodent chow diet (V1124-300, Ssniff Spezialdiäten GmbH, Soest/Germany) and water prior to the beginning of experiments.

2.1.1 Inbred mouse lines

129S6 and BL6J mice were obtained from Taconic (Hudson NY/USA) and Charles River (Wilmington MA/USA), respectively, and distinctly bred as individual inbred mouse lines inside the SPF facility. All experiments involving 129S6 and BL6J inbred mice were conducted with male animals. Importantly, these 129S6 and BL6J mice served not as direct wildtype (WT) controls in experiments involving knockout (KO) mice, but WT animals of the respective mouse lines were used for that purpose.

2.1.2 Cox7a1-KO mouse line

KO strategy and breeding:

Mice with a constitutive KO of the cytochrome *c* oxidase subunit 7a isoform 1 (Cox7a1) allele were generated, initially described [160] and kindly provided by Maik Hüttemann, Larry Grossman and colleagues. The KO is based on replacement of the first three exons of the Cox7a1 gene by a neomycin resistance cassette, thus impeding transcription of the open reading frame. Genotyping (see below) is performed with desoxyribonucleic acid (DNA) of genomic origin (gDNA), applying one forward primer, binding in the promoter region of the gene, and two different reverse primers. The WT allele is detected by a reverse primer binding in exon 2, generating a polymerase chain reaction (PCR) product of about 600 base pairs (bp). The KO allele is detected by application of a reverse primer binding within the neomycin cassette, resulting in a PCR product of about 1,000 bp.

Cox7a1-KO mice were imported into the SPF facility via embryonic transfer and bred on BL6J background. Breeding was generally conducted with heterozygous (HET) breeding pairs to obtain offspring of all genotypes. WT and HET littermates were used as controls for KO mice in all experiments. Experiments were conducted with male and female mice.

Genotyping:

Tail tips or ear punches were digested for at least 4 hours at 65°C in 200 µl tail buffer comprising 0.25 mg/ml proteinase K (Thermo Fisher Scientific, Waltham MA/USA) followed by heat inactivation at 95°C for 10 min. One µl of this solution was used as template for genotyping. Two PCRs per sample were conducted using one of two reverse primers, each in a total volume of 25 µl comprising 12.5 µl 2x ImmoMix (Bioline, London/UK), 400 nM forward and reverse primers and 1 µl template DNA. PCR was conducted as described in Table 1. Five µl of 6x DNA loading buffer was added to each PCR reaction and PCR products were separated in a 1.5% agarose gel (dissolved in TAE buffer comprising 5 µl/100 ml DNA dye (Roti®-GelStain, Carl Roth, Karlsruhe/Germany)). PCR products were detected at 312 nm or 366 nm.

Table 1: PCR program for genotyping of Cox7a1-KO mice.

Step	Temperature [°C]	Duration [sec]	Cycles
Initial denaturation	95	420	
Denaturation	95	10	x43
Primer annealing	60	20	
Elongation	72	30	
Final Elongation	72	300	

Tail buffer: 10 mM Tris (pH 8.3), 50 mM KCl, 0.45% Nonidet P40, 0.45% Tween 20
6x DNA loading buffer: 10 mM Tris (pH 7.6), 0.2% Orange G, 60% glycerol, 60 mM EDTA
TAE buffer: 40 mM Tris (pH 8.3), 0.15% acetic acid, 1 mM EDTA

Primers (produced by Eurofins MWG Operon, Ebersberg/Germany; sequences adopted from [160]):
Forward CGCCCATTTCACATTCTCAGCACTGGAG
WT reverse AAGAGCTTCTGCTTCTCTGCCAC
KO reverse ACGGTATCGCCGCTCCCGATTCGCAG

2.1.3 Ucp1-KO mouse line

KO strategy and breeding:

Mice carrying a constitutive knockout of the uncoupling protein 1 (Ucp1) allele were investigated. Ucp1-KO mice on hybrid background were generated and initially described by Leslie Kozak and coworkers [47]. Ucp1-KO mice were backcrossed on the congenic BL6J background [181]. Founder mice were kindly provided by Leslie Kozak and introduced into the in-house SPF facility to establish a colony, which was bred on the BL6J background. Among the six exons of the murine Ucp1 gene, exon 2 and partly exon 3 are replaced by a neomycin resistance cassette. Genotyping (see below) is based on application of one forward and two different reverse primers, producing WT and KO PCR-products of 371 bp and 198 bp, respectively.

Backup breeding was generally conducted with HET breeding pairs to obtain mice of all genotypes. In thermal imaging experiments (section 2.3.6), WT and HET littermates were used

as controls for KO mice. WT and KO mice obtained from HET breeding pairs were mated in homozygous WT/WT and KO/KO breeding pairs to obtain WT and KO mice used for experiments with adult animals. All experiments involving adult mice were conducted with male animals.

Genotyping:
Genotyping was performed as described above (section 2.1.2). One PCR per sample was conducted in a total volume of 25 µl, comprising 12.5 µl 2x ImmoMix, 400 nM forward primer, 400 nM WT and KO reverse primers and 1 µl template DNA. PCR was performed as described (Table 2). PCR products were separated in a 1.5% agarose gel.

Table 2: PCR program for genotyping of UCP1-KO mice.

Step	Temperature [°C]	Duration [sec]	Cycles
Initial denaturation	95	420	
Denaturation	97	10	x35
Primer annealing	53	15	
Elongation	72	20	
Final Elongation	72	180	

Primers (produced by Eurofins MWG Operon, Ebersberg/Germany):

Forward	CCCCTGTCAGGTGGGAT
WT reverse	CACCCACATTGTCCATGAAG
KO reverse	AGGGGAGGAGTAGAAGGTGG

2.2 Experimental diets

2.2.1 Diet composition

Mice received three different types of pelleted diets (10 mm diameter) during feeding experiments (Table 3). Diets were primarily characterized by differential fat content. A control diet was fed (referred to as low-fat control diet (LFCD)) comprising 5% fat (w/w) from soybean oil. Fat content of the LFCD was increased to 14% fat (w/w) by addition of 9% (w/w) experimental oil (section 2.2.3), thus obtaining intermediate-fat diets (IFD). High-fat diets (HFD) were characterized by 25% (w/w) total fat content comprising 5% soybean oil, 9% experimental oil and 11% palm oil. Fat content of IFD and HFD was increased at the expense of corn starch. The absolute amount of other nutrients was comparable in all types of diets.
Unless stated otherwise, all experimental food was sterilized by γ-irradiation and supplemented with 0.1 g/kg butylated hydroxytoluene (BHT) to minimize deterioration processes. BHT was added at the expense of corn starch. All food was obtained from Ssniff Spezialdiäten GmbH, Soest/Germany.

Table 3: Crude nutrient composition of experimental diets.

Type of diet	LFCD	IFD	HFD
Gross energy [MJ/kg][1]	18.6	20.5	22.8
Metabolizable energy [MJ/kg][2]	15.3	17.2	19.6
Metabolizable energy [MJ%][2]			
Protein	23	20	18
Fat	13	31	48
Carbohydrate	64	49	34
Crude nutrients [g/kg][2]			
Protein			
Casein	240	240	240
Fat			
Soybean oil	50	50	50
Experimental oil		90	90
Palm oil			110
Carbohydrate			
Corn starch	477.9	387.9	277.9
Sucrose	50	50	50
Maltodextrin	56	56	56
Cellulose	50	50	50
Other			
Vitamins	12	12	12
Anorganic Compounds	60	60	60
L-Cystine	2	2	2
Choline-Cl	2	2	2
BHT	0.1	0.1	0.1

[1]Determined by bomb calorimetry as described below (section 2.2.2). [2]According to manufacturer's information.

2.2.2 Gross energy

Food pellets were sampled from all types of diets for each batch ordered. Pellets were dried at 55°C for several days until no further weight change was detectable. Gross energy of pellets of approx. 1 g dry weight was determined by bomb calorimetry (bomb calorimeter 6300, Parr Instrument Company, Moline IL/USA). During the measurement, samples are completely combusted under high pressure in the presence of oxygen. Combustion leads to warming of a water bath that surrounds the bomb, and the difference in temperature before and after combustion is proportional to the energy content of the sample. The latter is determined via calibration of the calorimeter with a standard (benzoic acid) of known energy content.

A mean value was calculated for each type of diet irrespective of experimental fat source averaging gross energy of diets from all batches used (see Table 3). Energy intake of mice during experiments was calculated from food intake and gross energy of the respective batch fed in consideration of variable fat sources of IFDs and HFDs.

2.2.3 Fatty acid profile of diets

Mice were fed with IFDs and HFDs comprising 9% (w/w) experimental oil. Palm, fish and borage oil served as experimental fat sources. Commercial fatty acid analysis was conducted (Research Center Weihenstephan for Brewing and Food Quality) to clarify fatty acid composition of IFDs vs. LFCD (Table 4).

Table 4: Fatty acid composition of LFCD and IFDs determined by commercial fatty acid analysis.

Fatty acid methylester [%]	Structure[1]	ω	LFCD[2]	IFD palm[2]	IFD fish[2]	IFD borage[2]
Butyric	4:0		0.05			
Lauric	12:0		0.11	0.12	0.13	
Myristic	14:0		0.46	0.79	4.48	0.22
Pentadecanoic	15:0		0.06	0.05	0.35	
Palmitic	16:0		13.41	31.01	15.18	11.59
Palmitoleic	16:1, 9c		0.17	0.15	5.23	0.14
Heptadecanoic	17:0		0.11	0.10	0.36	0.08
Heptadecenoic	17:1, 9c		0.06		0.12	
Stearic	18:0		3.67	4.13	3.57	3.46
Oleic	18:1, 9c		25.44	33.36	16.91	20.59
cis-Vaccenic	18:1, c11		1.59	1.01	2.58	0.96
Linoleic	18:2, 9c,12c	n6	48.07	25.53	21.16	42.80
y-Linolenic	18:3, 6c,9c,12c	n6			0.23	12.03
Linolenic	18:3, 9c,12c,15c	n3	4.62	2.01	2.48	2.27
Arachidic	20:0		0.33	0.35	0.33	0.28
Conjugated Linoleic	18:2, 9c,11t				0.06	
Conjugated Linoleic	18:2, 10t,12c				0.09	
Eicosenoic	20:1, 11c		0.22	0.15	1.01	2.30
Arachidonic	20:4, 5c,8c,11c,14c	n6			0.73	
Behenic	22:0		0.43	0.18	0.20	0.25
Erucic	22:1, 13c				0.50	1.36
Docosadienoic	22:2, 13c,16c	n6	0.09			
Eicosapentaenoic	20:5, 5c,8c,11c,14c,17c	n3			10.40	
Docosapentaenoic	22:5, 7c,10c,13c,16c,19c	n3			1.19	
Docosahexaenoic	22:6,4c,7c,10c,13c,16c,19c	n3			6.62	
Lignoceric	24:0		0.17	0.06	0.23	0.11
Nervonic	24:1, 15c					0.83
others			0.24	0.00	2.87	0.24
not identified			0.70	1.00	3.00	0.50
Σ			100.00	100.00	100.0	100.00
Saturated fatty acids			18.99	36.79	25.14	15.99
Monounsaturated fatty acids			27.53	34.67	27.23	26.17
Polyunsaturated fatty acids			52.79	27.54	44.86	57.34
		Σ n6	48.16	25.53	22.29	54.96
		Σ n3	4.62	2.01	22.42	2.37
		n6/n3	10.41	12.73	0.99	23.16

[1]Structure specifies chain length, number of double bonds, position of double bonds and configuration (c=cis, t=trans).
[2]Ssniff article no: S5745-E720 (LFCD), S5745-E141 (IFD palm), S5745-E143 (IFD fish), S5745-E142 (IFD borage).

Addition of 11% palm oil to each of the three IFDs resulted in the generation of HFDs. Hypothetical fatty acid composition of HFDs (Table 5) was calculated based on results obtained from commercial fatty acid analysis of LFCD and IFDs.

Table 5: Hypothetical fatty acid composition of HFDs.

Fatty acid methylester [%]	Structure[1]	ω	HFD palm[2]	HFD fish[2]	HFD borage[2]
Butyric	4:0		0.01	0.01	0.01
Lauric	12:0		0.13	0.13	0.08
Myristic	14:0		0.87	2.93	0.55
Pentadecanoic	15:0		0.05	0.22	0.03
Palmitic	16:0		35.24	26.40	24.38
Palmitoleic	16:1, 9c		0.15	2.99	0.14
Heptadecanoic	17:0		0.09	0.24	0.08
Heptadecenoic	17:1, 9c		0.01	0.07	0.01
Stearic	18:0		4.23	3.92	3.86
Oleic	18:1, 9c		35.22	26.03	28.08
cis-Vaccenic	18:1, c11		0.87	1.75	0.84
Linoleic	18:2, 9c,12c	n6	19.98	17.54	29.63
y-Linolenic	18:3, 6c,9c,12c	n6		0.13	6.72
Linolenic	18:3, 9c,12c,15c	n3	1.36	1.63	1.51
Arachidic	20:0		0.35	0.34	0.31
Conjugated Linoleic	18:2, 9c,11t			0.04	
Conjugated Linoleic	18:2, 10t,12c			0.05	
Eicosenoic	20:1, 11c		0.13	0.61	1.33
Arachidonic	20:4, 5c,8c,11c,14c	n6		0.41	
Behenic	22:0		0.12	0.13	0.16
Erucic	22:1, 13c			0.28	0.76
Docosadienoic	22:2, 13c,16c	n6	0.02	0.02	0.02
Eicosapentaenoic	20:5, 5c,8c,11c,14c,17c	n3		5.81	
Docosapentaenoic	22:5, 7c,10c,13c,16c,19c	n3		0.67	
Docosahexaenoic	22:6,4c,7c,10c,13c,16c,19c	n3		3.70	
Lignoceric	24:0		0.03	0.13	0.06
Nervonic	24:1, 15c				0.47
others			0.05	1.77	0.18
not identified			1.08	2.07	0.79
Σ			100.00	100.00	100.00
Saturated fatty acids			41.16	34.66	29.56
Monounsaturated fatty acids			36.40	32.22	31.64
Polyunsaturated fatty acids			21.36	31.05	38.01
	Σ n6		20.00	18.20	36.44
	Σ n3		1.36	12.77	1.57
	n6/n3		14.68	1.42	23.25

[1]Structure specifies chain length, number of double bonds, position of double bonds and configuration (c=cis, t=trans).
[2]Ssniff article no: S5745-E722 (HFD palm), S5745-E147 (HFD fish), S5745-E146 (HFD borage).

Addition of experimental oils modified the dietary fatty acid composition to alter the ratio of n6 to n3 fatty acids. Fish oil containing IFD (IFD fish) was characterized by occurrence of the n3 fatty acids eicosapentaenoic and docosahexaenoic acid and decreased n6/n3 ratio compared to the other diets. Compared to other IFDs, borage oil containing IFD (IFD borage) was characterized by increased abundance of the n6 fatty acids linoleic and γ-linolenic acid and an increased n6/n3 ratio. The n6/n3 ratio of palm oil containing IFD (IFD palm) was comparable to LFCD and intermediate compared to fish and borage oil containing IFDs. Differential n6/n3 ratios of IFDs were well conserved in HFDs.

2.3 Animal experiments

2.3.1 Housing

Unless stated otherwise, all animal experimentation was conducted within the SPF facility. Mice were housed in individual ventilated cages at 23°C with *ad libitum* access to chow food and water prior to the beginning of all experiments. Housing of mice at 4°C, 20°C and 30°C or 31°C during experiments was conducted in constant climate cabinets (HPP749 and HPP750life, Memmert, Schwabach/Germany, or UniProtect, Zoonlab, Castrop-Rauxel/Germany) at 55-65% relative humidity and 12/12 hour light/dark cycle (5:00 am/pm CET). Mouse husbandry inside climate cabinets was conducted in an open cage system using type II (for 1-3 mice, 370 cm^2) and type II long (for 3-5 mice, 530 cm^2) cages. Unless stated otherwise, mice were group-housed and received *ad libitum* access to food and water. Housing at 4°C was conducted with single-caged mice to avoid social thermoregulation. Mice and food were weighed using a standard laboratory balance. In the respective experiments, body temperature was recorded between 7:30 and 9:00 am using a rectal probe (Almemo 2490, Ahlborn, Holzkirchen/Germany). All animal experimentation was conducted in accordance with the German animal welfare law.

2.3.2 Oral glucose tolerance test

In the morning of the test day, mice were single caged without food and fasted for 6 hours (8:00 am - 2:00 pm). Meanwhile, body composition was determined with a nuclear magnetic resonance instrument (mq 7.5, Bruker, Billerica MA/USA). Mice received an oral glucose load of 2.8 g/kg lean mass from a 40% glucose stock solution (B.Braun Melsungen AG, Melsungen/Germany). Blood was taken from a small incision on the distal end of the tail to measure blood glucose before (0 min) and 15, 30, 60 and 120 min after gavage using a whole blood monitor (FreeStyle Lite, Abbott, Wiesbaden/Germany). Fasting and oral glucose tolerance tests (oGTT) were performed at room temperature in all experiments irrespective of previous acclimation state. Total area under the curve (AUC) was calculated by the trapezoidal method [182] and served as measure for glucose tolerance.

2.3.3 Insulin tolerance test

Performance of insulin tolerance tests (ITT) was similar to the oGTT procedure described above (section 2.3.2). After a fasting period of 6 hours, single-caged mice received an intraperitoneal injection to administer insulin (Insuman Rapid 40 U/ml, Sanofi, Paris/France) in a dose of 0.75 U/kg lean mass using an insulin stock solution to inject a volume of 4-6 ml/kg body mass. Blood glucose was measured at the indicated time points. Fasting and ITT was performed at room temperature. The AUC served as measure for insulin sensitivity [182].

2.3.4 Repeated administration of CL-316243

CL-316243 (CL, disodium salt, Tocris Bioscience, Bristol/UK) was administered via intraperitoneal injection on seven consecutive days at the same time of the day. Stock solutions (CL dissolved in saline (B.Braun Melsungen AG, Melsungen/Germany)) were prepared to administer a volume of 5 ml/kg body mass. Vehicle-treated mice generally received an injection of 150 µl saline. Aliquots of stock solutions and saline were stored at -20°C and a fresh aliquot was thawed every day. During CL-treatment, body mass was measured every day prior to administration of CL. Body composition was measured via nuclear magnetic resonance on the first day and the day after the last CL-administration. Mice were killed approx. 24 hours after the last injection.

2.3.5 Indirect calorimetry and norepinephrine test

The norepinephrine (NE) test is a gold standard method to determine the capacity for non-shivering thermogenesis (NST) in mice [28, 183]. The test is based on interaction of NE with the β_3-adrenergic receptor. Injection of NE in high dose leads to acute and maximal stimulation of Ucp1-dependent mitochondrial respiration and thus heat production (HP) in brown adipose tissue (BAT). Thermogenic BAT activity is reflected in the oxygen consumption of the animal, which is recorded via indirect calorimetry. The magnitude of response is dependent on pretreatment of the animal.

NE-tests with Cox7a1-KO mice:

In the morning of the test day, body mass was determined and mice were placed in metabolic cages (3 liter volume) without food and water. The cages were connected to the indirect calorimetry setup (LabMaster, TSE Systems, Bad Homburg/Germany) inside a climate cabinet (TPK 600, Feutron, Greiz/Germany) preconditioned to 31°C. Oxygen consumption and carbon dioxide production of mice was recorded over a period of 4 hours (8:00 am - 12:00 pm) to determine basal metabolic rate (BMR) during fasting. The air of the cages was extracted with a flow rate of 33 l/h over a period of 1 min every 7 min, dried in a cooling trap and analyzed for oxygen and carbon dioxide content. Oxygen consumption and carbon dioxide production were determined by comparison of air from the cages with an empty reference cage. The BMR was calculated as the lowest mean of three consecutive oxygen consumption values, which had a coefficient of variation less than 5%.

After BMR measurement, mice were placed at room temperature and the climate cabinet was altered to 26°C (first test) or 20°C (second test) for at least 20 min to facilitate loss of heat to the environment produced in response to NE-administration in order to avoid hyperthermic reactions. Mice were injected subcutaneously with 1 mg/kg NE (Arterenol 1 mg/ml, Sanofi, Paris/France) and immediately reconnected to the indirect calorimetry setup. Oxygen consumption and carbon dioxide production were recorded as described above during a 1 min read every 3 min for 60-75 min. NE-tests were performed with two mice per single measurement. Up to three consecutive measurements were conducted per test day. Oxygen consumption data were smoothed by calculating a mean of three consecutive values. Maximal NE-stimulated (NE_{max}) oxygen consumption was obtained from the highest individual mean. Metabolic rates (MR), i.e. BMR and NE_{max}, were converted into HP according to the following equation [184]:

$$HP\ [mW] = (4.44 + 1.43 * RER) * MR\ [ml\ O_2/h]$$

The respiratory exchange ratio (RER) is the ratio of carbon dioxide production and oxygen consumption.

BMR represents the rate of energy expended at rest in thermoneutral environment and does not involve energy expenditure utilized for BAT-derived heat production [185-187]. In contrast, MR measured at NE_{max} reflects the sum of energy expenditure resulting from BMR and all NE-induced thermogenic processes beyond. Besides a general, pharmacological Ucp1-independent response, the latter is in large part accounted for by BAT activity [188, 189]. NST capacity was thus calculated as difference in HP between NE_{max} and BMR.

NE-tests with 129S6 and BL6J WT mouse lines:

NST capacity was determined as described above with slight modifications. BMR was measured at 31°C for 4 hours (7:00 am – 11:00 am) with a 1 min read every 5 min. BMR was calculated as the lowest mean of four oxygen consumption values with a coefficient of variation less than 5%. NE-tests were performed at 27°C. Prior to each NE-injection, the air from a reference cage was analyzed for oxygen and carbon dioxide content for a period of 5 min. One mouse was injected with NE during the last minute of reference measurement and immediately reconnected to the setup, thus ensuring temporal comparability between different measurements. Oxygen consumption and carbon dioxide production of the mouse were measured every 10 sec. After 65 min, the reference was measured for 5 more minutes to control for putative drifts in oxygen and carbon dioxide content. Four animals were tested per day in single, consecutive measurements.

Measurements were exclusively conducted with mice that were previously housed at 30°C for 4 weeks. Mice of such acclimation state have minimized NST capacity and therefore minimized NE-induced oxygen consumption. In this setting, various types of unspecific oxygen consumption peaks occurred that may result from activity of conscious animals rather than maximal BAT thermogenesis (Figure 7A). Moreover, drawn-out plateau-phases were observed within the first 30 min of measurement with no recognizable NE_{max}, and/or unspecific peaks

were observed suggesting NE_{max} to occur more than 30 min after NE administration (Figure 7B). The latter is in conflict with results obtained in cold-exposed mice that exhibit NE_{max} within 20 min after NE administration (compare section 3.1.2). Thus, a mean value was calculated from 50 consecutive oxygen consumption values (mean 50, Figure 7A and B), resulting in severe smoothing of oxygen consumption traces. The highest individual mean occurring within 30 min after NE administration was considered as true NE_{max}. BMR and NE_{max} were converted into HP as described above. NST capacity was calculated as difference in HP between NE_{max} and BMR.

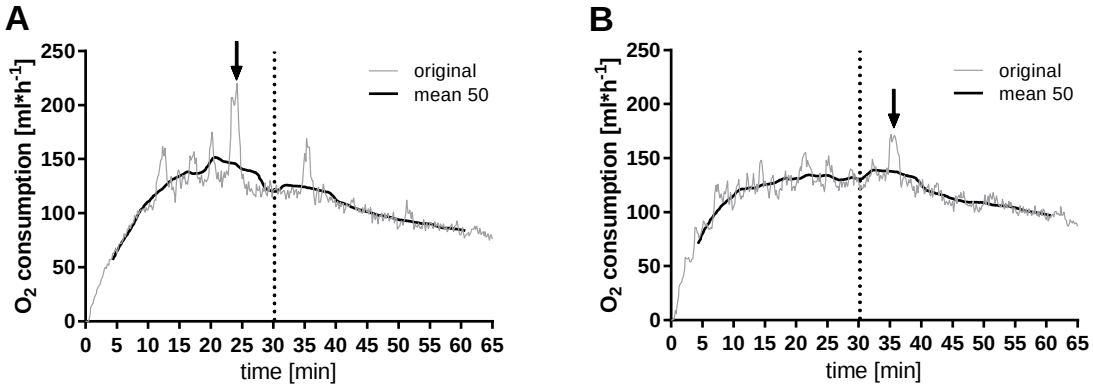

Figure 7: Representative oxygen consumption traces from NE-tests performed with mice acclimated to 30°C. (A) and (B) represent individual measurements with different mice. Original oxygen consumption and deduced traces from the mean of 50 consecutive original values (mean 50) are depicted. X-axis displays time after NE-administration. Dotted vertical line at 30 min indicates threshold for determination of true NE_{max}. Arrows exemplify unspecific peaks leading to putative misinterpretation of NE_{max}.

2.3.6 Infrared thermal imaging

Thermal imaging was applied to determine skin surface temperature of mice as surrogate measure for BAT-derived HP. Imaging was conducted with newborn mice of the Cox7a1-KO and Ucp1-KO mouse lines. HET animals were mated to obtain litters with offspring of all genotypes (WT, HET, KO). Entire litters were subjected to thermal imaging within the first three days of life. Neonates were withdrawn from their dams and prone-placed on multiwell-plates. An individual series of pictures (at least 6) was taken from each litter using a thermal imaging device (T890, Testo, Lenzkirch/Germany). Imaging was conducted at room temperature to achieve BAT activation. Pups were killed by decapitation and tail tips were sampled for post-mortem genotyping as described above (see sections 2.1.2 and 2.1.3).

Image analysis was conducted with software delivered with the thermal imaging device (IRSoft version 3.1, Testo, Lenzkirch/Germany). The warmest spot within a defined region in the upper dorsal area was determined for each animal on each picture, referred to as interscapular skin surface temperature (iSST). A mean iSST was calculated for each individual animal using data from serial pictures as technical replicates. Within each litter, an averaged iSST was calculated for HET animals. Finally, the difference between this averaged HET-iSST and iSST of each individual animal within that litter was calculated to standardize data obtained from different litters.

2.4 Molecular analyses of brown and white adipose tissues

2.4.1 Tissue dissection

Tissues were dissected immediately after death of mice via exposure to carbon dioxide, snap-frozen in liquid nitrogen and stored at -80°C until use, or fixed in paraformaldehyde for histological analyses (section 2.4.5). If necessary, frozen tissue samples were grinded in liquid nitrogen to obtain homogenous aliquots for multiple molecular analyses.

2.4.2 RNA isolation and quantitative real-time PCR

Deep-frozen tissue samples (subcutaneous inguinal white adipose tissue (iWAT), visceral gonadal WAT (gWAT), BAT from the suprasternal region, heart and liver) were homogenized in 1 ml TRIsure (Bioline, London/UK) according to the manufacturer's instructions using a dispersing instrument (Ultra-Turrax D-1, Miccra GmbH, Mühlheim/Germany). Ribonucleic acid (RNA) was precipitated and 700 µl of this solution was added to a spin column of a commercial RNA isolation kit (SV Total RNA Isolation System, Promega, Fitchburg WI/USA) and centrifuged for 15 sec with 8,000 g at room temperature. The residual volume was added to the column and centrifuged for 1 min with 12,000 g at room temperature. Further processing was performed according to the protocol of the RNA isolation kit. RNA was eluted in 50 µl of nuclease-free water. RNA concentration was determined spectrophotometrically at 260 nm with a plate reader (Infinite® 200 PRO NanoQuant, Tecan Group Ltd., Männedorf/Switzerland).
RNA integrity of random samples was validated using a Bioanalyzer system (2100, Agilent Technologies, Santa Clara CA/USA). The method is based on a conventional gel electrophoresis that is run in chip-format to reduce separation time and sample consumption. Eukaryotic 18S and 28S ribosomal RNA fragments are detected by laser-induced fluorescence. In consideration of degradation products within the electrophoretic trace, a dimensionless RNA integrity number is calculated that allows evaluation of RNA integrity. The RNA integrity number ranges from 0 (completely degraded) to 10 (perfectly intact). Samples were diluted in nuclease-free water (25-100 ng/µl) and denatured for 2 min at 70°C. RNA integrity was determined according to the manufacturer's protocol (Agilent RNA 6000 Nano Kit). The RNA integrity number of all samples tested ranged between 7.5 and 9.5, which was considered as sufficiently intact for synthesis of complementary DNA (cDNA), which was conducted with a commercial kit (QuantiTect® Reverse Transcription Kit, Qiagen, Hilden/Germany). This kit contains poly-deoxythymidine oligonucleotides and random hexamer primers that allow subsequent amplification of messenger RNAs (mRNA) by the use of PCR primers targeting the coding sequence or untranslated regions. Reverse transcription of 500 ng template RNA was conducted in a final volume of 10 µl according to the manufacturer's protocol.
Quantitative real-time PCR (qRT-PCR) was conducted on 384 well plates in a total volume of 12.5 µl comprising 6.25 µl 2x SensiMix SYBR No-ROX (Bioline, London/UK), 250 nM or 800 nM forward and reverse primers, and 1 µl template cDNA (diluted 1:10). To ensure comparability, all samples of the same experiment were run in triplicates on the same plate. Primers for

qRT-PCR (Table 6) were applied to generate a PCR product of up to 300 bp, characterized either by spanning at least one intron of multi-exon genes, or by annealing within an exon/intron-border to exclude quantification of PCR products derived from gDNA. Specificity of primers and PCR product length were validated by *in silico* PCR (https://genome.ucsc.edu/).

Table 6: Primers for qRT-PCR.

Target mRNA	Primer forward	Primer reverse	Product length cDNA [bp]	Product length gDNA [bp]
Cidea[1]	TGCTCTTCTGTATCGCCCAGT	GCCGTGTTAAGGAATCTGCTG	113	/
Cox7a1	CCGACAATGACCTCCCAGTA	TGTTTGTCCAAGTCCTCCAA	171	723
Cox7a2	CCCTCCTCTACAGAGCCACA	CGAGCGTTGATGAAACTGAA	143	814
Eef2	ACCTGCCTGTCAATGAGTCC	CAGCATGTGGCAGTATCAGG	242	505
Gtf2b[2]	TGGAGATTTGTCCACCATGA	GAATTGCCAAACTCATCAAAACT	66	1433
Hsp90	AGGAGGGTCAAGGAAGTGGT	TTTTTCTTGTCTTTGCCGCT	215	314
Tbp	ACTTCACATCACAGCTCCCC	CTTCGTGCAAGAAATGCTGA	244	6951
Ucp1	TCTCTGCCAGGACAGTACCC	AGAAGCCCAATGATGTTCAG	238	2745

All primers were produced by Eurofins MWG Operon, Ebersberg/Germany. Cidea=cell death-inducing DNA fragmentation factor, alpha subunit-like effector A; Cox7a1=cytochrome *c* oxidase subunit 7a isoform 1; Cox7a2=cytochrome *c* oxidase subunit 7a isoform 2; Eef2=eukaryotic translation elongation factor 2; Gtf2b=general transcription factor 2b; Hsp90=heat shock protein 90 alpha (cytosolic), class B member 1; Tbp=TATA box binding protein; Ucp1=uncoupling protein 1. [1]Sequences adopted from [163]. [2]Sequences adopted from [12].

Expression levels of target genes were quantified by a standard curve, consisting of pooled cDNA that was diluted with factor 2 in at least 8 steps. SYBR-green based detection of PCR products (LightCycler® 480 Instrument II, Roche, Basel/Switzerland) was conducted during 45 cycles, which was complemented by a melting curve to screen for unspecific PCR products (Table 7).

Table 7: PCR program for qRT-PCR.

Step	Temperature [°C]	Duration [sec]	Cycles
Initial denuration	95	420	
Denaturation	97	10	x45
Primer annealing	53	15	
Elongation	72	20	
Melting curve	60-95	0.11°C/sec	

Expression levels of target mRNAs were normalized as indicated in figure legends. Due to the multiplicity of experimental setups, different strategies for normalization were applied:

(1) If possible, gene expression was normalized to a single housekeeping gene that was not regulated by determining factors of the experimental setup.

(2) Depending on mouse strains or treatments, large variability of individual genes required normalization to the mean of multiple housekeeping genes in the respective experiments.

(3) The NormFinder algorithm (http://moma.dk/normfinder-software), a mathematical model to identify the optimal normalization gene among a set of candidates [190], was applied when an appropriate housekeeper was not identified by other strategies.

2.4.3 Measurement of cytochrome *c* oxidase activity

Deep-frozen BAT-samples from the interscapular region (iBAT) were homogenized in an appropriate volume (300-500 µl) of detergent-containing tissue buffer using a potter-type homogenizer (5 ml, Sartorius, Göttingen/Germany), thus generating a tissue homogenate comprising solubilized cytochrome *c* oxidase (CCO). The homogenate was ultrasonicated (Sonoplus HD 2070, Bandelin, Berlin/Germany) and centrifuged for 2 min with 16,000 g at room temperature. The supernatant was collected, centrifuged a second time and cleared from residual fat. The protein concentration of the homogenate was determined according to the Biuret method. Ten µl of the tissue homogenate was diluted with 990 µl of Biuret reagent. The absorption of the sample was measured spectrophotometrically (Genesys 10 Bio, Thermo Fisher Scientific, Waltham MA/USA) at 540 nm after short incubation time.

The activity of CCO was measured polarographically as oxygen consumption of the homogenate using a Clark-type oxygen electrode (Digital Model 10, Rank Brothers, Cambridge/UK). The electrode consists of a platinum cathode and a silver anode in 3 M potassium chloride environment, which are separated from the sample-containing measurement chamber by an oxygen-permeable Teflon membrane. Reduction of oxygen at the electrode generates an electrical current that is proportional to the oxygen partial pressure inside the chamber, which is influenced by the oxygen consumption of CCO. Enzyme activity is initiated by addition of its substrate cytochrome *c*, which is kept in reduced state by presence of ascorbic acid.

The activity of CCO was measured in a total volume of 700 µl measurement buffer, comprising 20 mM ascorbic acid as well as 5 mM ADP (allosteric CCO activator) or an ATP regenerating system that sustains high levels of ATP (allosteric CCO inhibitor). Oxygen consumption was recorded during a titration (1-30 µM) or as point measurement at 30 µM cytochrome *c* (Sigma-Aldrich, St.Louis MO/USA).

The activity of CCO was measured in an aliquot of 50 µg total protein from the iBAT homogenate. Since CCO is a mitochondrial enzyme, CCO activity may be influenced by mitochondrial abundance and thus the proportion of mitochondrial protein in the aliquot. Mitochondrial abundance of BAT is influenced by recruitment of NST capacity [28] and comparability among treatment groups is therefore limited. To get more physiological insights, CCO activity was extrapolated to depot size considering total protein yield from the tissue, thus reflecting the total oxidative capacity of iBAT.

Tissue buffer:	10 mM Hepes (pH 7.4), 40 mM KCl, 2 mM EGTA, 10 mM KF, 1% (v/v) Tween 20 and 2 µM oligomycin, supplemented either with 1 mM PMSF or 0.1% (v/v) protease/phosphatase inhibitor cocktail (Sigma-Aldrich, St.Louis, MO/USA)
Measurement buffer:	50 mM KH_2PO_4, 2 mM EGTA, 1% (v/v) Tween 20 and 2 µM oligomycin
Biuret reagent:	80 mM NaOH, 8 mM $C_4H_4KNaO_6(H_2O)_4$, 3 mM $CuSO_4(H_2O)_5$, 4.5 mM KJ and 0.1% (w/v) sodium deoxycholate
ATP regenerating system:	5 mM ATP, 5 mM $MgSO_4$, 10 U/ml pyruvate kinase (Roche, Basel/Switzerland) and 10 mM phosphoenolpyruvic acid

2.4.4 SDS-PAGE and Western Blot

Sodium dodecyl sulfate polyacrylamide gel electrophoresis (SDS-PAGE) was conducted with total protein derived from iBAT homogenates used to measure CCO activity (section 2.4.3) or with freshly prepared homogenates. Deep-frozen tissue samples were homogenized (Ultra-Turrax D-1, Miccra GmbH, Mühlheim/Germany) in lysis buffer (iBAT 10 µl/mg; iWAT 5 µl/mg) and centrifuged for 15 min with 16,000 g at 4°C. The supernatant was collected, centrifuged a second time and cleared from residual fat. Protein concentration was determined with the bicinchoninic acid method using a commercial microplate kit (Pierce™ BCA Protein Assay Kit, Thermo Fisher Scientific, Waltham MA/USA) according to the manufacturer's instruction.

An appropriate volume of 2x sample buffer was added to 25-30 µg of protein. The mixture was incubated at 95°C for 5 min. Proteins were resolved in a 12.5% SDS-PAGE (Mini PROTEAN® Tetra Cell System, BioRad Laboratories Inc., Hercules CA/USA, or Twin ExW S, Peqlab, Erlangen/Germany) and blotted onto a nitrocellulose membrane (1 mA/cm^2 for 45-60 min) by the use of a semi-dry blotting-system (Trans-Blot® Semidry Transfer Cell, BioRad Laboratories Inc., Hercules CA/USA). Membranes were incubated over night at 4°C in TBS comprising 3% bovine serum albumin. Primary antibodies were incubated for 1.5 hours at room temperature (Table 8). Membranes were washed with TBST and infrared dye-conjugated secondary antibodies were incubated for 1.5 h at room temperature (Table 8). The infrared signal and thus target proteins were detected with an infrared imaging system (Odyssey imager, LI-COR Biosciences, Lincoln NE/USA). Target proteins were identified by application of a molecular weight marker (PageRuler™ Prestained Protein Ladder, Thermo Fisher Scientific, Waltham MA/USA). Signals were densitometrically quantified using software delivered with the imaging system (Odyssey software version 3.0, LI-COR Biosciences, Lincoln NE/USA). Results were inter-blot standardized by calculating a mean value from all individual quantified signals of one target protein on the same blot. Each individual signal was normalized to its mean. Finally, standardized Ucp1 levels were normalized to standardized pan-actin levels.

Table 8: Antibodies for Western Blot.

Target protein	Molecular weight [kD]	Primary antibody dilution	Secondary antibody[3]
Pan-actin[1]	43	1:2500,1:5000	donkey-anti-mouse
Ucp1[2]	32	1:10000	goat-anti-rabbit

All antibodies were diluted in TBST. [1]Primary antibody dilution was dependent on batch (Anti-Actin clone c4, Merck Millipore, Billerica MA/USA). [2]Anti-hamster-IgG [191] with reliable detection of murine Ucp1 [192]. [3]All secondary antibodies were diluted 1:20000. Secondary antibodies were conjugated with infrared dyes 680 or 800CW (LI-COR Biosciences, Lincoln NE/USA).

Relative expression of Ucp1 protein was measured in a small aliquot of total depot protein, thus providing information on expression levels on a 'per cell basis'. Depot size and thus cell number may, however, be influenced by treatment. In consideration of total protein yield from the tissue, normalized Ucp1 expression was extrapolated to depot size. SDS-PAGE was conducted with protein derived from iBAT, which is the largest of all murine BAT depots, thus allowing estimation of the total abundance of heat-producing Ucp1 in a mouse for a physiological comparison of NST capacity.

Lysis buffer:	50 mM Tris, 1% (v/v) NP-40, 0.25% (w/v) sodium deoxycholate, 150 mM NaCl, 1 mM EDTA and 0.1% (v/v) protease/phosphatase inhibitor cocktail (Sigma-Aldrich, St.Louis MO/USA)
2x sample buffer:	62.5 mM Tris (pH 6.8), 25% (v/v) glycerol, 2% (w/v) SDS and 0.1% (w/v) bromophenol blue
12.5% resolving gel:	41.7% (v/v) acrylamide stock solution (Rotiphorese® Gel 30, Carl Roth, Karlsruhe/Germany), 375 mM Tris (pH 8.8), 0.1% (w/v) SDS, 0.05% (w/v) AMPS and 0.05% (v/v) TEMED
5% stacking gel:	16% (v/v) acrylamide stock solution, 125 mM Tris (pH 6.8), 0.1% (w/v) SDS, 0.06% (w/v) AMPS and 0.2% (v/v) TEMED
Electrophoresis buffer (pH 8.3):	25 mM Tris, 250 mM glycine and 1% (w/v) SDS. pH was adjusted with glycine.
Transfer buffer (pH 9.2):	48 mM Tris, 1.3 mM glycine and 20% (v/v) methanol. pH was adjusted with glycine.
TBS:	20 mM Tris (pH 7.6) and 137 mM NaCl
TBST:	TBS with 0.1% (v/v) Tween 20

2.4.5 Histology

One lobe of every iWAT depot was placed in 4% (w/v) paraformaldehyde and 0.0024% (w/v) picric acid immediately after dissection. The tissue was fixed for several days. Tissues were stored in 70% ethanol until dehydration (Table 9) and paraffin-embedding was conducted.

Table 9: Protocols for dehydration and hematoxylin/eosin-staining of iWAT samples.

Step	Dehydration		Hematoxylin/eosin-staining	
	Incubation in	**Duration [min]**	**Incubation in**	**Duration [min]**
1	70% ethanol	60	xylol	3
2	70% ethanol	60	xylol	3
3	80% ethanol	60	100% ethanol	2
4	96% ethanol	60	96% ethanol	2
5	96% ethanol	60	70% ethanol	1
6	100% ethanol	60	H_2O	1
7	100% ethanol	60	hemalum[2]	4
8	100% ethanol	60	H_2O	2
9	xylol	60	eosin[2]	2
10	xylol	60	70% ethanol	1
11	Paraplast[1]	60	96% ethanol	1
12	Paraplast[1]	60	100% ethanol	1
13			100% ethanol	1.5
14			xylol/ethanol (1:1)	1.5
15			xylol	2
16			xylol	2

[1]Obtained from VWR International GmbH, Darmstadt/Germany. [2]Obtained from Medite GmbH, Burgdorf/Germany.

Five µM sections were mounted on object slides and dried for at least 24 hours at 37°C until hematoxylin/eosin-staining was conducted (Table 9). This staining facilitates discrimination of cellular compartments by differential coloring: hematoxylin, characterized by blue color, stains basophile structures like nuclei, whereas eosin causes red staining of eosinophil structures like cytoplasmic compounds [193]. Stained sections were immediately covered with mounting medium (Roti®-Histokitt, Carl Roth, Karlsruhe/Germany), dried for at least 24 hours and analyzed under a microscope (Inverted microscope DMI4000B, Leica, Wetzlar/Germany) using similar adjustments for all sections of the same experiment.

2.4.6 Oxylipin analysis

Commercial oxylipin analysis was conducted in collaboration with the MetaToul metabolomics and fluxomics platform, Toulouse, France. One lobe of iWAT was grinded in liquid nitrogen and an aliquot of each sample (17-89 mg) was sent on dry ice. In total, 33 molecules were quantified (Table 10).

Oxylipins are oxygenated metabolites derived from n6 and n3-polyunsaturated fatty acids, generally referred to as docosanoids and eicosanoids. The latter includes different subclasses depending on biosynthesis pathway (Table 10). Biosynthesis occurs via non-enzymatic and enzymatic pathways, including cyclooxygenase (COX), lipoxygenase (LOX) and cytochrome P450 (CYP450) enzymes. Oxylipins were analyzed as described using a rapid, high-sensitivity method to quantify various molecules in a single run [168]. The method has already been described for application to samples of WAT [194]. Basically, tissues are spiked with internal standards (deuterium-labelled eicosanoids, see Table 11) and subjected to methanol extraction for the purpose of lipid species enrichment. Subsequently, oxylipins are separated from undesired metabolites by solid phase extraction. Oxylipins are eluted and the solvent is evaporated with nitrogen. Samples are reconstituted prior to analysis by liquid chromatography and mass spectrometry.

Table 10: Quantified oxylipins and their synthesis pathways.

Class[1]	Pathway[2]	Series	Precursor[3]	Compound
Prostaglandin	COX	n6	DGLA	PGA_1
			AA	PGD_2
				PGE_2
				6-keto-$PGF_{1\alpha}$
				$PGF_{2\alpha}$
				11β-$PGF_{2\alpha}$
				15-deoxy-PGJ_2
		n3	EPA	PGE_3
isoprostane	non-enzymatic	n6	AA	8isoPGA_2
thromboxane	COX	n6	AA	TxB_2
leukotrien	LOX	n6	AA	LTB_4
		n3	EPA	LTB_5
lipoxin	LOX	n6	AA	LxA_4
				LxB_4
hydroxyeicosatetraenoic acid	LOX	n6	AA	5-HETE
				5-oxo-ETE
				8-HETE
				12-HETE
				15-HETE
				5,6-DiHETE
hydroxyeicosapentaenoic acid	non-enzymatic	n3	EPA	18-HEPE
octadecanoid	LOX	n6	LA	9-HODE
				13-HODE
Docosanoid[4]	LOX	n3	DHA	7MaR1
				14-HDoHE
				17-HDoHE
				PDx
				RvD1
				RvD2
epoxyeicosatrienoic acid	CYP450	n6	AA	5,6-EET
				8,9-EET
				11,12-EET
				14,15-EET

Quantified oxylipins and their synthesis pathways are illustrated in Figure 6. Classification of oxylipins and their biosynthesis pathways refer to formal names of quantified compounds (see Table 11). [1]Classification was conducted according to compound LIPID MAPS IDs (see Table 11). [2]COX=cyclooxygenase; LOX=lipoxygenase; CYP450=cytochrome P450 enzymes. [3]DGLA=dihomo-γ-linolenic acid; AA=arachidonic acid; EPA=eicosapentaenoic acid; LA=linoleic acid; DHA=docosahexaenoic acid. [4]Docosanoids include maresins (MaR), hydroxy-DHA (HDoHE), protectins (PD) and resolvins (Rv).

Table 11: Common and systematic names of quantified oxylipins and eicosanoid standards.

Common name	Formal name	LIPID MAPS ID*
Oxylipins		
PGA_1	9-oxo-15S-hydroxy-prosta-10,13E-dien-1-oic acid	LMFA03010005
PGD_2	9α,15S-dihydroxy-11-oxo-prosta-5Z,13E-dien-1-oic acid	LMFA03010004
PGE_2	9-oxo-11α,15(S)-dihydroxy-prosta-5Z,13E-dien-1-oic acid	LMFA03010003
6-keto-$PGF_{1\alpha}$	6-oxo-9α,11α,15(S)-trihydroxy-prost-13E-en-1-oic acid	LMFA03010001
$PGF_{2\alpha}$	9α,11α,15S-trihydroxy-prosta-5Z,13E-dien-1-oic acid	LMFA03010002
11B-$PGF_{2\alpha}$	9α,11β,15S-trihydroxy-prosta-5Z,13E-dien-1-oic acid	LMFA03010036
15-deoxy-PGJ_2	11-oxo-prosta-5Z,9,12E,14E-tetraen-1-oic acid	LMFA03010021
PGE_3	9-oxo-11α,15(S)-dihydroxy-prosta-5Z,13E,17Z-trien-1-oic acid	LMFA03010135
8isoPGA$_2$	9-oxo-15S-hydroxy-(8β)-prosta-5Z,10,13E-trien-1-oic acid	n/a
TxB_2	9α,11,15(S)-trihydroxythromba-5Z,13E-dien-1-oic acid	LMFA03030002
LTB_4	5(S),12(R)-dihydroxy-6Z,8E,10E,14Z-eicosatetraenoic acid	LMFA03020001
LTB_5	5(S),12(R)-dihydroxy-6Z,8E,10E,14Z,17Z-eicosapentaenoic acid	LMFA03020010
LxA_4	5(S),6(R),15(S)-trihydroxy-7E,9E,11Z,13E-eicosatetraenoic acid	LMFA03040001
LxB_4	5(S),14(R),15(S)-trihydroxy-6E,8Z,10E,12E-eicosatetraenoic acid	LMFA03040002
5-HETE	5(S)-hydroxy-6E,8Z,11Z,14Z-eicosatetraenoic acid	LMFA03060002
5-oxo-ETE	5-oxo-6E,8Z,11Z,14Z-eicosatetraenoic acid	LMFA03060011
8-HETE	(±)8-hydroxy-5Z,9E,11Z,14Z-eicosatetraenoic acid	LMFA03060086
12-HETE	12(S)-hydroxy-5Z,8Z,10E,14Z-eicosatetraenoic acid	LMFA03060007
15-HETE	15(S)-hydroxy-5Z,8Z,11Z,13E-eicosatetraenoic acid	LMFA03060001
5,6-DiHETE	11-trans-5(S),6(R)-dihydroxy-7E,9E,11E,14Z-eicosatetraenoic acid	n/a
18-HEPE	(±)-18-hydroxy-5Z,8Z,11Z,14Z,16E-eicosapentaenoic acid	LMFA03070033
9-HODE	(±)-9-hydroxy-10E,12Z-octadecadienoic acid	LMFA02000151
13-HODE	(±)-13-hydroxy-9Z,11E-octadecadienoic acid	LMFA02000228
7MaR1	7(S),14(R)-dihydroxy-4Z,8E,10Z,12Z,16Z,19Z-docosahexaenoic acid	n/a
14-HDoHE	(±)14-hydroxy-4Z,7Z,10Z,12E,16Z,19Z-docosahexaenoic acid	LMFA04000030
17-HDoHE	(±)17-hydroxy-4Z,7Z,10Z,13Z,15E,19Z-docosahexaenoic acid	LMFA04000032
PDx	10(S),17(S)-dihydroxy-4Z,7Z,11E,13Z,15E,19Z-docosahexaenoic acid	LMFA04000047
RvD1	7(S),8(R),17(S)-trihydroxy-4Z,9E,11E,13Z,15E,19Z-docosahexaenoic acid	LMFA04000074
RvD2	7S,16R,17S-trihydroxy-4Z,8E,10Z,12E,14E,19Z-docosahexaenoic acid	LMFA04000007
5,6-EET	(±)5(6)-epoxy-8Z,11Z,14Z-eicosatrienoic acid	LMFA03080002
8,9-EET	(±)8(9)-epoxy-5Z,11Z,14Z-eicosatrienoic acid	LMFA03080003
11,12-EET	(±)11(12)-epoxy-5Z,8Z,14Z-eicosatrienoic acid	LMFA03080004
14,15-EET	(±)14(15)-epoxy-5Z,8Z,11Z-eicosatrienoic acid	LMFA03080001
Standards		
LxA_4-d5	5(S),6(R),15(S)-trihydroxy-7E,9E,11Z,13E-eicosatetraenoic acid-19,19,20,20,20-d5	
LTB_4-d4	5(S),12(R)-dihydroxy-6Z,8E,10E,14Z-eicosatetraenoic-6,7,14,15-d4 acid	
5-HETE-d8	5(S)-hydroxy-6E,8Z,11Z,14Z-eicosatetraenoic-5,6,8,9,11,12,14,15-d8 acid	

Trivial names of compounds are indicated in Table 10. *LIPID MAPS ID (http://www.lipidmaps.org) refers to formal names. If necessary, synonymous denomination was checked with the Chemspider database (http://www.chemspider.com).

2.5 Statistics

Graphs were generated with GraphPad Prism 6 (GraphPad Software Inc., La Jolla CA/USA). All data are presented as mean values, as mean values ± standard deviation or as individual values with the group mean indicated as a horizontal line. Statistical analyses were conducted with SigmaPlot 12.0 (Systat Software Inc., San Jose CA/USA) or GraphPad Prism 6. Statistical tests were applied as indicated in figure legends. Significant differences are indicated by asterisks or printed characters. P-values <0.05 were considered as statistically significant.

Normal distribution was tested using the Shapiro-Wilk normality test. Two normally distributed or non-normally distributed groups were compared by t-test or Mann-Whitney Rank Sum test, respectively. Three or more normally distributed groups were compared by One Way analysis of variance (ANOVA) and Holm-Sidak post-test. Three or more non-normally distributed groups were compared by Kruskal-Wallis One Way ANOVA on Ranks and Dunn's multiple comparison test. Two Way ANOVA and Holm-Sidak post-test was used to compare two or more groups with respect to two variables. When Two Way ANOVA was impossible to apply due to unequal group sizes, effects were compared as indicted by One Way ANOVA or multiple t-tests with the Holm-Sidak correction method. Two Way repeated measures (RM) ANOVA and Holm-Sidak post-test was used to compare one variable between two groups that was repeatedly measured over time. Three Way ANOVA and Holm-Sidak post-test was applied to compare a repeatedly measured variable among experimental groups that differed with respect to two characteristics. The coefficient of determination (R^2) was determined by correlation analysis using the Pearson correlation coefficient. Regression lines are indicated for significant correlations only.

3 RESULTS

3.1 The role of Cox7a1 for non-shivering thermogenesis in mice

Brown adipose tissue (BAT) provides non-shivering thermogenesis (NST) to small mammals in order to maintain normothermia in a subthermoneutral environment. The identification of indispensable components in the molecular machinery of this tissue constitutes an essential need to understand and manipulate the regulation of BAT activation that is linked to an increase in systemic energy expenditure.

The function of Cox7a1 for brown adipocytes has not yet been elucidated. Cox7a1, a well-known brown adipocyte marker gene, is a cold-responsive protein of BAT [146] as well as one of two alternative isoforms for subunit 7a of mitochondrial cytochrome *c* oxidase (CCO). The alternative isoform Cox7a2 is ubiquitously found whereas Cox7a1 is abundantly expressed in heart and skeletal muscle where its ablation blunts CCO activity, causing cardiac myopathy and impaired skeletal muscle function [160, 161]. Cold-induced upregulation of Cox7a1 in BAT may thus adjust CCO activity to increased uncoupling protein 1 (Ucp1) mediated proton leak in mitochondria of the cold-activated tissue. Consequently, ablation of Cox7a1 may impair NST caused by insufficient oxidative capacity. Wildtype (WT) and Cox7a1 knockout (KO) mice were employed to test this hypothesis.

3.1.1 Molecular characterization of the respiratory capacity in BAT

Cox7a1 is predominantly expressed in skeletal muscle and heart and affects CCO activity in these tissues [160, 161]. Its relevance for CCO activity in BAT has not yet been addressed. The abundance of Cox7a1 and Cox7a2 mRNA was similar in BAT and heart, and high Cox7a1 expression of heart compared to other tissues was well-reflected in BAT (Figure 8A). This specific expression pattern indicates Cox7a1 to be of similar importance in BAT and heart.

Cox7a1 is a cold-induced protein of BAT [146]. To recapitulate this effect, WT and Cox7a1-KO mice were housed at different temperature conditions to measure Cox7a1 and Cox7a2 mRNA expression in BAT (Figure 8B). Importantly, Cox7a1 mRNA was not detected in Cox7a1-KO mice of any acclimation state. In line with a role for NST, Cox7a1 expression was lowest in WT mice housed under thermoneutral conditions (31°C), whereas cold-exposure (4°C) led to a duration-dependent upregulation. In contrast, Cox7a2 expression was not significantly influenced by housing temperature in both WT and Cox7a1-KO mice. Expression of Cox7a2 was comparable between WT and KO mice at any acclimation state, indicating that Cox7a2 did not compensate for the loss of Cox7a1 at mRNA level.

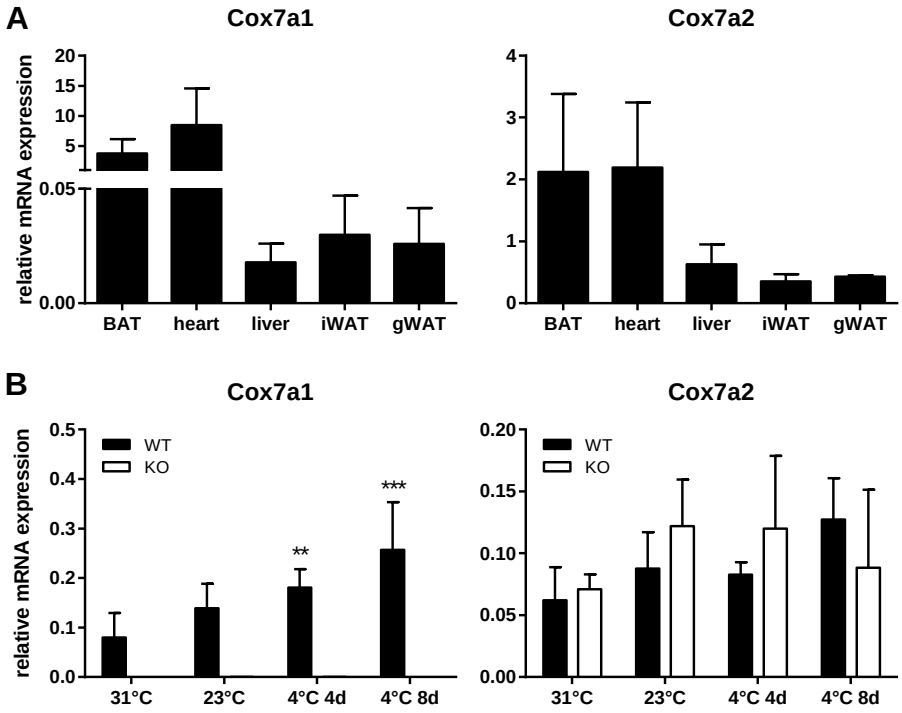

Figure 8: Cox7a1 and Cox7a2 mRNA expression. (A) Expression levels of target genes were compared between brown adipose tissue (BAT), heart, liver, subcutaneous inguinal white adipose tissue (iWAT) and visceral gonadal WAT (gWAT). Tissues were obtained from chow-fed WT mice housed at 23°C (n=3). Data were normalized to Gtf2b expression. (B) Expression levels of target genes in BAT from chow-fed WT and Cox7a1-KO mice housed at 31°C for 2 weeks, permanently at 23°C or at 4°C for 4 days and 8 days (n=4-6). Data were normalized to the mean of Gtf2b, Eef2, TBP and HSP90. Data were analyzed by Two Way ANOVA and Holm-Sidak post-test using mice housed at 31°C as control group. Asterisks indicate significant effect of housing temperature (** $p<0.01$; *** $p<0.001$).

Housing of mice in thermoneutral environment leads to paling of the typical dark brown color of murine BAT, whereas it is intensified in cold-exposed mice [2]. Thus, the color of BAT is associated with NST capacity and serves as an approximate, visual indicator for BAT function. In Cox7a1-KO mice, appearance of interscapular BAT (iBAT) was comparable to that of WT mice (Figure 9A). Short-term cold-exposure appeared to slightly intensify the brown color as compared to BAT of mice housed room temperature (23°C). Moreover, BAT appeared to be larger in cold-exposed mice, which was reflected in dissected tissue mass (Figure 9B). Dissected mass of BAT was increased both by cold-exposure and housing at thermoneutral environment compared to room temperature. No differences were observed between WT and KO mice.

Protein levels of Ucp1 were quantified as measure for BAT recruitment (Figure 9C and D). Housing of mice at 23°C resulted in an elevation of Ucp1 levels compared to 31°C, indicating conventional housing temperatures to represent a state of mild cold-exposure for mice. At 4°C, Ucp1 levels were even more increased and the magnitude of effect was dependent on housing time. There were, however, no differences in Ucp1 levels between WT and Cox7a1-KO mice.

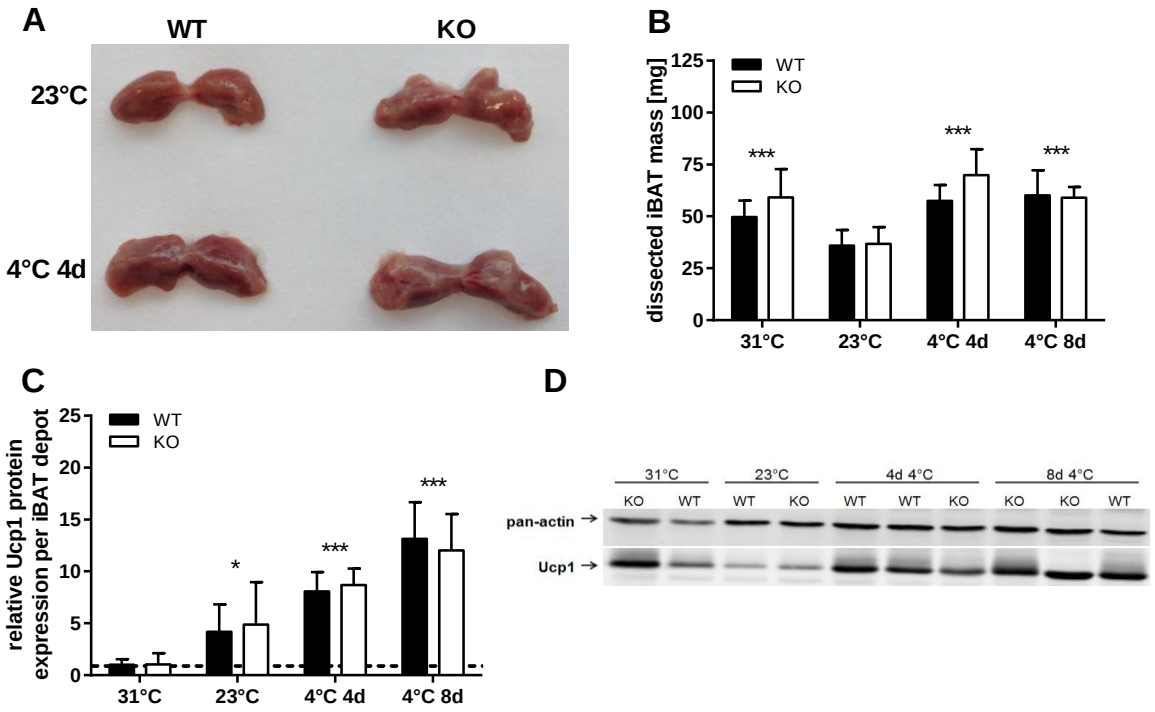

Figure 9: Indices of BAT recruitment in WT and Cox7a1-KO mice. Chow-fed animals were housed at 31°C for 2 weeks, permanently at 23°C or at 4°C for 4 days or 8 days, respectively (n=4-6). (A) Morphological appearance of BAT dissected from the interscapular region (iBAT) of WT and Cox7a1-KO mice housed at 23°C or at 4°C for 4 days. (B) Dissected wet tissue mass of iBAT. Data were analyzed by Two Way ANOVA and Holm-Sidak post-test using mice housed at 23°C as control group. Significant differences between WT and KO mice were not detected. Asterisks indicate an effect of housing temperature (*** $p<0.001$). (C) Relative Ucp1 protein levels in iBAT. Data are expressed as fold-change of expression measured in WT mice housed at 31°C. Data were analyzed by Two Way ANOVA and Holm-Sidak post-test using mice housed at 31°C as control group. Significant differences between WT and KO mice were not detected. Asterisks indicate significant effect of reduced housing temperature (* $p<0.05$; *** $p<0.001$). (D) Representative Western Blot conducted with 30 µg of total iBAT protein.

Expression of Cox7a1 is upregulated in cold-activated BAT [146] and ablation of this protein affects CCO activity in other tissues characterized by high Cox7a1 expression [160, 161]. Thus, CCO activity was investigated in tissue homogenates of BAT. Measurements were conducted during a titration of cytochrome *c* (1-30 µM) in the presence of adenosine di- (ADP) or triphosphate (ATP), which serve as allosteric CCO activator and inhibitor, respectively [195, 196] (Figure 10). In both measurements, CCO activity was similarly dependent on housing temperature. The activity of CCO was lowest in mice housed at 31°C and tended to be higher in mice kept at 23°C. The effect of cold-exposure was dependent on housing time, resulting in a clear upregulation of CCO activity after 8 days at 4°C. Neither absolute CCO activity nor the magnitude of adaptive response was, however, in any acclimation state affected by the presence or absence of Cox7a1.

In summary, Cox7a1 mRNA expression was regulated by housing temperature of mice and reflected high expression levels of heart, supporting a putative role of this isoform for CCO activity and thermogenesis in BAT. Ablation of Cox7a1 did, however, neither influence CCO activity nor Ucp1 expression in this tissue, indicating an intact thermogenic BAT function in KO mice on the molecular and cellular level.

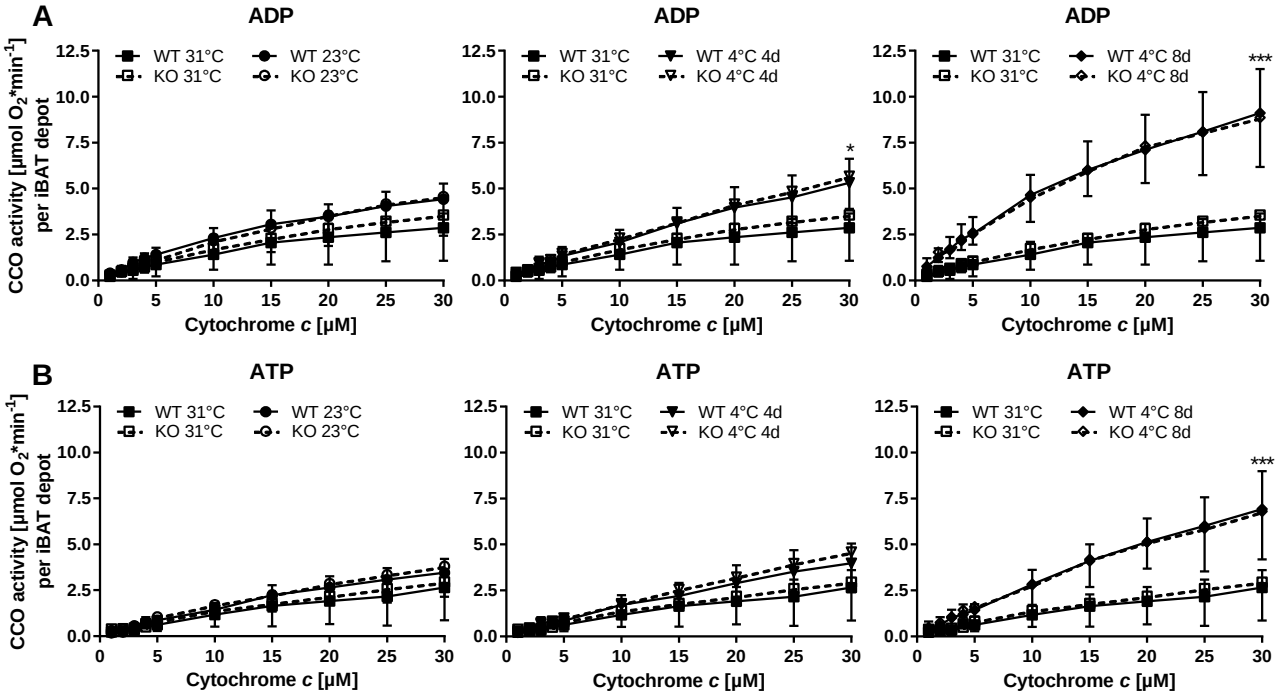

Figure 10: Cytochrome *c* oxidase (CCO) activity in iBAT derived from WT and Cox7a1-KO mice. Chow-fed mice were housed at 31°C for 2 weeks, permanently at 23°C or at 4°C for 4 days or 8 days, respectively (n=4-6). Oxygen consumption was measured in tissue homogenates during a titration of cytochrome *c* (1-30 µM) in the presence of (A) ADP or (B) ATP. The activity of CCO at 31°C was repeatedly depicted to evaluate the effect of mild (23°C) and severe (4°C) cold-exposure. Statistical analysis was conducted for oxygen consumption of CCO in the presence of 30 µM cytochrome *c* using Two Way ANOVA and Holm-Sidak post-test. Asterisks (* $p<0.05$; *** $p<0.001$) indicate significant effect of temperature. Differences between WT and Cox7a1-KO mice were not detected.

3.1.2 Adaptive heat production in WT and Cox7a1-KO mice

Cox7a1 is a cold-responsive protein of BAT and may therefore play a role for NST. Molecular measures of thermogenic BAT function in tissue homogenates were similarly regulated in WT and Cox7a1-KO mice, suggesting normal NST capacity. However, heat production (HP) in brown adipocytes of a living animal is the result of the coordinated interaction of multiple cellular pathways and ablation of Cox7a1 may affect this system by other mechanisms. WT and Cox7a1-KO mice were subjected to norepinephrine (NE) tests to directly investigate BAT-derived HP (Figure 11). In the course of this test, mice were injected with NE to activate Ucp1 positive cells throughout the body thus mimicking the acute effect of physiological BAT activation by reduced ambient temperature. Since BAT represents the major site for Ucp1 positive cells, NE-induced oxygen consumption is basically interpreted as result of basal metabolic rate (BMR) and BAT-derived NST. Maximal oxygen consumption induced by a very high dose of NE thereby reflects the maximal NST capacity of a mouse.

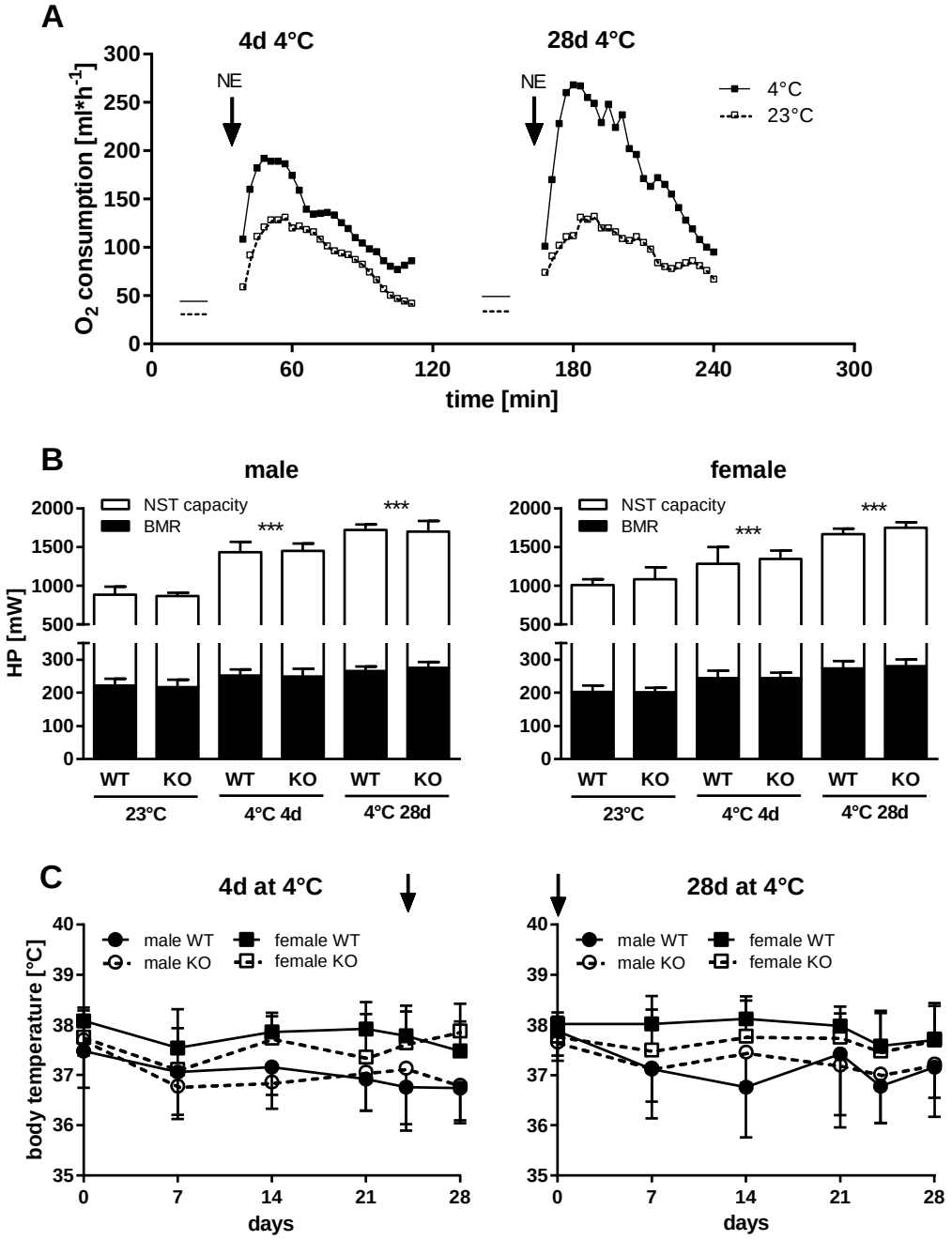

Figure 11: NST capacity of WT and Cox7a1-KO mice. Male and female mice of both genotypes were subjected to two consecutive norepinephrine (NE) tests to measure BAT-derived heat production (HP) of animals in room temperature-acclimated state (at the age of 12-13 weeks) and 4 weeks later after 4 days or 28 days of cold-exposure, respectively (n=5). All mice were single-caged and received chow-diet throughout the entire experiment. (A) Representative oxygen consumption traces exemplarily depicted for two different WT mice subjected either to acute or to chronic cold-exposure. Basal metabolic rate (BMR) was measured before NE-administration (indicated by arrows) and is indicated as horizontal line. (B) Maximal NE-induced oxygen consumption (NE_{max}) and BMR were converted into HP. The capacity for NST was calculated as the difference in HP between NE_{max} and BMR. Data were analyzed by Two Way ANOVA and Holm-Sidak post-test using data obtained in room temperature-acclimated state as control group. Asterisks indicate significant effect of cold-exposure. The degree of significance (*** $p<0.001$) was identical for all three parameters tested (BMR, NE_{max} and NST capacity). Differences between the genotypes were not detected. (C) Rectal body temperature in male and female WT and Cox7a1-KO mice. Arrows indicate the onset of cold-exposure in the respective groups. Data were analyzed separately for males and females using Two Way RM ANOVA and Holm-Sidak post-test. Significant differences between WT and KO mice were not detected at any time point.

Two consecutive NE-tests were performed with male and female mice. The first test was in all animals performed in room temperature-acclimated state, whereas the second test was performed 4 weeks later after acute (4 days) or chronic (28 days) housing at 4°C. As expected, oxygen consumption in all acclimation states was rapidly increased after NE-administration (Figure 11A), reaching maximal levels after 15-20 min referred to as maximal NE-stimulatable oxygen consumption (NE_{max}). Both BMR and NE_{max} were similarly regulated by temperature, being lowest in room temperature-acclimated state with pronounced elevation under cold exposure. Oxygen consumption was converted into heat production and NST capacity was calculated as difference in HP between NE_{max} and BMR (Figure 11B). The capacity for NST gradually increased by cold-exposure, indicating that short-term housing at 4°C is already effective but not sufficient to maximize NST capacity. In line with such regulation, rectal body temperature was well defended during cold-exposure and fairly constant throughout the experiment (Figure 11C). Females tended to have a slightly higher body temperature compared to males (38°C vs. 37°C), although HP in any acclimation state was comparable between both sexes. All parameters tested were, however, comparable between WT and Cox7a1-KO mice, indicating that Cox7a1 is not required for BAT-derived HP in adult mice.

BAT-derived HP was measured in a mouse model characterized by constitutive KO of Cox7a1. Putative differences in NST capacity of adult animals may be masked by compensatory mechanisms in other tissues. Maturation of BAT in altricial species such as mice occurs shortly after birth [49, 197, 198]. Since Cox7a1 expression is first detectable on developmental day 17 in mixed tissues of murine embryos [159], this maturation process may be influenced by KO of Cox7a1 thus affecting heat production of neonates.

Murine neonates are characterized by the lack of protective fur. This property not only increases dermal heat loss and therefore the need for adaptive HP, but also allows thermal imaging. To see whether such an approach is indeed suitable for the detection of impaired NST, neonates of the Ucp1-KO mouse line were employed since adult Ucp1-KO mice are well-known for their impaired BAT function [47]. Mice were obtained from heterozygous (HET) breeding pairs and entire litters were subjected to thermal imaging within the first three days of life. For identification and handling purposes, mice were placed face-down on multiwell plates (Figure 12A). The location of iBAT coincided in most neonates with the detection of the warmest spot within the dorsal area (Figure 12B), referred to as interscapular skin surface temperature (iSST). Among Ucp1-KO mice, iSST was comparable between WT and HET mice, whereas it was reduced by more than 1°C in KO mice (Figure 12C). These results clearly indicate that iSST is a suitable measure to detect defective NST by infrared thermal imaging with murine neonates of a constitutive knockout model. Accordingly, this method was applied to neonates of the Cox7a1-KO mouse line (Figure 12D and E). WT, HET and KO mice exhibited, however, comparable iSST, indicating that NST capacity in pups is not affected by the presence or absence of Cox7a1.

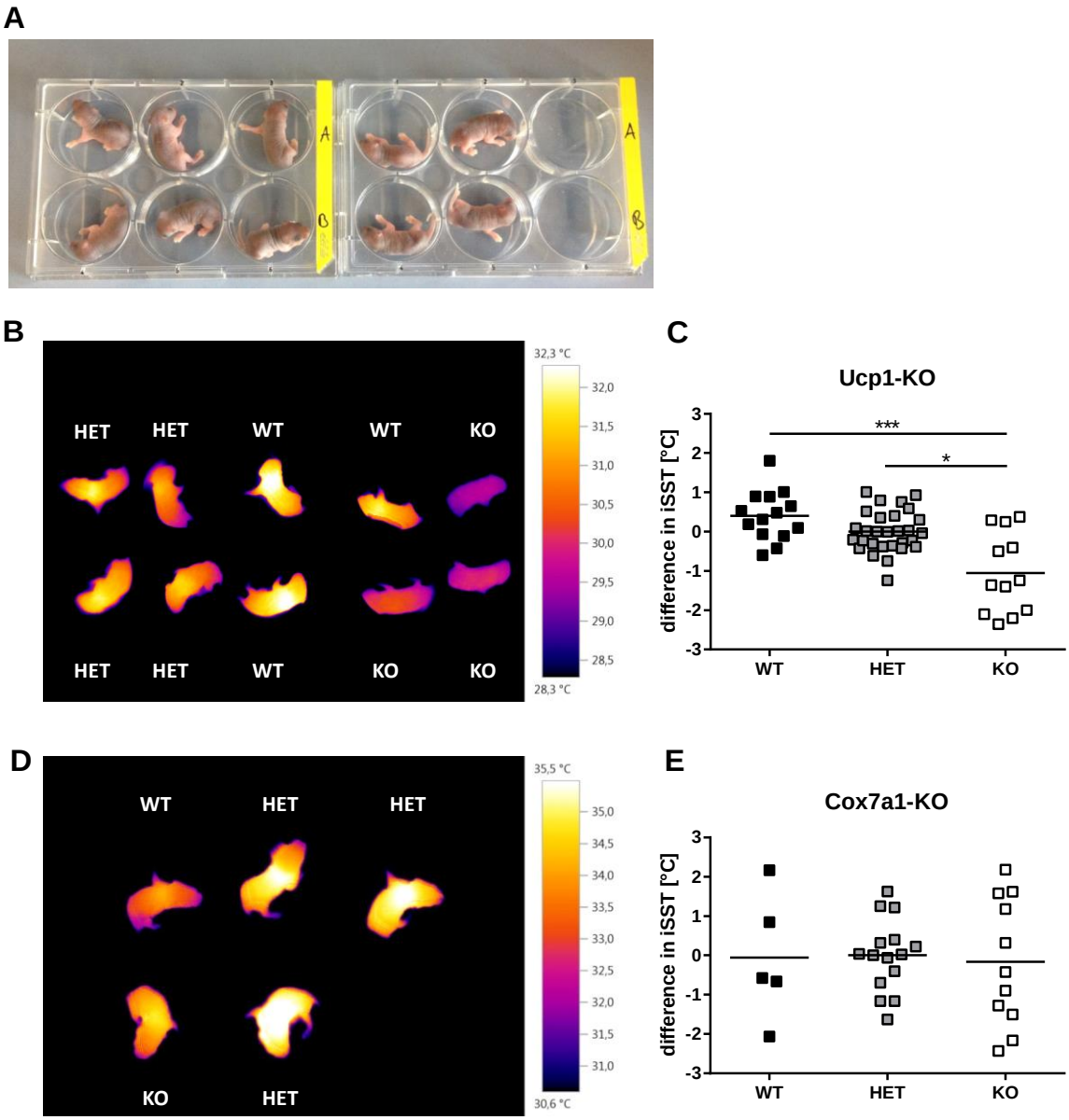

Figure 12: Infrared thermal imaging with neonates of the Ucp1-KO (A-C) and Cox7a1-KO (D+E) mouse lines. Pups of both mouse lines were obtained from heterozygous (HET) breeding pairs and whole litters were subjected to imaging within the first three postnatal days. (A) Pups were placed in multiwell plates for identification purposes. A series of thermal profile pictures was generated. Representative images are depicted for (B) Ucp1-KO mice (N=7, n=12-29) and (D) Cox7a1-KO mice (N=5, n=5-15). Interscapular skin surface temperature (iSST) was determined as described (section 2.3.6) and used as measure for BAT activity. Data for (C) Ucp1-KO mice and (E) Cox7a1-KO mice are expressed as difference in iSST between HET mice and WT or KO mice, respectively. Datasets were analyzed by One Way ANOVA on Ranks and Dunn's multiple comparison test (* $p<0.05$; *** $p<0.001$). Differences between mice of the Cox7a1-KO mouse line were not detected.

In summary, cold-exposure of mice increased Cox7a1 expression in BAT and affected molecular indices of BAT recruitment. In line with elevated Ucp1 levels and CCO activity, NST capacity was markedly increased in cold-exposed adult mice. All parameters tested were, however, not affected by ablation of Cox7a1. Moreover, BAT activity was reduced in Ucp1-KO but not Cox7a1-KO pups. These results indicate that Cox7a1 is not required for BAT-derived NST in mice.

3.1.3 Abundance of brite adipocytes in white adipose tissue

The occurrence of Ucp1-expressing cells is not restricted to BAT. Thermogenic competent brite adipocytes are found in white adipose tissue (WAT) of mice in response to cold-exposure [9] or adrenergic stimulation [19]. The abundance of those cells can be approximated by determination of brown adipocyte marker gene expression. One of many candidates is Cox7a1, which is consistently upregulated in WAT of cold-exposed mice [162]. Ablation of Cox7a1 may thus affect the induction of brite adipocytes in WAT of mice during cold-exposure.

The subcutaneous inguinal depot (iWAT) is prone to browning and was therefore investigated in mice kept at 23°C or 4°C. At 23°C, cells appeared largely unilocular whereas the portion of multilocular cells increased with housing time at 4°C, indicating a gradual increase in the abundance of brite adipocytes (Figure 13).

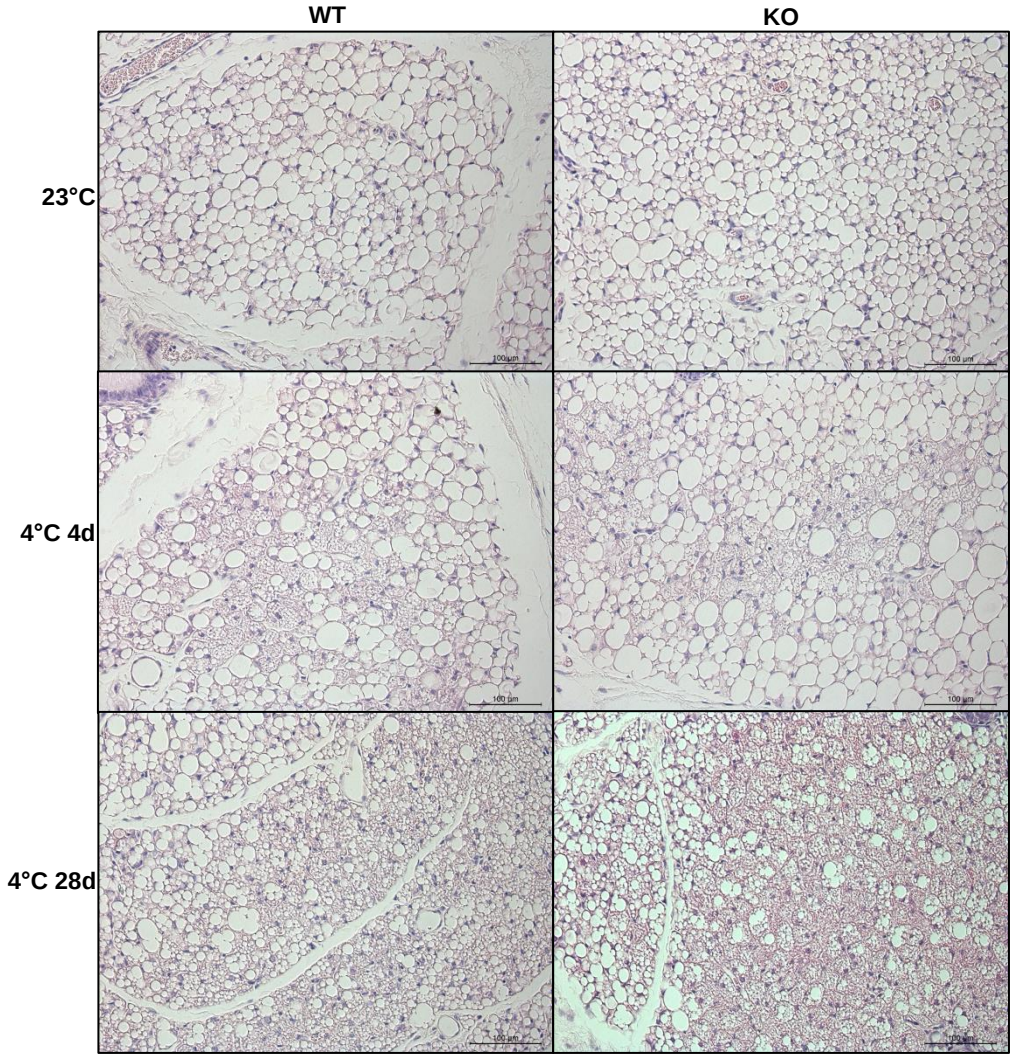

Figure 13: Hematoxylin/eosin-stained sections of inguinal white adipose tissue (iWAT). Tissue was obtained from chow-fed WT and Cox7a1-KO mice aged 16 weeks, housed at room temperature (23°C) or at 4°C for 4 days or 28 days, respectively (n=5).

In line with iWAT morphology, Ucp1 protein was hardly detectable in iWAT of mice housed at 23°C (Figure 14). After 4 weeks at 4°C, Ucp1 levels in iWAT were comparable to those found in BAT at 23°C, indicating a strong browning effect. Female mice tended to be less responsive than male mice. Neither the abundance of multilocular cells nor Ucp1 protein levels were, however,

differentially affected between WT and Cox7a1-KO mice, indicating that browning of WAT is not dependent on the presence or absence of Cox7a1.

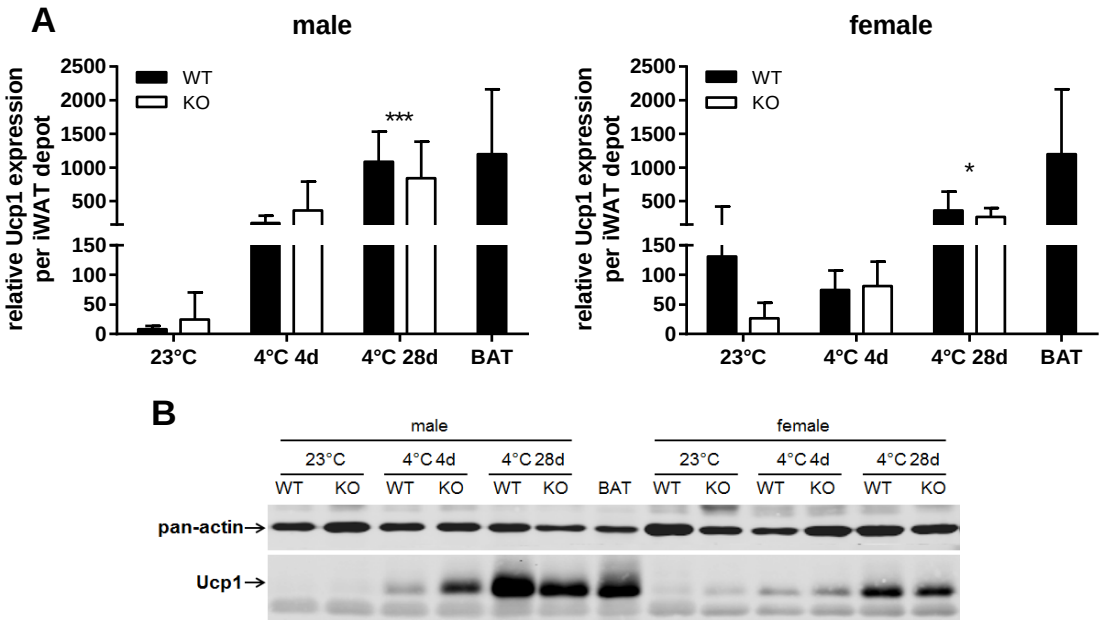

Figure 14: Ucp1 protein levels in iWAT of WT and Cox7a1-KO mice. Chow-fed animals were housed at room temperature (23°C) or subjected to cold-exposure (4°C) for 4 days or 28 days, respectively (n=5). Tissue was obtained at the age of 16 weeks. (A) Relative Ucp1 protein expression per iWAT depot in male and female mice. Data were analyzed by Two Way ANOVA and Holm-Sidak post-test using mice housed at 23°C as control group. Differences between WT and KO mice were not identified. Asterisks indicate significant effect of cold-exposure (* $p<0.05$; *** $p<0.001$). BAT obtained from male mice housed at 23°C (n=4) was employed as positive control. (B) Representative Western Blot conducted with 30 µg of total protein.

3.1.4 Response to hypercaloric feeding

Besides its function for the maintenance of core body temperature, BAT mediates diet-induced thermogenesis (DIT) [106]. This mechanism involves BAT as regulator of body mass development in the response to hypercaloric feeding, suggesting that defective BAT function may result in excessive body mass accumulation.

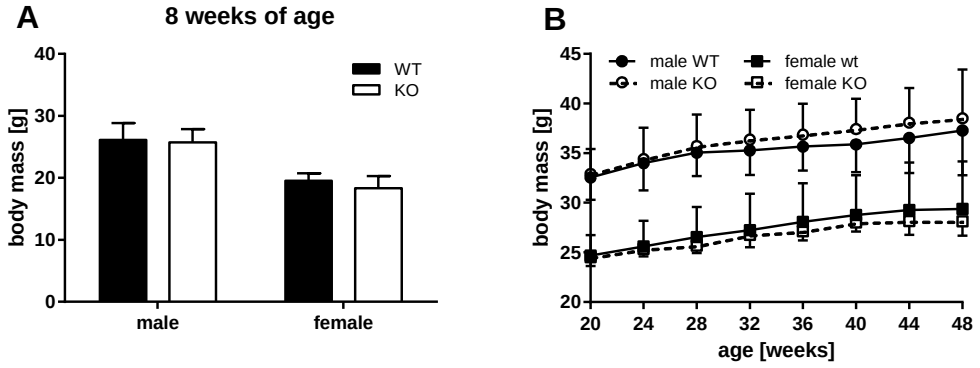

Figure 15: Body mass of chow diet-fed WT and Cox7a1-KO mice. Animals were housed at 23°C and subject to regular husbandry throughout life. (A) Body mass at the age of 8 weeks (n=8-14). (B) Body mass determined in another cohort of mice between 20 and 48 weeks of age (n=7-10). Data were analyzed by Two Way ANOVA (A) or Two Way RM ANOVA (B) and Holm-Sidak post-test. Significant differences between male or female WT and KO mice were not detected at any age.

In fact, neither young (Figure 15A) nor aged (Figure 15B) Cox7a1-KO mice differed in body mass development from WT mice when fed with chow-diet at 23°C throughout life without experimental intervention. Male mice were subjected to a feeding experiment to further investigate the effect of Cox7a1-ablation on BAT function in the context of DIT (Figure 16). The experiment was conducted at 31°C to minimize the activity of BAT for the purpose of thermoregulation, which may affect the development of diet-induced obesity (DIO) in mouse models with defective BAT function [107, 108].

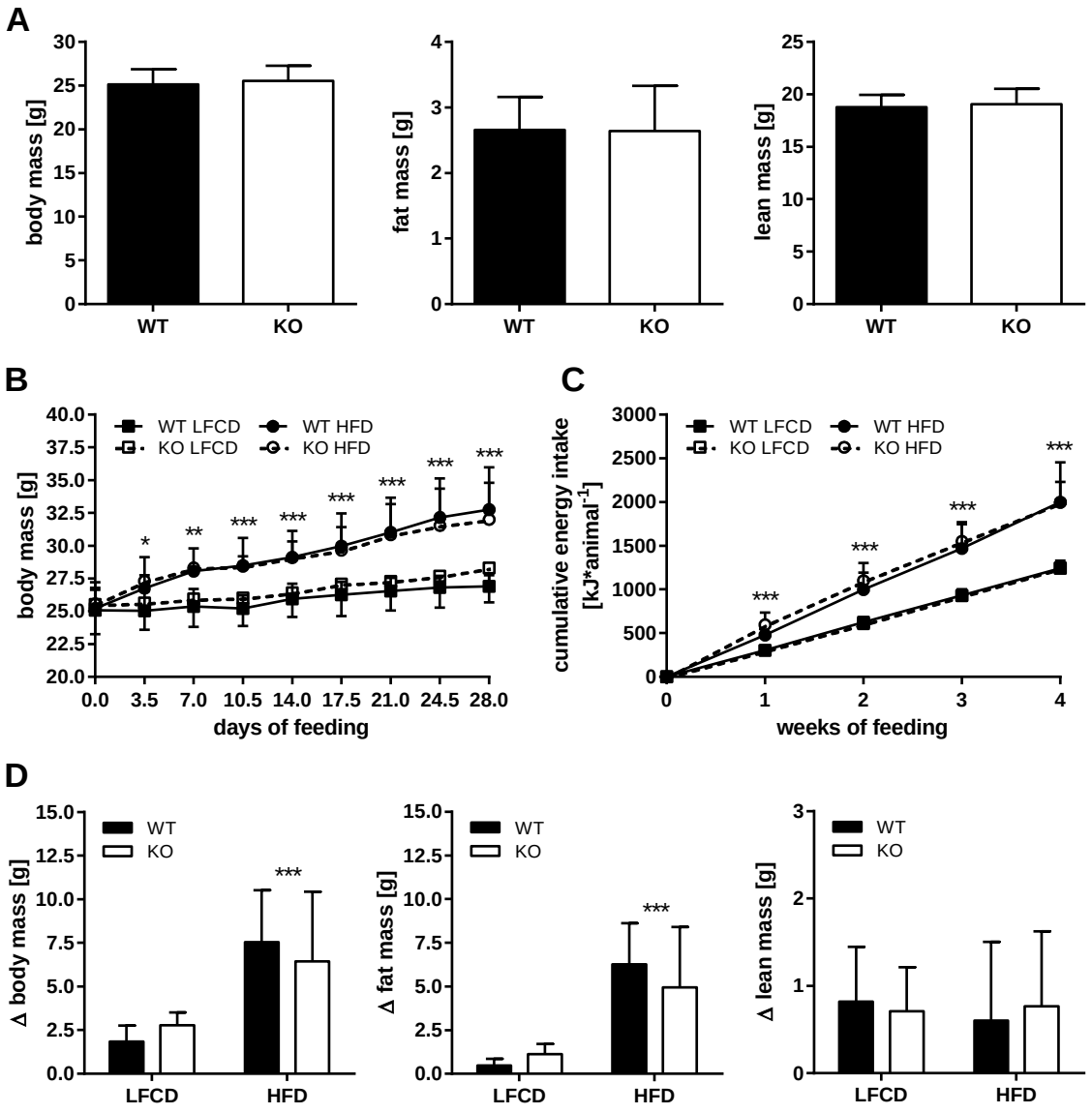

Figure 16: Feeding experiment with WT and Cox7a1-KO mice. Male mice were housed at 31°C and exposed to a low-fat control diet (LFCD) or a high-fat diet (HFD) for 4 weeks at the age of 10 weeks (n=6). Diets were not supplemented with BHT. (A) Body, fat and lean mass of WT and Cox7a1-KO mice at the beginning of HFD-feeding (day 0). Data were analyzed by t-test (body and fat mass) or Mann-Whitney Rank Sum Test (lean mass). Differences between WT and KO mice were not detected. (B) Body mass development and (C) cumulative energy intake during HFD-feeding. Both datasets were analyzed by Three Way ANOVA and Holm-Sidak post-test. Asterisks indicate significant difference between LFCD and HFD-fed mice (* $p<0.05$; ** $p<0.01$; *** $p<0.001$). Differences between genotypes were not identified. (D) Changes in body, fat and lean mass between beginning (day 0) and end (day 28) of HFD-feeding. Each dataset was analyzed by Two Way ANOVA and Holm-Sidak post-test. Asterisks indicate significant effect of HFD-feeding (*** $p<0.001$). Differences between WT and KO mice were not detected.

All WT and Cox7a1-KO mice were initially fed with a low-fat control diet (LFCD) at 31°C for 2 weeks before half of the mice was administered a high-fat diet (HFD). At the beginning of HFD-feeding, Cox7a1-KO mice did not differ from WT mice regarding body mass and body composition (Figure 16A). The HFD was fed for 4 weeks in total and has been shown to induce DIO and impaired glucose tolerance in mice of the C57BL/6J strain within this time frame when these are fed at 23°C [199]. In line with this, body mass development of HFD-fed mice differed from that of LFCD-fed mice throughout the experiment (Figure 16B). As expected, HFD-fed mice exhibited constantly increased energy intake (Figure 16C). This resulted in an elevated total body mass gain that was largely attributable to increased fat mass gain (Figure 16D). There were, however, no differences between WT and Cox7a1-KO mice.

Similarly, glucose tolerance of LFCD and HFD-fed mice at the end of the feeding period was not affected by the presence or absence of Cox7a1 (Figure 17A). Surprisingly, glucose tolerance was comparable between LFCD and HFD-fed mice of both genotypes (Figure 17B), although it is usually impaired in C57BL/6J mice fed a HFD at 23°C [199]. This phenotype may be related to the recruitment state of BAT, which was minimized due to long-term housing at 31°C. Minimal NST capacity may thus either impair glucose tolerance in LFCD-fed mice or abrogate the adverse effect of HFD on glucose tolerance but not on DIO development.

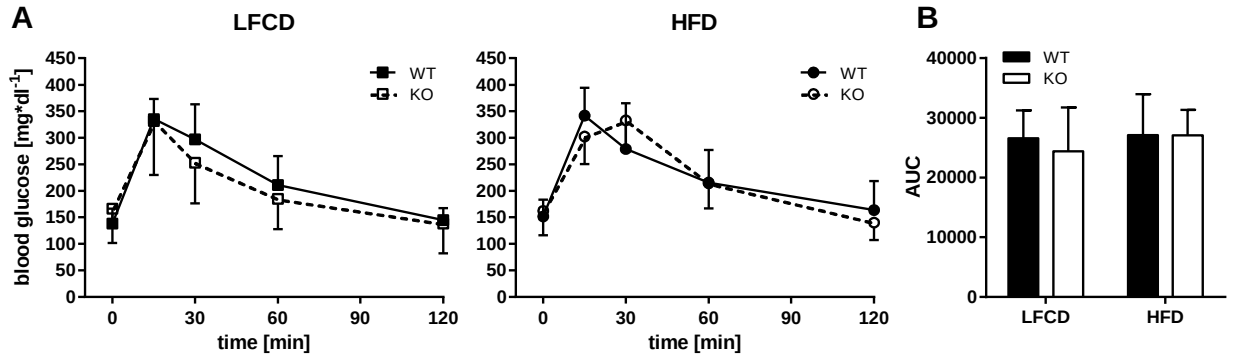

Figure 17: Glucose tolerance of WT and Cox7a1-KO mice. Animals were housed at 31°C and fed with LFCD or HFD. Diets were not supplemented with BHT. Glucose tolerance was assessed after 4 weeks of HFD-feeding at the age of 14 weeks (n=6). (A) Blood glucose levels over time before (0 min) and after glucose gavage. (B) Total area under the curve (AUC) of blood glucose levels. Datasets were analyzed by Two Way RM ANOVA (A) or Two Way ANOVA (B) and Holm-Sidak post-test. Significant differences between genotypes were neither detected at any time point nor in response to a diet.

Taken together, Cox7a1 is a cold-responsive protein of BAT and a widely used marker gene for brown and brite adipocytes. This protein is required for maximal CCO activity in heart and skeletal muscle characterized by high Cox7a1 abundance. In BAT, however, knockout of Cox7a1 neither affected CCO activity nor adaptive heat production. Moreover, Cox7a1 was not required for browning of WAT or the response to hypercaloric feeding. These data collectively indicate that Cox7a1 is dispensable for BAT function.

3.2 The capacity for NST of inbred mouse strains

The thermogenic function of BAT is hypothesized to influence systemic glucose homeostasis since adaptive heat production is supported by the oxidation of glucose taken up from the bloodstream. An increased capacity for NST may cause increased glucose uptake into the tissue thus affecting blood glucose clearance. Such effect may be complemented by the abundance of brite adipocytes, which represent an additional pool of thermogenic cells in WAT. The assessment of NST capacity is a prerequisite to investigate the relationship between brown and brite adipocyte function and glucose tolerance, involving monogenic models or the comparison of different inbred mouse strains as polygenic alternative. In this regard, two different mouse strains, 129S6/SvEvTac (129S6) and C57BL/6J (BL6J), were characterized with respect to their NST capacity.

3.2.1 Effect of ambient temperature on brown and brite adipocyte recruitment

Mice of the 129S6 and BL6J strains were kept at 30°C (thermoneutral condition) and 20°C (mild cold-exposure) and fed with LFCD. After 4 weeks of acclimation, mice were killed and adipose tissues were dissected. The mass of iWAT was higher in 129S6 mice compared to BL6J mice under both housing conditions (Figure 18). There was no difference in iBAT mass between the strains when mice were housed at 30°C. Mild cold-exposure decreased iBAT mass in both strains, but had a stronger effect in BL6J mice. Thus, iBAT mass is regulated dependent on the need for NST, whereas iWAT mass is primarily determined by genetic background.

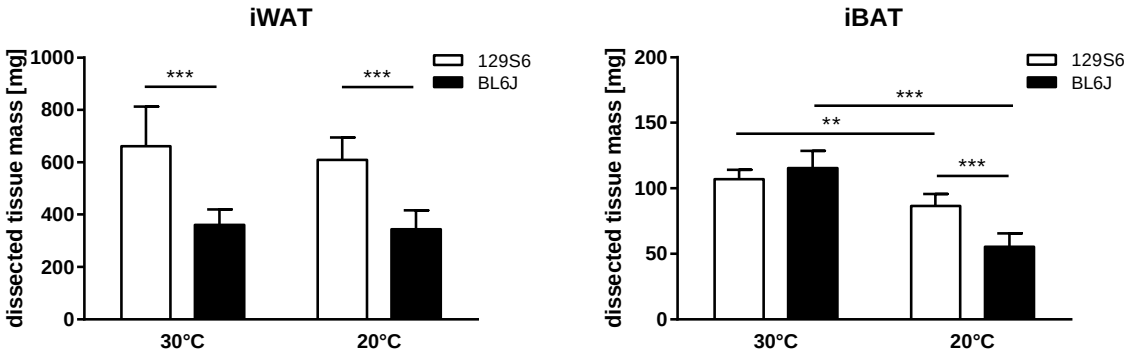

Figure 18: Dissected wet tissue mass of iWAT and iBAT from 129S6 and BL6J mice. At the age of 8 weeks, animals were housed at 30°C and 20°C and fed with LFCD for 4 weeks (n=6). Datasets were analyzed using Two Way ANOVA and Holm-Sidak post-test (** p<0.01; *** p<0.001).

Among the various murine WAT depots, iWAT is a subcutaneous depot generally considered to have a high propensity for browning. At 30°C, iWAT of 129S6 mice was a heterogeneous mixture of large unilocular and smaller paucilocular adipocytes, indicating brite cells to be present even under conditions when the need for Ucp1-mediated NST is minimized (Figure 19). In contrast, iWAT of BL6J mice was at 30°C composed of a rather homogenous population of unilocular white adipocytes which appear, however, to be smaller in size compared to white adipocytes in iWAT of 129S6 mice.

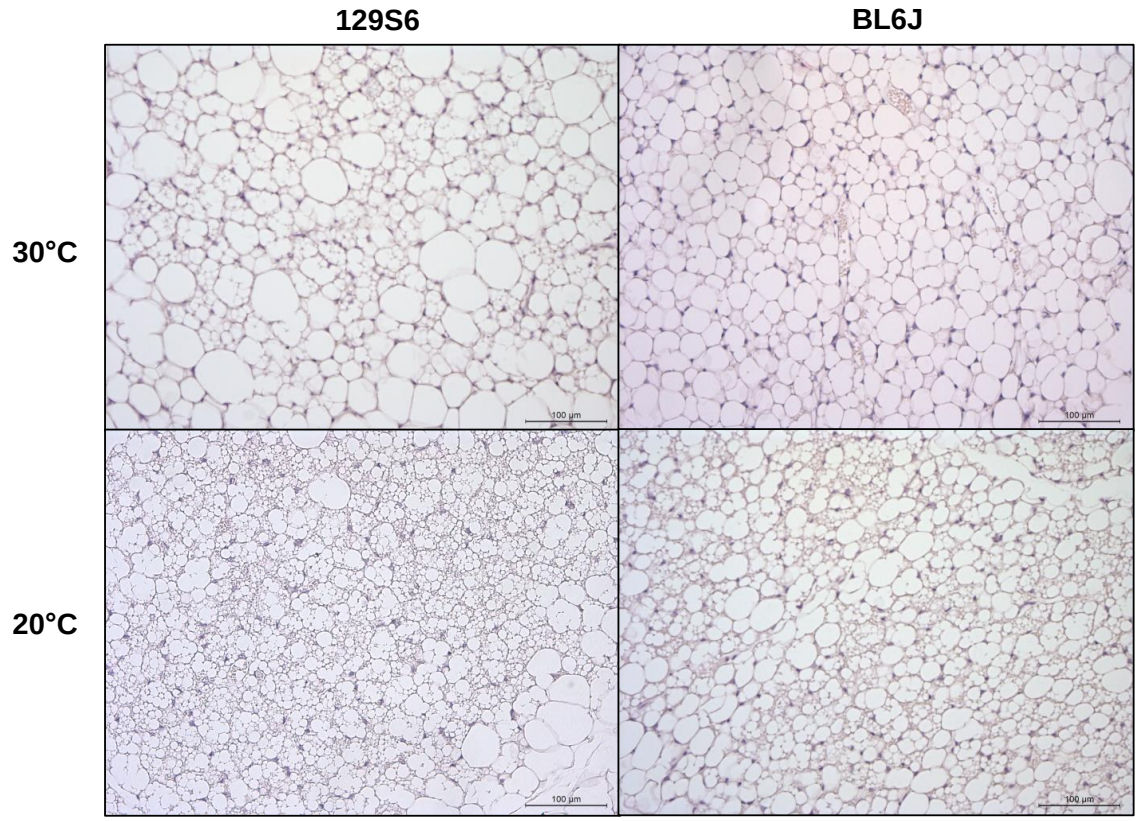

Figure 19: Hematoxylin/eosin-stained sections of iWAT from 129S6 and BL6J mice. At the age of 8 weeks, animals were housed at 30°C and 20°C and fed with LFCD for 4 weeks (n=6).

Housing of 129S6 mice at 20°C shifted the appearance of paucilocular adipocytes towards multilocular brown-like morphology. Although more pronounced in 129S6 mice, the abundance of these cells is increased in both strains at 20°C compared to 30°C, indicating the recruitment of brite adipocytes under mild cold-exposure (Figure 19). The brown adipocyte marker genes Ucp1, cell death-inducing DNA fragmentation factor, alpha subunit-like effector A (Cidea) and Cox7a1 were determined as an additional measure for browning (Figure 20).

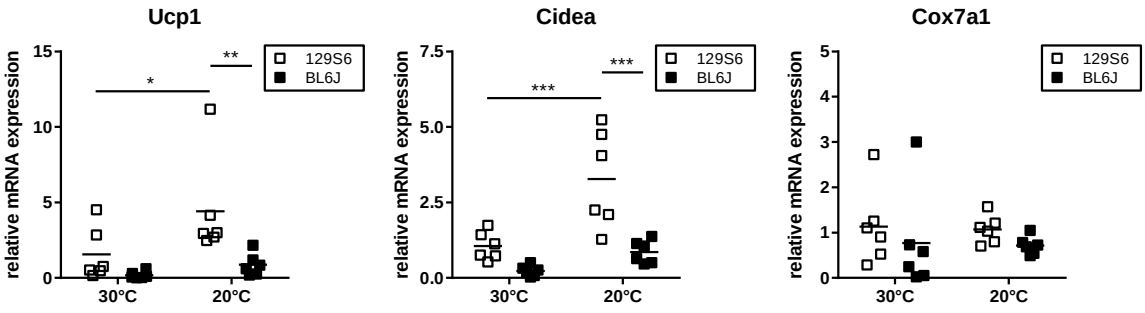

Figure 20: Relative expression of brown adipocyte marker genes Ucp1, Cidea and Cox7a1 in iWAT of 129S6 and BL6J mice. At the age of 8 weeks, animals were housed at 30°C and 20°C and fed with LFCD for 4 weeks (n=6). Expression levels of target genes were normalized to Gtf2b expression. All datasets were analyzed by Two Way ANOVA and Holm-Sidak post-test (* p<0.05; ** p<0.01; *** p<0.001).

At 30°C, there were no significant differences in Ucp1 expression between BL6J and 129S6 mice. Expression of Ucp1 was clearly increased in 129S6 mice at 20°C compared to 30°C,

whereas BL6J mice only tended to show a cold-induced response. This regulation indicates 129S6 mice to have a higher propensity for the adaptive recruitment of brite cells. Regulation of the Ucp1 gene was well reflected in Cidea but not Cox7a1 levels. As strain-specific differences in iWAT mass (Figure 18) may potentiate differences in gene expression and iWAT morphology, 129S6 mice likely exhibit a significantly higher abundance of brite adipocytes on the physiological level (per depot) both at 30°C and at 20°C.

Protein levels of Ucp1 and the activity of CCO were determined in iBAT as molecular markers for NST capacity (Figure 21). Both Ucp1 levels and CCO activity were similar between 129S6 and BL6J mice when these were housed at 30°C, indicating the capacity for BAT-derived heat production to be similar under this housing condition.

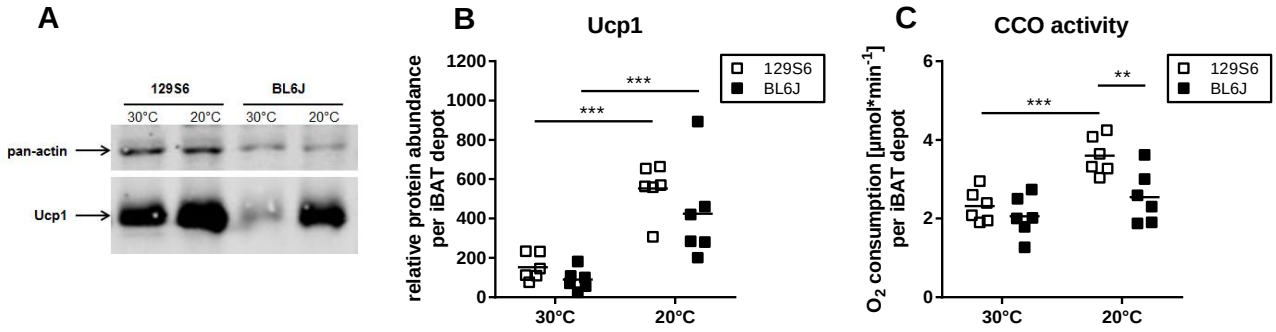

Figure 21: Characteristics of NST capacity in iBAT of 129S6 and BL6J mice. At the age of 8 weeks, animals were housed at 30°C and 20°C and fed with LFCD for 4 weeks (n=6). (A) Representative Western Blot with 25 µg total iBAT protein. (B) Ucp1 protein levels normalized to pan-actin levels per iBAT depot. (C) Cytochrome *c* oxidase (CCO) activity per iBAT depot. Oxygen consumption of tissue homogenates was measured in the presence of 5 mM ADP and 30 µM cytochrome *c*. Datasets (B+C) were analyzed by Two Way ANOVA and Holm-Sidak post-test (** p<0.01; *** p<0.001).

At 20°C, Ucp1 expression and CCO activity were increased in both strains though with a higher magnitude of effect in 129S6 mice (Figure 21), indicating a higher propensity for the adaptive recruitment of NST in this strain. Of note, physiological levels (per depot) of Ucp1 expression and CCO activity were not reflected on the cellular level (in a defined aliquot of total protein) but resulted from differences in depot size (Figure 18).

3.2.2 Heat production in 129S6 and BL6J mice

Mice of the 129S6 and BL6J strains were characterized by similar Ucp1 levels and oxidative capacity in BAT when these were housed at 30°C for 4 weeks, indicating similar NST capacity. However, the abundance of multilocular cells in iWAT was higher in 129S6 mice under this condition. Moreover, 129S6 mice exhibited increased iWAT mass compared to BL6J mice, which may in turn affect Ucp1-dependent heat production on the physiological level. To investigate this issue, mice of both strains acclimated to 30°C were subjected to NE-tests to determine NST capacity.

Oxygen consumption of mice was recorded before and after NE-administration to measure BMR and NE_{max}, respectively. Injection of NE resulted in a rapid rise of oxygen consumption over basal (BMR≈33 ml/h in both strains), peaking after 24-25 min with subsequent decline

over time in both strains (Figure 22A). The magnitude of oxidative response was more pronounced in 129S6 mice. This was reflected in a faster increase of oxygen consumption at the beginning of the measurement persisting as generally higher oxygen consumption over time, and consequently resulting in a higher NE_{max}.

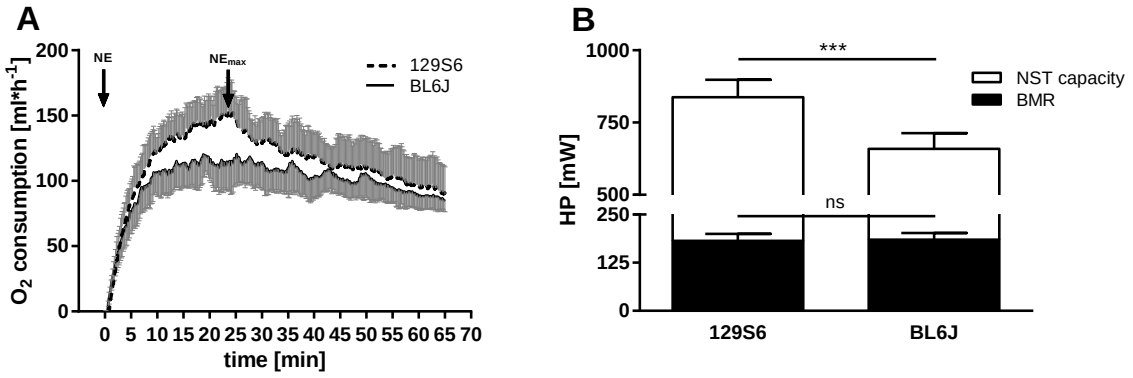

Figure 22: NST capacity of 129S6 and BL6J mice. At the age of 8 weeks, animals were housed at 30°C and 20°C and fed with LFCD (n=22-26). After 4 weeks, mice were subjected to a norepinephrine (NE) test. (A) Averaged (± standard deviation) oxygen consumption traces measured by indirect calorimetry. Arrows indicate time of NE-injection and the approximate time of maximal NE-stimulated oxygen consumption (NE_{max}) in both strains. (B) Basal (BMR) and NE-induced, Ucp1-dependent (NST capacity) heat production (HP). The latter was calculated as difference in HP between NE_{max} and BMR. Statistical analysis was conducted by Mann-Whitney Rank Sum Test (BMR) or t-test (NST capacity and NE_{max}). Asterisks indicate differences between 129S6 and BL6J mice in both NST capacity and NE_{max} with identical degree of significance (*** $p<0.001$).

Basal (BMR) and maximal (NE_{max}) oxygen consumption were converted into HP to calculate the difference between both measures, representing NST capacity (Figure 22B). Differences in NE_{max} were well reflected in NST capacity, which was significantly higher in 129S6 mice.

3.2.3 Effect of CL-316243 on brown and brite adipocyte recruitment

Housing at subthermoneutral environment represents a condition of adrenergic stimulation that consequently results in the recruitment of NST. Such environmental effect can be mimicked on the pharmacological level by administration of specific β_3-adrenergic agonists. Mice of the 129S6 and BL6J strains were housed at 30°C and fed with LFCD to minimize endogenous NST capacity. After 7 weeks, mice were subjected to CL-316243 (CL) treatment to recapitulate the effect of mild cold-exposure on Ucp1 expression in BAT and WAT. On seven consecutive days, CL was repeatedly administered in different doses, three of which below (0.008, 0.04 and 0.2 mg/kg/day) and one above (5 mg/kg/day) the dose of 1 mg/kg/day, which has been shown to robustly increase Ucp1 expression in BAT and WAT of mice [200]. Vehicle-treated mice served as negative control.

Prior to beginning of CL-treatment, body mass and body composition were determined as reference for phenotypic changes (Figure 23A). Mice of the 129S6 strain had slightly higher body mass than BL6J mice. This was accompanied by a more than 3-fold higher amount of fat mass in 129S6 mice, whereas the amount of lean mass was higher in BL6J mice. Notably, all

129S6 mice treated with the highest dose of CL (5 mg/kg/day) died or lapsed into a severe torpor-like state within 24 hours after the first injection. This treatment group was therefore excluded from the experiment. Such phenotype was not observed in BL6J animals, suggesting different sensitivity to β_3-adrenergic stimulation. Body composition of the remaining treatment groups was again assessed one day after the last CL-administration to calculate drug-induced changes (Figure 23C). In 129S6 mice, CL caused a reduction of body mass in a dose-dependent manner and had maximal efficacy in a dose of 0.04 mg/kg/day. The effect was not further stimulatable by a higher dose and was fully explainable by changes in fat mass. Changes in body composition were less pronounced in BL6J mice. Total energy intake during the treatment period tended to increase with CL-dose in BL6J mice whereas a dose-dependent reduction of energy intake was observed in 129S6 mice (Figure 23B). This difference in energy intake between vehicle and CL-treated 129S6 mice was, however, insufficient to explain the CL-induced loss of fat mass (Table 12), indicating differences in energy expenditure as causative factor.

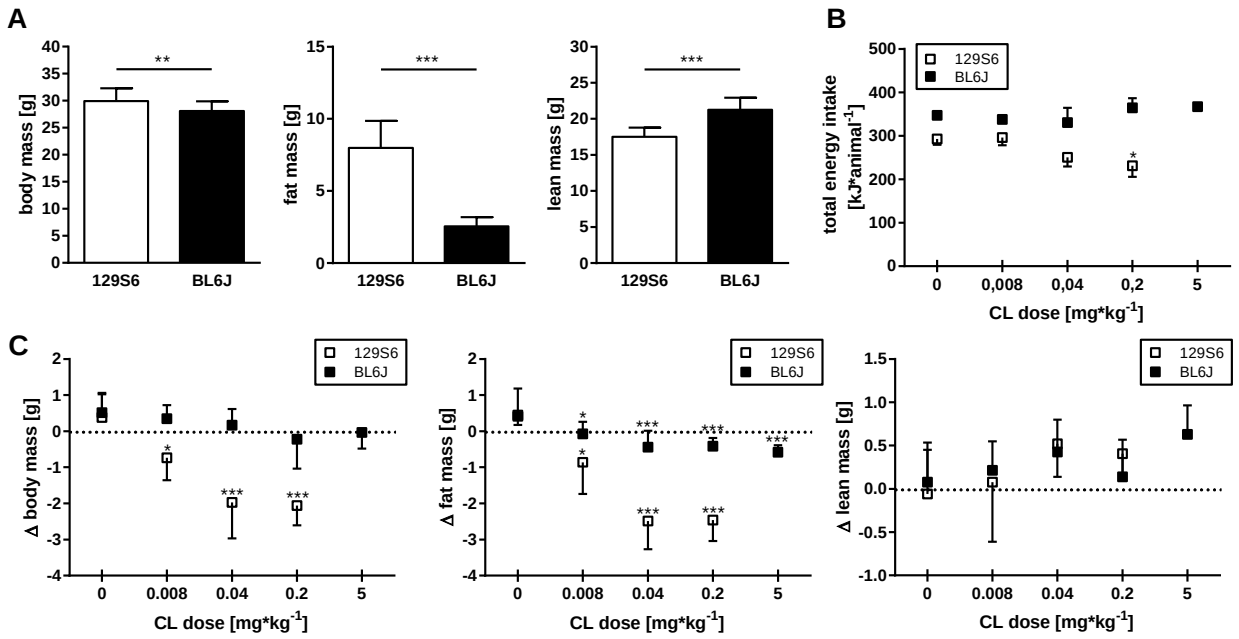

Figure 23: Effect of CL-treatment on body composition and food intake of 129S6 and BL6J mice. At 8 weeks of age, mice were housed at 30°C and fed with LFCD. After 7 weeks, CL was administered on seven consecutive days in different doses. (A) Body, fat and lean mass of mice after 7 weeks of LFCD-feeding prior to CL-treatment (n=22-30). Data were statistically evaluated via t-test (body mass) and Mann-Whitney Rank Sum Test (fat mass and lean mass; ** p<0.01; *** p<0.001). (B) Total cumulative energy intake after 7 days of CL-treatment (n=5-6). Application of Two Way ANOVA was impossible due to unequal group sizes. Thus, statistical analysis was conducted separately for each strain using One Way ANOVA on Ranks and Dunn's multiple comparison test with vehicle-treated mice as control group (0 mg/kg). Asterisks indicate significant differences between CL-treated and control mice (* p<0.05). (C) Difference in body, fat and lean mass between beginning and end of CL-treatment (n=5-6). Statistical analysis was conducted separately for each strain using One Way ANOVA and Holm-Sidak post-test with vehicle-treated mice as control group. Asterisks indicate significant differences between CL-treated and control mice (* p<0.05; *** p<0.001).

Table 12: Comparison of total energy intake and energetic costs of fat mass change during CL-treatment of 129S6 mice.

CL dose [mg/kg/day]	0	0.008	0.04	0.2
Δ fat mass [g][1]	0.45 ± 0.73	-0.86 ± 0.88	-2.49 ± 0.78	-2.46 ± 0.59
Energy content of Δ fat mass [kJ][2]	16 ± 26	-31 ± 32	-89 ± 28	-88 ± 21
difference vehicle vs.CL		**47**	**105**	**104**
Total energy intake [kJ][3]	293 ± 14	296 ± 17	250 ± 21	231 ± 26
difference vehicle vs. CL		**-3**	**43**	**62**

Data represent mean ± standard deviation (n=5-6). [1]Difference in fat mass between beginning and end of CL-administration (compare Figure 23C). [2]Sum of stored energy that is gained or lost due to fat mass change, assuming portions of fat and protein of 90.8% and 0.79%, respectively, per g of adipose tissue [201], and an energy content of 39.3 kJ/g fat and 23.5 kJ/g protein [202]. Energetic costs of fat mass formation and depletion were not considered. [3]Total energy intake during CL-treatment (compare Figure 23B).

Brite adipocytes are capable of mediating Ucp1-dependent thermogenesis and their abundance may thus contribute to energy expenditure. Administration of CL led to significant changes in Ucp1 expression in iWAT of both strains (Figure 24A). Maximal Ucp1 expression was achieved with 0.2 mg/kg/day, indicating higher doses to exceed what is required to maximally induce browning of WAT.

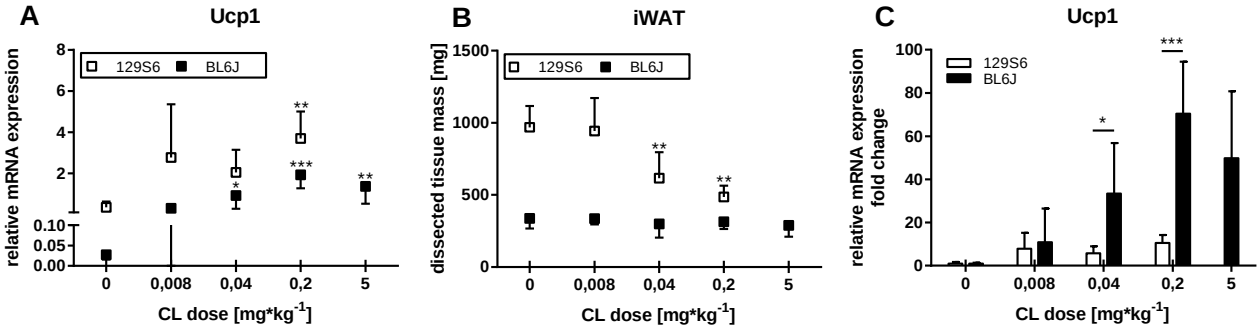

Figure 24: Effect of CL-treatment on iWAT of 129S6 and BL6J mice. At 8 weeks of age, mice were housed at 30°C and fed with LFCD for 7 weeks. Tissues were dissected after 1 additional week characterized by repeated administration of CL in different doses (n=5-6). (A) Relative Ucp1 mRNA levels in iWAT. Data were normalized to Eef2 expression. Application of Two Way ANOVA was impossible due to unequal group sizes. Data were analyzed separately for each strain using One Way ANOVA and Holm-Sidak post-test (BL6J) or One Way ANOVA on Ranks and Dunn's multiple comparison test (129S6) with vehicle-treated mice as control group. Asterisks indicate significant differences between CL-treated and vehicle-treated mice (* p<0.05; ** p<0.01; *** p<0.001). (B) Dissected iWAT wet tissue mass. Data were analyzed separately for each strain using One Way ANOVA and Holm-Sidak post-test with vehicle-treated mice as control group. Asterisks indicate significant difference between CL-treated and control mice (** p<0.01). (C) Relative Ucp1 mRNA levels in iWAT. Data are normalized to Eef2 levels and expressed as fold change of expression level observed in the control group (0 mg/kg) of the respective strain. Differences between the strains were analyzed by multiple t-tests using the Holm-Sidak correction method for multiple comparisons. Asterisks indicate significant differences between strains at the indicated CL doses (* p<0.05; *** p<0.001).

The expression of Ucp1 was higher in 129S6 mice under all conditions and may be potentiated by differential iWAT mass (Figure 24B). Administration of CL did not affect iWAT mass in BL6J mice, whereas it was dose-dependently reduced in 129S6 mice. This phenotype may be related to the abundance of brite cells using stored fat as local source for energy expenditure thus depleting fat mass as consequence. The magnitude of Ucp1-response to CL treatment was more pronounced in BL6J mice (Figure 24C), indicating a higher propensity for the recruitment of brite cells. Expression of Ucp1 in vehicle-treated mice was, however, higher in the

129S6 strain (Figure 24A), indicating the responsivity of BL6J mice to be improved due to a greater difference between basal levels and the physiological maximum.

Additionally, CL-treatment caused a significant reduction of iBAT mass in both strains in dose-dependent manner (Figure 25A). Vehicle-treated mice of the 129S6 strain had higher iBAT mass compared to BL6J mice, a difference that was equalized by a dose of 0.2 mg/kg/day. Protein levels of Ucp1 in iBAT tended to be upregulated by CL-treatment in both strains, although significant differences were not observed (Figure 25B). Treatment of BL6J mice with the highest dose returned Ucp1 levels towards baseline (vehicle). Mice of the 129S6 strain generally tended to express Ucp1 at a higher level than BL6J mice, indicating higher NST capacity in BAT.

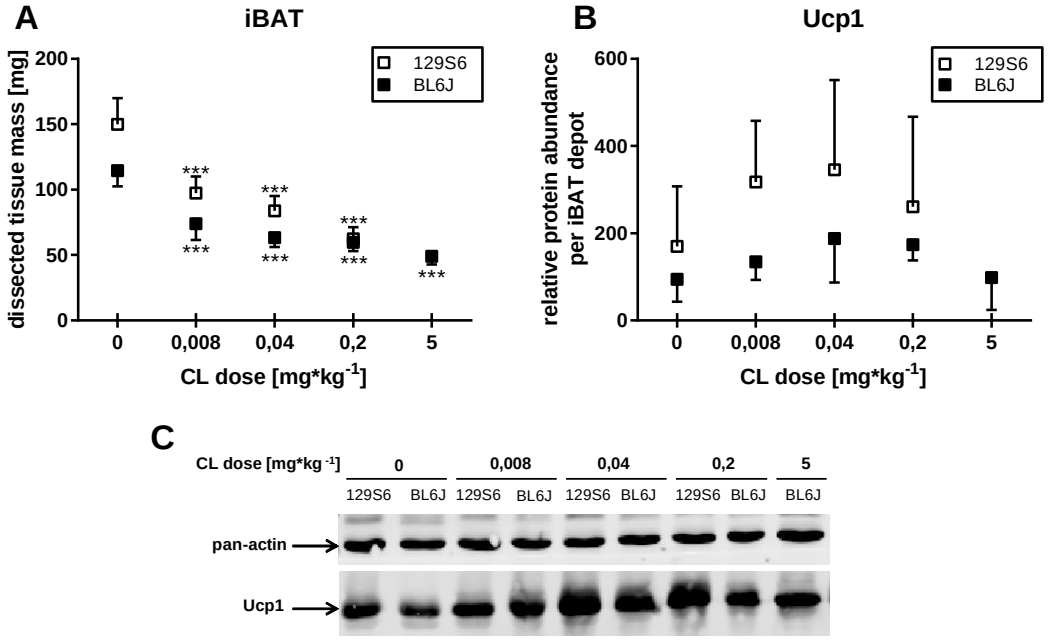

Figure 25: Effect of CL-treatment on iBAT of 129S6 and BL6J mice. At the age of 8 weeks, mice were housed at 30°C and fed with LFCD for 7 weeks. Tissues were dissected after 1 additional week characterized by repeated administration of CL in different doses (n=5-6). (A) Dissected iBAT wet tissue mass. Application of Two Way ANOVA was impossible due to unequal group sizes. Data were analyzed separately for each strain using One Way ANOVA and Holm-Sidak post-test with vehicle-treated mice as control group. Asterisks indicate significant difference induced by CL-treatment (*** $p<0.001$). (B) Ucp1 protein levels per iBAT depot normalized to pan-actin levels. Data were analyzed by One Way ANOVA on Ranks and Dunn's multiple comparison test with vehicle-treated mice as control group. Significant differences induced by CL-treatment were not detected. (C) Representative Western Blot conducted with 30 µg of total iBAT protein.

Taken together, 129S6 and BL6J mice are two inbred mouse strains characterized by differential NST capacity. When acclimated to 30°C, 129S6 mice exhibited higher NE-stimulatable HP, whereas Ucp1 expression in BAT and brite fat was stimulatable with a higher magnitude of effect at 20°C. This effect of mild cold-exposure was well-reflected on the pharmacological level, indicating 129S6 mice to exhibit an improved ability for the adaptive recruitment of NST. Thus, 129S6 and BL6J serve as polygenic model system to investigate the effect of differential thermogenic BAT and brite fat function on systemic blood glucose clearance.

3.3 Dietary modification of brite adipocyte abundance

Browning of WAT is stimulatable by environmental temperature or pharmacological treatment and may contribute to systemic energy expenditure and blood glucose clearance by enhancing NST capacity. The cyclooxygenase enzyme (COX) is as central regulator of brite cell recruitment [165, 166] as well as a key enzyme in the metabolization of polyunsaturated fatty acids. In fact, browning of WAT is associated with downstream metabolites of the COX-mediated conversion of arachidonic acid (AA) [165, 166]. Thus, COX constitutes a cellular target that may be suitable for a nutritional intervention as alternative strategy for the recruitment of brite cells. Feeding a diet rich in AA itself or in its precursors may beneficially affect brite adipocyte abundance via increased production of browning-associated eicosanoids.

3.3.1 Thermogenic properties of WAT and BAT

Mice of the 129S6 and BL6J strains were subjected to a feeding experiment characterized by administration of diets with differential fatty acid composition. Subsequent to four weeks of initial LFCD-feeding, mice were assigned to four different groups, one of which continued with LFCD and three were switched to intermediate-fat diets (IFD). Compared to LFCD, IFDs were increased in fat content by addition of palm oil (IFD palm), fish oil (IFD fish) or borage oil (IFD borage; see Table 3). The latter was characterized by a high n6/n3 ratio and increased abundance of the n6 fatty acids linoleic and γ-linolenic acid (compare Table 4), which are AA precursors. Fish oil-comprising IFD was characterized by a very low n6/n3 ratio as well as increased abundance of the n3 fatty acids eicosapentaenoic and docosahexaenoic acid, which are AA competitors for the COX-reaction. Palm oil-comprising IFD was intermediate and most similar to LFCD regarding the n6/n3 ratio and served as control-IFD. Feeding of LFCD and IFDs was conducted at 30°C. The experiment was performed in the open animal facility Thalhausen (not specified pathogen free). Tissues were dissected after 4 weeks of IFD-feeding (Figure 26).

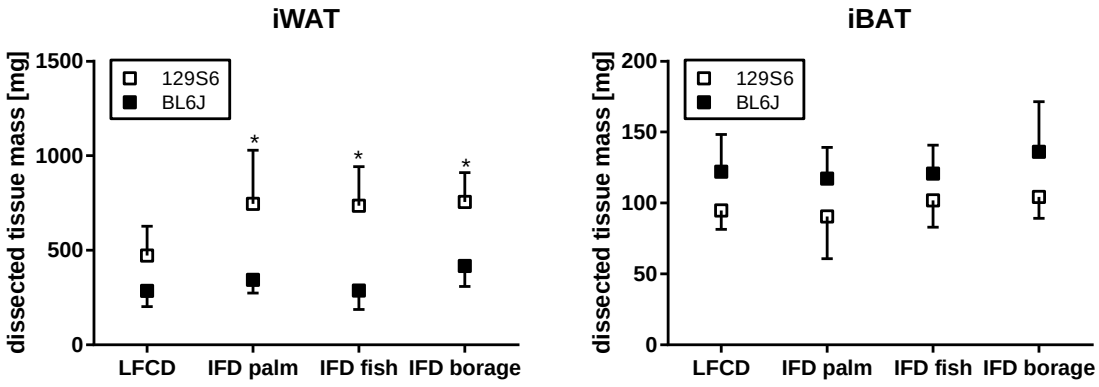

Figure 26: Dissected wet tissue masses of iWAT and iBAT from 129S6 and BL6J mice. At the age of 14 weeks, mice were fed with LFCD or one of three intermediate-fat diets (IFD) comprising palm, fish or borage oil as additional fat source. Diets were fed at 30°C in the facility Thalhausen. Tissues were dissected after 4 weeks of IFD-feeding (n=5). Data were analyzed by Two Way ANOVA and Holm-Sidak post-test using LFCD-fed mice as control group. Asterisks indicate significant effect (* $p<0.05$) of IFD-feeding compared to LFCD within the 129S6 strain.

Elevated fat content of IFDs increased dissected tissue mass of iWAT in 129S6 but not BL6J mice. The magnitude of this effect was not influenced by the dietary fatty acid composition. The mass of iBAT was neither affected by dietary fat content nor fatty acid composition.

Brown adipocyte marker gene expression was determined in iWAT to investigate the effect of diets on brite cell recruitment. The expression of Ucp1, Cidea and Cox7a1 was differentially affected in 129S6 and BL6J mice (Figure 27). In 129S6 mice, elevated fat content of IFDs vs. LFCD decreased gene expression with the strongest magnitude of effect in borage-fed animals. Interestingly, similar results were observed in BL6J mice when these were fed with fish and palm oil-comprising IFDs whereas borage oil appeared to attenuate IFD-induced downregulation of marker gene expression. Although all effects were weakly pronounced and subject to large variation, these data indicate that an elevation of dietary fat content negatively affects brite adipocyte abundance in both strains. Borage oil-comprising IFD thereby acts in strain-specific manner.

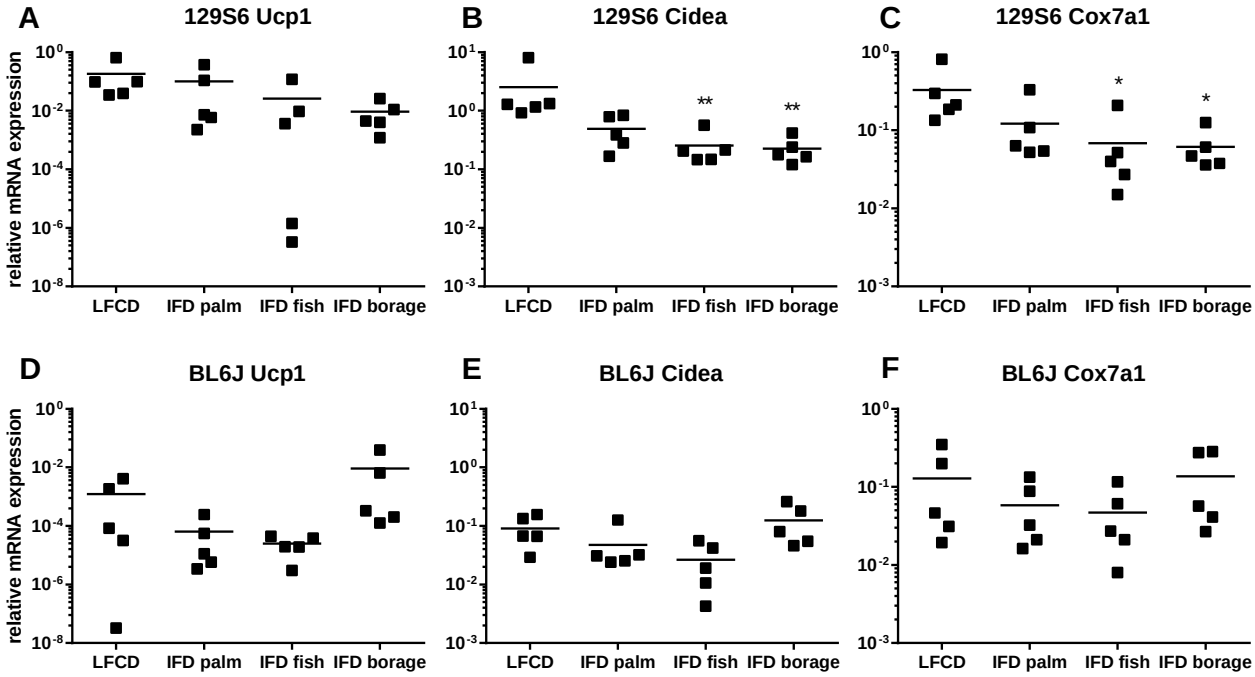

Figure 27: Relative mRNA levels of Ucp1, Cidea and Cox7a1 expression in iWAT of 129S6 and BL6J. At the age of 14 weeks, mice of both strains were fed with LFCD or one of three IFDs comprising palm, fish or borage oil as additional fat source. Diets were fed at 30°C in the facility Thalhausen. Tissues were dissected after 4 weeks of IFD-feeding (n=5). Expression levels of target genes in iWAT were normalized to Gtf2b expression. Due to high standard deviations, y-axis has logarithmic scaling. Statistical analysis was conducted using One Way ANOVA on Ranks and Dunn's multiple comparison test (A, B, C and D) or One Way ANOVA and Holm-Sidak post-test (E and F). LFCD-fed mice were used as control group. Asterisks indicate significant effect of IFD-feeding compared to LFCD (* $p<0.05$; ** $p<0.01$).

Brite adipocytes are characterized by a multilocular phenotype. In line with previous observations (Figure 19), the abundance of multilocular adipocytes was clearly higher in iWAT of LFCD-fed 129S6 than BL6J mice (Figure 28). Among 129S6 mice, adipocytes with multiple smaller lipid droplets were also detectable in mice that received palm oil-comprising IFD whereas they were completely absent in fish and borage oil fed mice.

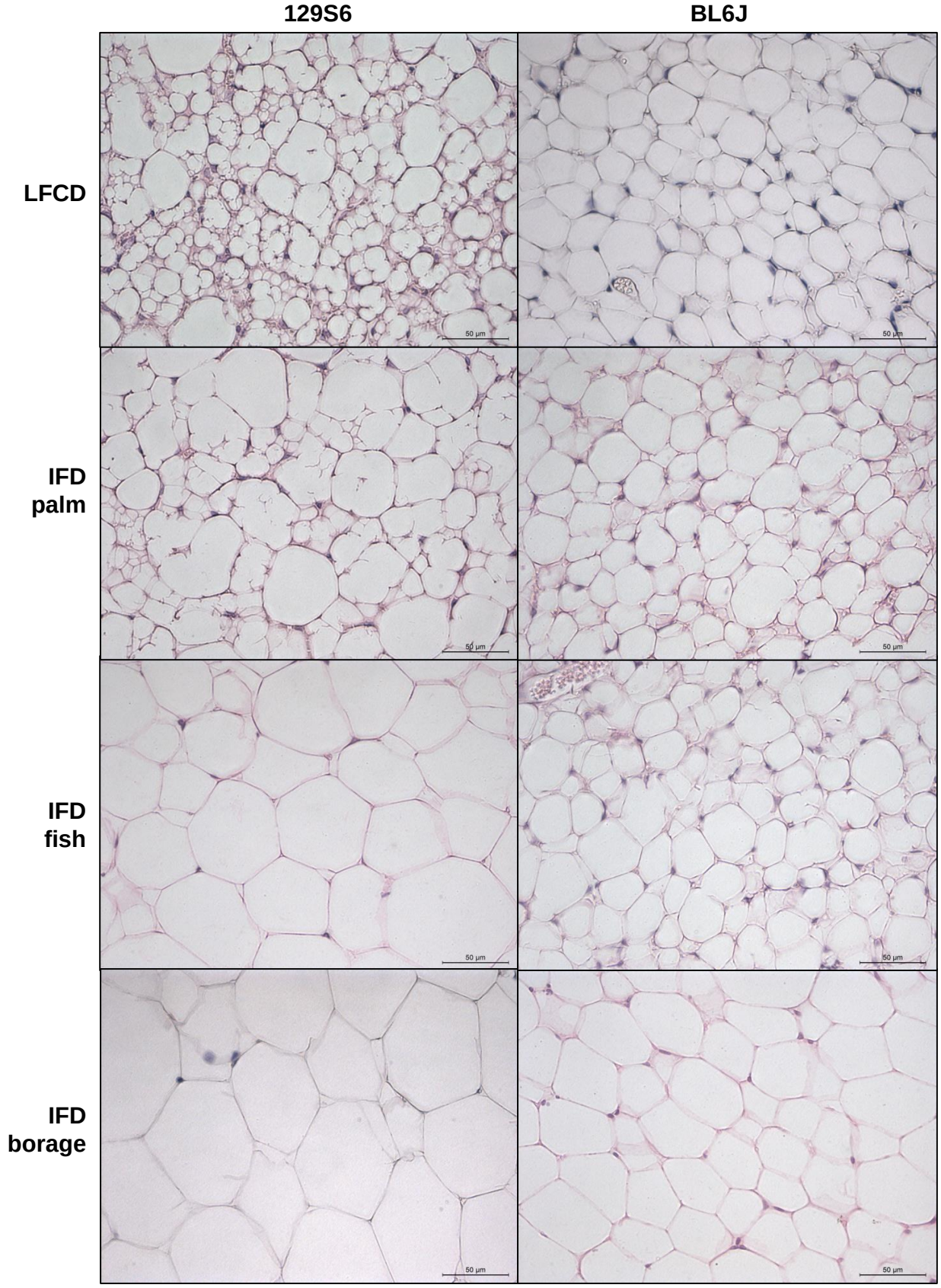

Figure 28: Hematoxylin/eosin-stained section of iWAT from 129S6 and BL6J mice. At the age of 14 weeks, mice of both strains were fed with LFCD or one of three IFDs comprising palm, fish or borage oil as additional fat source. Diets were fed at 30°C in the facility Thalhausen. Tissues were dissected after 4 weeks of IFD-feeding (n=5).

Additionally, this lack of multilocular morphology was accompanied by increased adipocyte size. In BL6J mice, the overall morphological appearance of iWAT was characterized by unilocular cells of smaller size than in 129S6 mice, and was largely comparable between LFCD-fed mice and animals that received palm or fish oil. Interestingly, adipocytes of borage-fed BL6J mice had a hypertrophic, unilocular appearance, which was not in line with the relative increase of Ucp1 expression in iWAT of this group (compare Figure 27D).

Protein levels of Ucp1 were determined in iBAT (Figure 29) to investigate whether diet-induced effects are restricted to WAT. Generally, Ucp1 levels were higher in 129S6 than BL6J mice under all conditions tested. In 129S6 mice, Ucp1 levels were comparable between mice fed with LFCD and palm oil-comprising IFD. Levels of Ucp1 tended to be elevated in fish and borage oil-fed mice, indicating an effect of extraordinary n6/n3 ratios. In BL6J mice, Ucp1 levels were neither affected by fat content nor fat source.

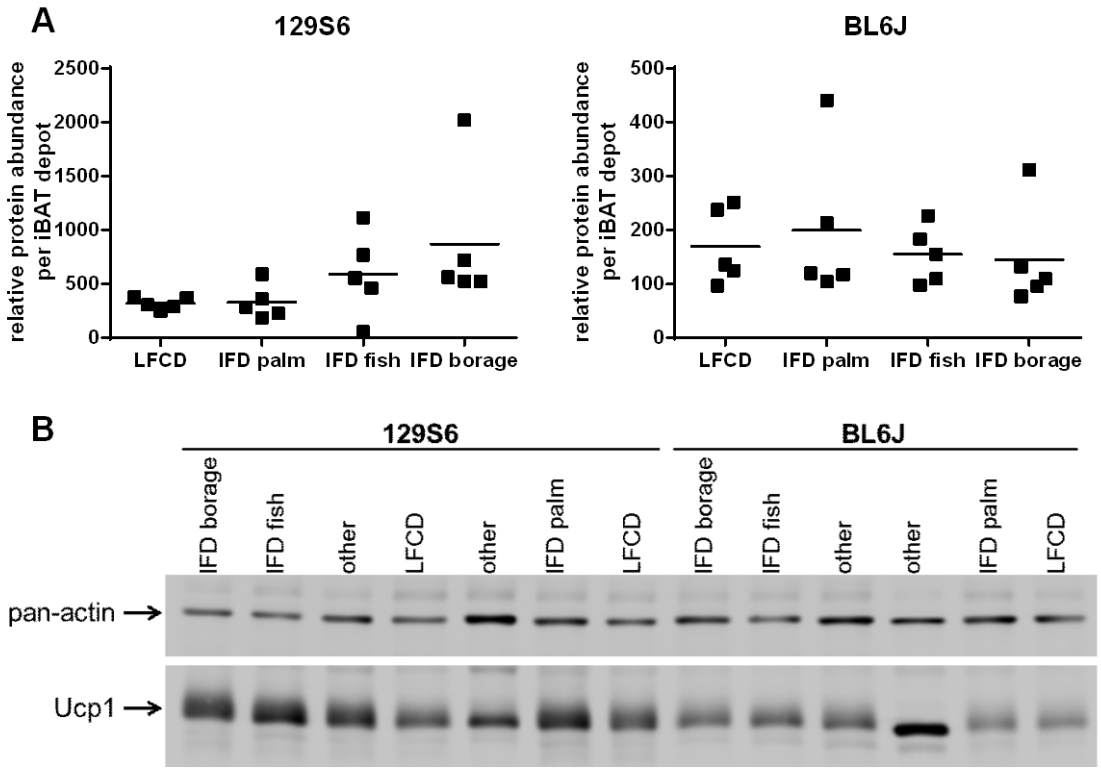

Figure 29: Ucp1 protein levels in iBAT of 129S6 and BL6J mice. At the age of 14 weeks, mice of both strains were fed with LFCD or one of three IFDs comprising palm, fish or borage oil as additional fat source. Diets were fed at 30°C in the facility Thalhausen. Tissues were dissected after 4 weeks of IFD-feeding (n=5). (A) Normalized Ucp1 expression per iBAT depot. Both datasets were analyzed by One Way ANOVA on Ranks and Dunn's multiple comparison test using LFCD-fed mice as control group. Significant differences induced by IFD-feeding were not detected. (B) Representative Western Blot with 30 µg of total protein. Of note, samples of mice fed with other diets (denominated as 'other') were loaded on the same SDS-PAGE but will not be further addressed in this thesis.

3.3.2 Analysis of oxylipin abundance in WAT

The COX enzyme contributes to the metabolization of n6 and n3 fatty acids and concurrently is a regulator of brite adipogenesis [165, 166]. Mice of the 129S6 and BL6J strains were fed with three different IFDs characterized by differential fatty acid composition (see section 3.3.1), thus shifting the dietary n6/n3 ratio from intermediate (IFD palm) towards very low (IFD fish) or very high (IFD borage). These diets were fed at thermoneutral ambient for 4 weeks in total. Oxylipin analysis was conducted to see whether this modification of food-derived precursors alters the local production pattern of eicosanoids in iWAT.

A small aliquot of a single iWAT lobe was subjected to analysis. In total, 33 molecules were quantified, 30 of which were detected in at least 1 sample. Metabolite abundance was extrapolated to lobe (depot) size and compared among the three diet groups. Based on this, compounds were divided into three categories (Table 13): (1) borage-associated, comprising metabolites that were exclusively detected in iWAT of borage oil-fed animals or upregulated in borage oil-fed mice compared to other diet-groups; (2) fish associated, comprising metabolites that were exclusively detected in iWAT of fish oil-fed mice or upregulated in fish oil-fed mice compared to other diet-groups; and (3) other metabolites, that were not distinctly enriched in borage or fish oil-fed mice, that were not regulated at all by diet or that were undetectable in all samples of one strain. Categorization resulted in the identification of 9 borage-associated and 9 fish-associated metabolites. Among these, 4 borage-associated and 6 fish-associated metabolites were enriched in both 129S6 and BL6J mice. None of all quantified metabolites was distinctly enriched in iWAT of palm oil-fed mice. Thus, extraordinary dietary n6/n3 ratios are capable of modifying the pattern of eicosanoids produced in iWAT causing the enrichment of single n6 or n3-derived compounds. Accordingly, the percentage of all n3-derived metabolites was increased in fish oil-fed animals of both strains (Figure 30). The percentage of n6 and n3-derived metabolites in iWAT was similar between palm and borage oil-fed mice. Based on the intermediate n6/n3 ratio of palm oil-comprising IFD, these data indicate that a reduction but not further elevation of this ratio alters the overall percentage of n6-derived metabolites.

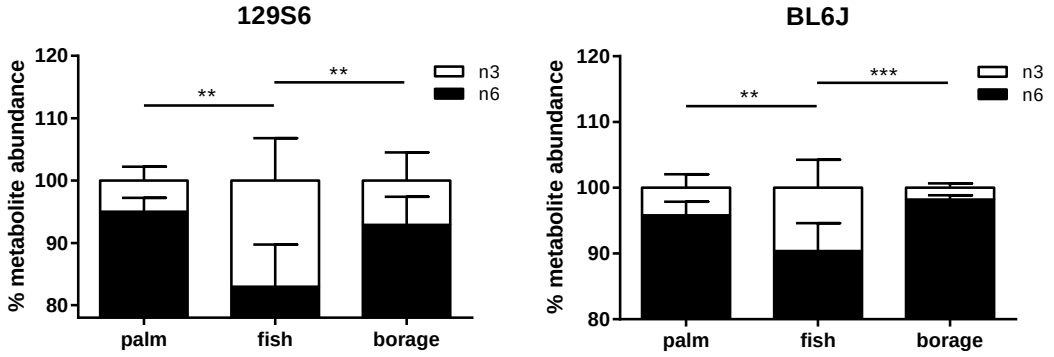

Figure 30: Percentage of n6 and n3-derived metabolites in total iWAT oxylipin abundance. 129S6 and BL6J mice received palm, fish and borage oil-comprising IFDs at 30°C. After 4 weeks, iWAT was dissected and subjected to oxylipin analysis (n=5). Oxylipins were classified by origin (n6 or n3). Datasets were analyzed by Two Way ANOVA and Holm-Sidak post-test to compare diet-effects for each class of metabolites (** $p<0.01$; *** $p<0.001$). Significant differences between diet-groups were reflected in both classes of metabolites with identical degree of significance.

Table 13: Summary of diet-effects on oxylipin abundance in iWAT of 129S6 and BL6J mice.

Category	Subcategory	129S6	BL6J
borage-associated	borage only	LxA_4	LxA_4*
		5,6-DiHETE*	
	↑ borage vs. fish+palm	$PGF_{2\alpha}$	PGA_1*
		PGE_2	TxB_2*
		PGA_1	
		12-HETE	
	↑ borage vs. fish	6-keto-$PGF_{1\alpha}$	6-keto-$PGF_{1\alpha}$*
			$PGF_{2\alpha}$
	↑ borage vs. palm		5-HETE
fish-associated	fish only	PGE_3	PGE_3
		11β-$PGF_{2\alpha}$	7MaR1
		7MaR1	
	↑ fish vs. borage+palm	PDx	PDx
		18-HEPE	18-HEPE
		17-HDoHE	17-HDoHE
		14-HDoHE	14-HDoHE
	↑ fish vs. palm		LTB_4
			9-HODE
other	↑ borage+fish vs. palm		5-oxo-ETE
	not regulated by diet	TxB_2	PGE_2*
		PGD_2	PGD_2
		8isoPGA_2	8isoPGA_2*
		LTB_5	15-deoxy-PGJ_2
		LTB_4	13-HODE
		15-deoxy-PGJ_2	15-HETE
		13-HODE	8-HETE
		9-HODE	12-HETE
		15-HETE*	14,15-EET
		8-HETE	11,12-EET
		5-HETE*	8,9-EET
		14,15-EET*	5,6-EET
		5-oxo-ETE*	
		11,12-EET*	
		8,9-EET*	
		5,6-EET*	
	not detected		11β-$PGF_{2\alpha}$
			LTB_5
			5,6-DiHETE

Mice of the 129S6 and BL6J strains were fed with IFDs for 4 weeks at 30°C. The effect of dietary fat source (palm oil, fish oil or borage oil) on oxylipin abundance [pg/depot] in both strains was investigated by Two Way ANOVA and Holm-Sidak post-test for each metabolite (n=5). Compounds were categorized based on the identification of statistically significant differences (at least $p<0.05$) by multiple comparisons or based on their occurrence in single diet-groups only. LxB_4, RvD1 and RvD2 were omitted since they were not detected in any diet-group of both strains. ↑ indicates upregulation of metabolites in one group compared to one or two other groups. *Significantly correlated with Ucp1 expression in iWAT (compare Table 14).

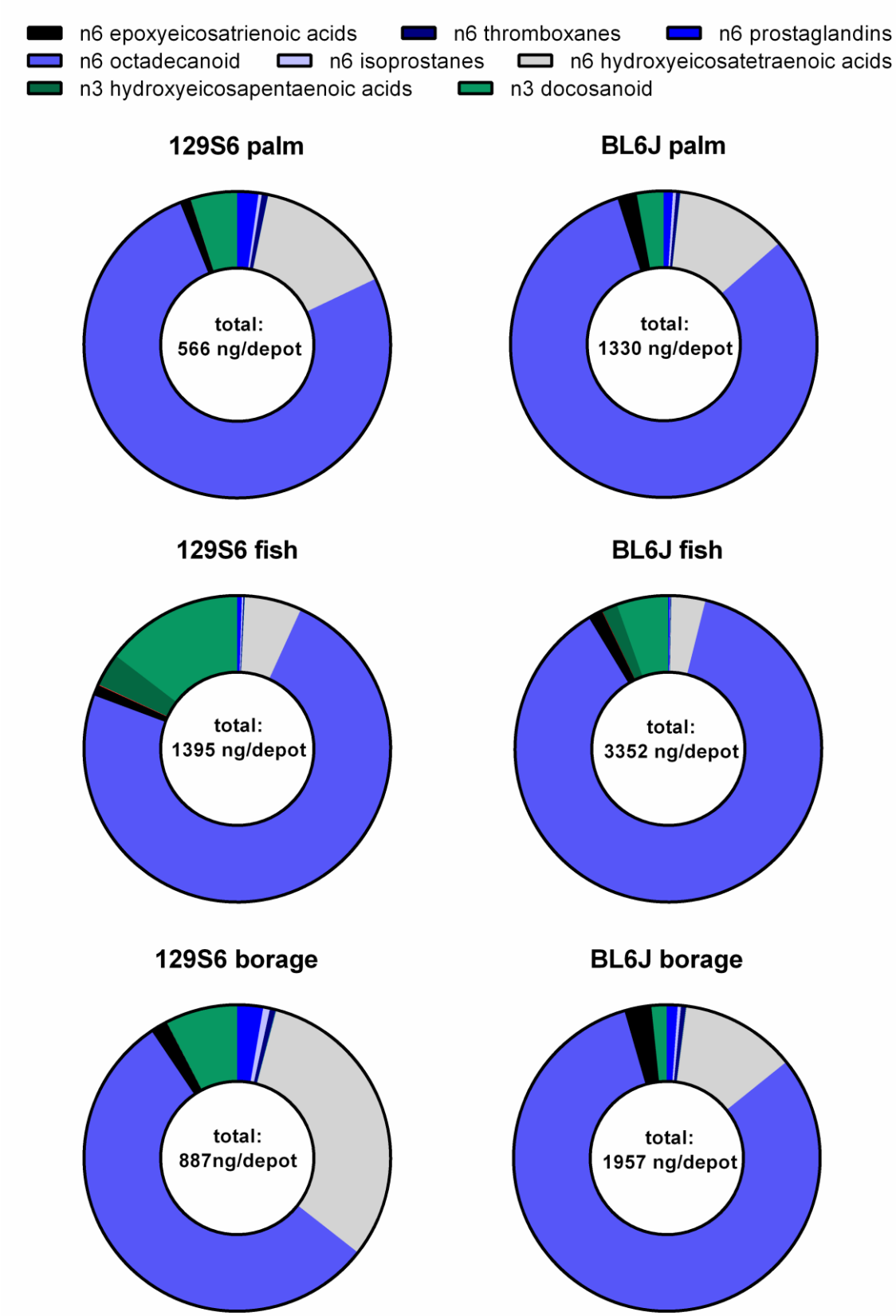

Figure 31: Averaged abundance of metabolite classes as percentage of total iWAT oxylipin abundance. 129S6 and BL6J mice received palm, fish and borage oil-comprising IFDs at 30°C. After 4 weeks, iWAT was dissected and subjected to oxylipin analysis (n=5). Oxylipins were classified as indicated in figure legend based on their chemical structure and biosynthesis pathway (compare Figure 6 and Table 10). n6 leukotriens, n6 lipoxins, n3 prostaglandins and n3 leukotriens were omitted in figure legend due to very low abundance (0.00-0.05%) in all treatment groups.

Based on their biosynthesis and chemical structure (compare Figure 6 and Table 10), the entity of n6 and n3-derived metabolites was further classified (Figure 31). The most abundant class of metabolites (55-88% of total metabolite abundance) in both strains and all diet-groups was represented by n6 octadecanoids derived from Lipoxygenase (LOX) mediated conversion of linoleic acid. Hydroxyeicosatetraenoic acids (HETEs) derived from LOX-mediated conversion of AA represented the second most abundant group of n6-derived metabolites (6-32%). 12-HETE, accounting for an important proportion of the abundance of this metabolite class, was enriched in borage-fed 129S6 but not BL6J mice (compare Table 13). This observation largely explains the remarkable difference between borage-fed mice of both strains regarding the percentage of HETEs in total metabolite abundance.

Generally, the percentage of metabolite classes was most comparable between palm and borage-fed animals (Figure 31). In fish oil-fed mice, the percentage of n6-derived metabolites (especially COX-derived thromboxanes, prostaglandins and isoprostanes as well as HETEs) was reduced at the expense of n3-derived metabolites. This phenotype was most pronounced for docosanoids, which are metabolites derived from LOX-mediated conversion of n3 docosahexaenoic acid, as well as 18-hydroxyeicosapentaenoic acid (18-HEPE), a fish-associated metabolite derived from n3 eicosapentaenoic acid (compare Figure 6).

Interestingly, the absolute abundance of all metabolites per depot (see Figure 31) consistently tended to be more than 2-fold higher in BL6J than 129S6 mice comparing the individual diet groups. Tissue masses of iWAT were, however, consistently higher in 129S6 mice (compare Figure 26), indicating a lower density of quantified metabolites in iWAT of this strain.

Collectively, modulation of the dietary n6/n3 ratio resulted in a modification of the eicosanoid pattern and affected brown adipocyte marker gene expression in iWAT of 129S6 and BL6J mice. Correlation analysis was conducted to investigate the relationship between the abundance of oxylipins and Ucp1 expression to identify putative candidate compounds that may contribute to the browning of WAT (Table 14). In 129S6 and BL6J mice, there were 8 and 6 metabolites, respectively, that were strongly and significantly correlated with Ucp1 expression. All correlations were positive, indicating that increased abundance of these metabolites positively affects Ucp1 expression or vice versa. All of these compounds were derived from metabolization of n6 fatty acids. There was not a single compound that was consistently correlated with Ucp1 expression in both mouse strains. In 129S6 mice, Ucp1 expression was exclusively correlated with HETEs and epoxyeicosatrienoic acids, which are derived from LOX and Cytochrome P450-mediated conversion of AA, respectively (compare Figure 6). One of these metabolites, 5,6-dihydroxy-eicosatetraenoic acid (5,6-DiHETE), was found in iWAT of borage oil-fed mice only, whereas the abundance of all other compounds was not regulated by the diets (compare Table 13). This indicates that the dietary fatty acid composition does not substantially influence the abundance of oxylipins associated with browning of WAT in 129S6 mice. In BL6J mice, Ucp1 expression was correlated with COX-derived prostaglandins, isoprostanes and thromboxanes as well as LOX-derived lipoxin A_4 (LxA_4). Interestingly, most of these compounds were categorized as borage-associated (compare Table 13), indicating that

supplementation of borage oil favors the production of oxylipins associated with browning of WAT in BL6J mice.

Table 14: Summary of correlation analysis between oxylipin abundance and Ucp1 mRNA expression in iWAT.

Class	Series	Compound	129S6		BL6J	
			R^2	significance	R^2	significance
prostaglandin	n6	PGA_1	0.28	ns	0.33	p<0.05
		PGD_2	0.00	ns	0.17	ns
		PGE_2	0.01	ns	0.54	p<0.01
		6-keto-$PGF_{1\alpha}$	0.16	ns	0.35	p<0.05
		$PGF_{2\alpha}$	0.24	ns	0.30	ns
		11β-$PGF_{2\alpha}$	0.12	ns	0.00	ns
		15-deoxy-PGJ_2	0.02	ns	0.26	ns
	n3	PGE_3	0.00	ns	0.12	ns
isoprostane	n6	8isoPGA_2	0.22	ns	0.72	p<0.001
thromboxane	n6	TxB_2	0.08	ns	0.55	p<0.01
leukotrien	n6	LTB_4	0.19	ns	0.00	ns
leukotrien	n3	LTB_5	0.14	ns	0.00	ns
lipoxin	n6	LxA_4	0.01	ns	0.42	p<0.05
hydroxyeicosatetraenoic acid	n6	5-HETE	0.54	p<0.01	0.12	ns
		5-oxo-ETE	0.64	p<0.01	0.02	ns
		8-HETE	0.13	ns	0.09	ns
		12-HETE	0.10	ns	0.15	ns
		15-HETE	0.38	p<0.05	0.06	ns
		5,6-DiHETE	0.46	p<0.05	0.00	ns
hydroxyeicosapentaenoic acid	n3	18-HEPE	0.00	ns	0.11	ns
octadecanoid	n6	9-HODE	0.16	ns	0.03	ns
		13-HODE	0.16	ns	0.04	ns
docosanoid	n3	7MaR1	0.01	ns	0.14	ns
		14-HDoHE	0.01	ns	0.14	ns
		17-HDoHE	0.01	ns	0.12	ns
		PDx	0.01	ns	0.13	ns
epoxyeicosatrienoic acids	n6	5,6-EET	0.67	p<0.01	0.01	ns
		8,9-EET	0.62	p<0.01	0.02	ns
		11,12-EET	0.67	p<0.01	0.00	ns
		14,15-EET	0.63	p<0.01	0.00	ns

Mice of the 129S6 and BL6J strains received palm, fish and borage oil-comprising IFDs at 30°C. After 4 weeks, iWAT was dissected and subjected to oxylipin analysis (n=5). Expression of Ucp1 mRNA (compare Figure 27) and abundance of oxylipins in iWAT [pg/aliquot] were extrapolated to depot size. R^2 was calculated using the Pearson correlation coefficient. Correlation analysis was conducted for each strain including mice of all diet-groups. Several animals of initially 5 per group were excluded from the analysis due to extraordinary high Ucp1 expression (129S6: 1 in fish oil group and 2 in palm oil group; BL6J: 2 in borage oil group). The metabolites LxB_4, RvD1 and RvD2 were measured but not detected in any sample.

Taken together, modification of the dietary fatty acid composition affected the production of oxylipins in WAT of mice. The percentage of n3-derived metabolites was increased by administration of fish oil, whereas the replacement of dietary palm oil by borage oil resulted in the enrichment of single, n6-derived metabolites. Administration of these fat sources via a diet that is characterized by a moderately elevated fat content appeared to decrease brite

adipocyte abundance compared to an LFCD, although this phenotype was weakly pronounced and not consistently reflected on the level of gene expression and adipocyte morphology. Expression of Ucp1 in WAT of 129S6 and BL6J mice was exclusively correlated with n6-derived metabolites, indicating that increased production of these respective compounds may favor brite adipogenesis. In 129S6 mice, the abundance of compounds associated with Ucp1 expression was not affected by the dietary fat source. In BL6J mice, Ucp1 expression was associated with metabolites enriched in WAT of borage oil-fed animals, suggesting that this fat source may affect brite adipocyte abundance in strain-specific manner. Collectively, the identified metabolites associated with Ucp1 expression in WAT serve as candidate compounds that may favor brite adipogenesis, although their actual browning potential remains to be elucidated.

3.4 Glucose tolerance of 129S6 and BL6J mice

Adaptive thermogenesis in BAT is supported by oxidation of glucose taken up from systemic blood circulation. Functional BAT and brite fat in high abundance has been shown to improve blood glucose clearance in mice [118, 119]. The capacity for Ucp1-mediated heat production may thus be related to glucose homeostasis. Mice of the 129S6 and BL6J strains, characterized by differences in NST capacity, were employed to test this hypothesis.

3.4.1 Non-obesogenic conditions

Mice of the 129S6 and BL6J strains were housed at 30°C and 20°C and fed with LFCD for 4 weeks. As demonstrated above (sections 3.2.1 and 3.2.2), NST capacity of 129S6 mice is higher under both housing conditions. Mice were subjected to oral glucose tolerance tests (oGTT) to investigate whether this phenotype influences blood glucose clearance. Fasting and oGTTs were conducted at room temperature (23°C ± 1°C) to challenge BAT function in all mice to the same extent. Thus, differences in glucose tolerance between treatment groups were not affected by acute effects of ambient temperature but influenced by NST capacity as result of acclimation.

Both strains did not differ in the regulation of blood glucose levels over time when mice were housed at 30°C (Figure 32A). Housing of mice at 20°C caused higher blood glucose levels in BL6J mice although the absolute amount of initial increment and subsequent decline after glucose gavage appeared to be similar between the strains. The total area under the curve (AUC) was calculated as measure for glucose tolerance (Figure 32B). As expected, glucose tolerance was not different between the strains when mice were housed at 30°C. A reduction of housing temperature led to an improvement of glucose tolerance in both strains, indicating attenuated blood glucose clearance in response to housing at thermoneutrality, representing a condition of minimized NST capacity. The effect of mild cold-exposure on glucose tolerance was more pronounced in 129S6 mice.

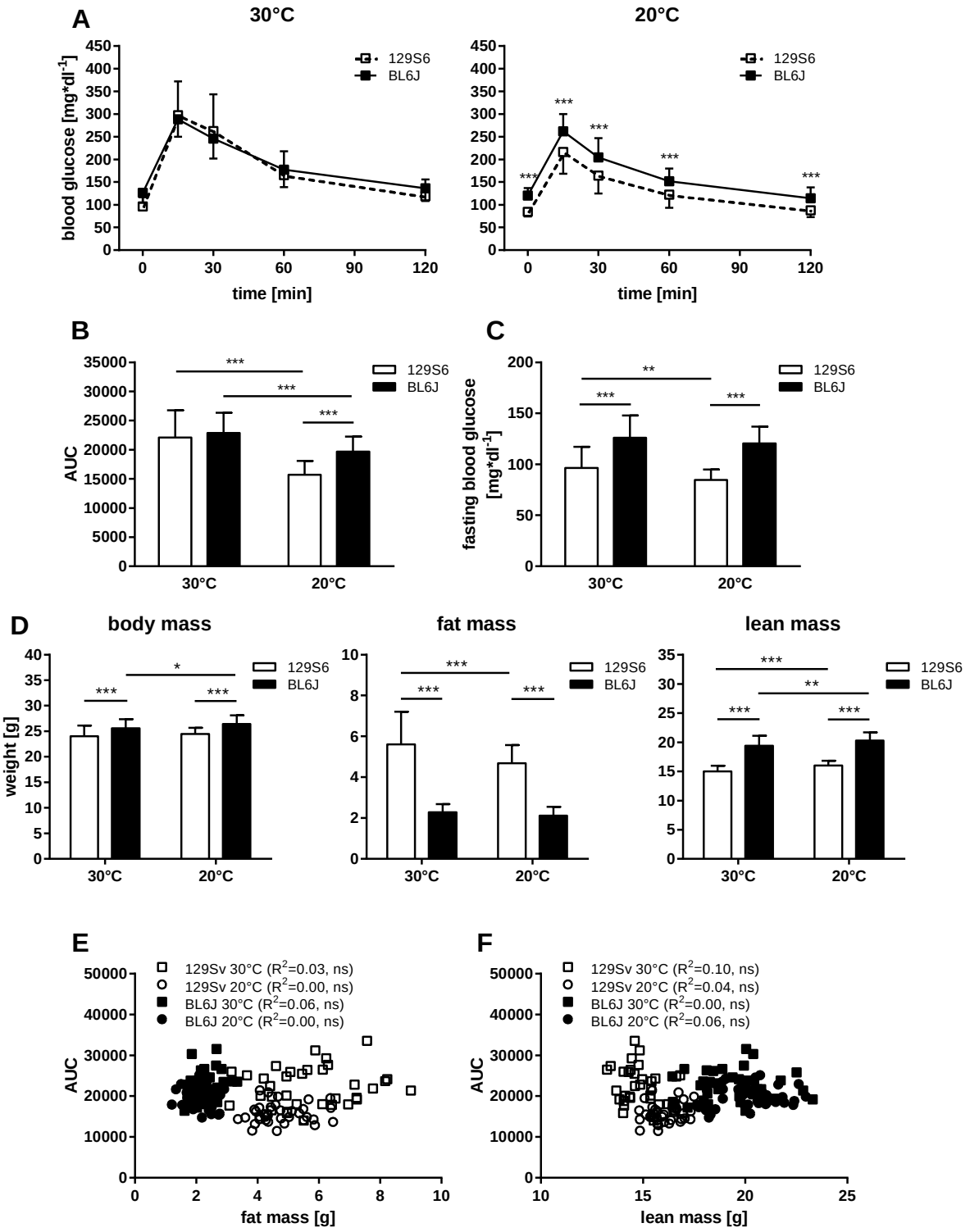

Figure 32: Body composition and glucose tolerance of 129S6 and BL6J mice under non-obesogenic conditions. At the age of 8 weeks, mice were housed at 30°C and 20°C and fed with LFCD. Body composition and glucose tolerance were assessed after 4 weeks of feeding (n=36). (A) Blood glucose levels during oral glucose tolerance tests (oGTT) before (0 min) and after glucose gavage. Each dataset was analyzed by Two Way RM ANOVA and Holm-Sidak post-test. Asterisks indicate significant differences between treatment groups at the indicated time points (*** p<0.001). (B) Total area under the curve (AUC) of blood glucose levels measured during oGTTs. (C) Fasting blood glucose levels before glucose gavage. (D) Body, fat and lean mass. Datasets (B-D) were analyzed by Two Way ANOVA and Holm-Sidak post-test (* p<0.05; ** p<0.01; *** p<0.001). (E) Relationship between glucose tolerance (AUC) and fat mass, and (F) AUC and lean mass. The relationship between two variables was analyzed in each group using the Pearson correlation coefficient. R^2 is indicated in figure legends.

In contrast to glucose tolerance, fasting blood glucose was marginally affected by housing temperature but predominantly influenced by strain-specific variation at both housing temperatures (Figure 32C).

In line with previous observations (Figure 23), there were significant differences in body composition between both strains (Figure 32D). Mice of the 129S6 strain exhibited a higher amount of fat mass, whereas lean mass was elevated in BL6J mice. This phenotype was not affected by housing temperature. Glucose tolerance (AUC) was not correlated with fat (Figure 32E) or lean mass (Figure 32F), indicating that blood glucose clearance is not predictable from body composition in this dataset.

Collectively, these data indicate that blood glucose clearance is affected by housing temperature and genetic background in the context of differential NST capacity when mice are fed with non-obesogenic LFCD. Elevated NST capacity of 129S6 versus BL6J mice did not affect attenuated blood glucose clearance induced by thermoneutral housing, but appeared to benefit the improvement of glucose tolerance under mild cold-exposure. As an elevation of the dietary fat content represents a challenge for glucose tolerance, differences in NST capacity may as well play a role in the response to hypercaloric feeding.

3.4.2 Hypercaloric conditions

An elevation of the dietary fat content commonly results in body mass gain, body fat accumulation and impairment of glucose tolerance in obesity-prone mouse strains. Considering that BAT mediates DIT by dissipating excess energy from food [106], an improved ability for adaptive thermogenesis may enhance blood glucose clearance attenuating the adverse effect of a hypercaloric challenge. The significance of NST capacity in the development of DIO and glucose intolerance was thus investigated.

After administration of LFCD at 30°C or 20°C (see previous section), 129S6 and BL6J mice were distributed into experimental groups stratifying differences in body mass, and switched to one of three IFDs characterized by a moderate elevation of the dietary fat content. These IFDs comprised fish oil, borage oil or palm oil and differed in fatty acid composition to alter the dietary n6/n3 ratio. As demonstrated before (section 3.3), feeding of these IFDs at 30°C modifies the eicosanoid pattern of iWAT and influences Ucp1 levels and adipocyte morphology in 129S6 and BL6J mice. Thus, IFD feeding was considered as ‘priming period’ that may affect the propensity for DIO and impaired glucose tolerance. Such relationship was tested by subsequent feeding of HFDs, characterized by a further elevation of fat content (compare Table 3).

Mice of all treatment groups gained body mass over time (Figure 33). There were no significant differences in body mass development between fish, borage and palm oil-fed mice in both strains when mice were subjected to IFD-feeding. After transition to HFD-feeding, there was a tendency for lower body mass gain in 129S6 mice fed a palm oil-containing diet, whereas fish oil-fed mice tended to gain most body mass. This phenotype was as well observed in

BL6J mice at 20°C, where body mass of fish oil-fed mice evolved significantly different from palm oil and borage oil-fed mice after 1.5 weeks (at day 66) of HFD-feeding.

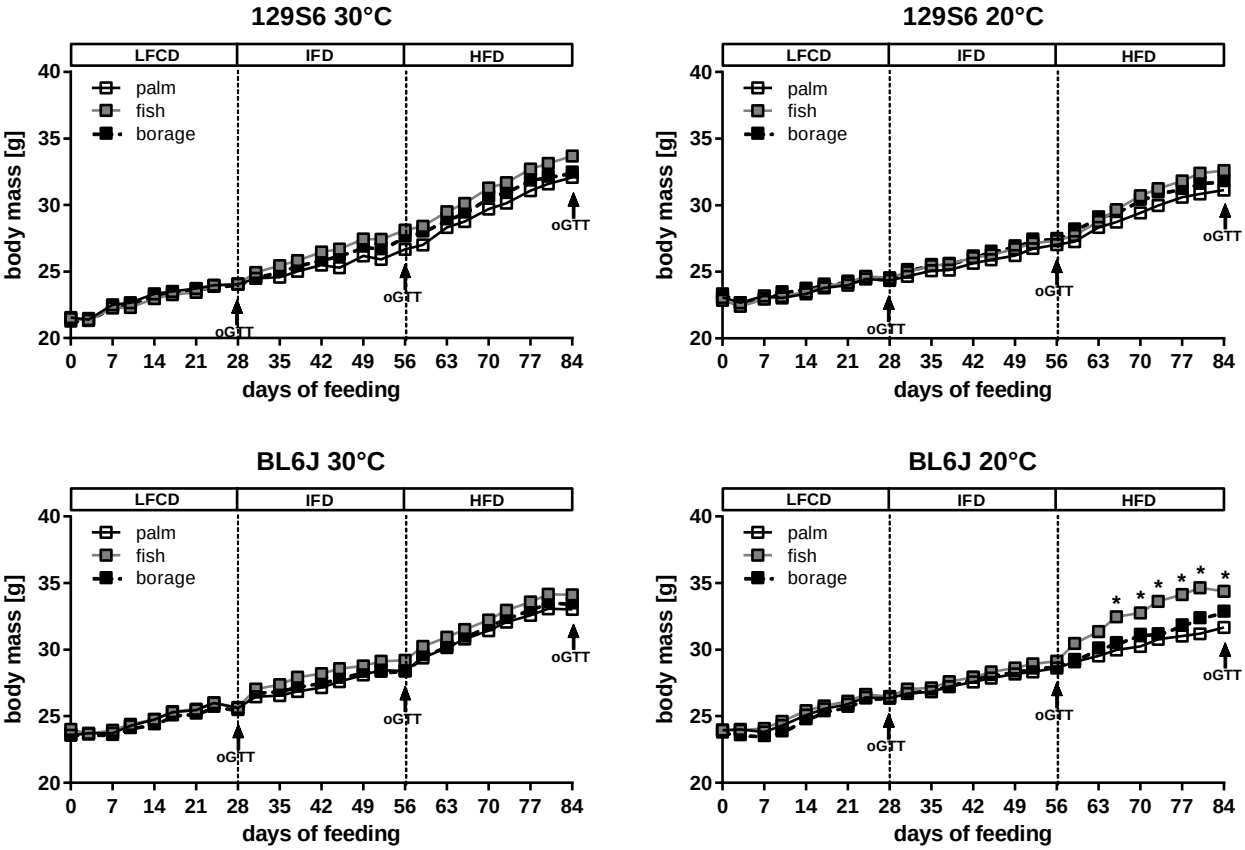

Figure 33: Body mass development of 129S6 and BL6J mice during LFCD, IFD and HFD-feeding. At the age of 8 weeks, mice were housed at 30°C and 20°C and gradually fed with LFCD, IFD and HFD. Each type of diet was fed for 4 weeks. Palm, fish and borage oil were contained as alternative fat sources in IFD and HFD. Depicted data represent averaged body mass of treatment groups at indicated time points (n=12). Standard deviations were omitted for reasons of clarity. Vertical dashed lines indicate diet change. oGTTs were performed at the end of each feeding interval as indicated by arrows. Body mass over time was analyzed by Two Way RM ANOVA and Holm-Sidak post-test in each of the 4 datasets. Asterisks indicate significant differences ($p<0.05$) between fish oil-fed mice and mice from either one or both of the other diet groups. Significant differences between borage and palm oil-fed mice were not identified.

In line with differences in body mass development, total body mass gain during HFD-feeding at 20°C was significantly different between fish oil and palm oil-fed BL6J mice, and largely attributable to differences in fat mass gain (Figure 34B). Interestingly, cumulative energy intake among BL6J mice housed at 20°C during HFD-feeding was slightly reduced in the fish oil-fed group (Figure 34C), indicating that increased fat mass gain of these mice under HFD is not explainable by sheer differences in energy intake.

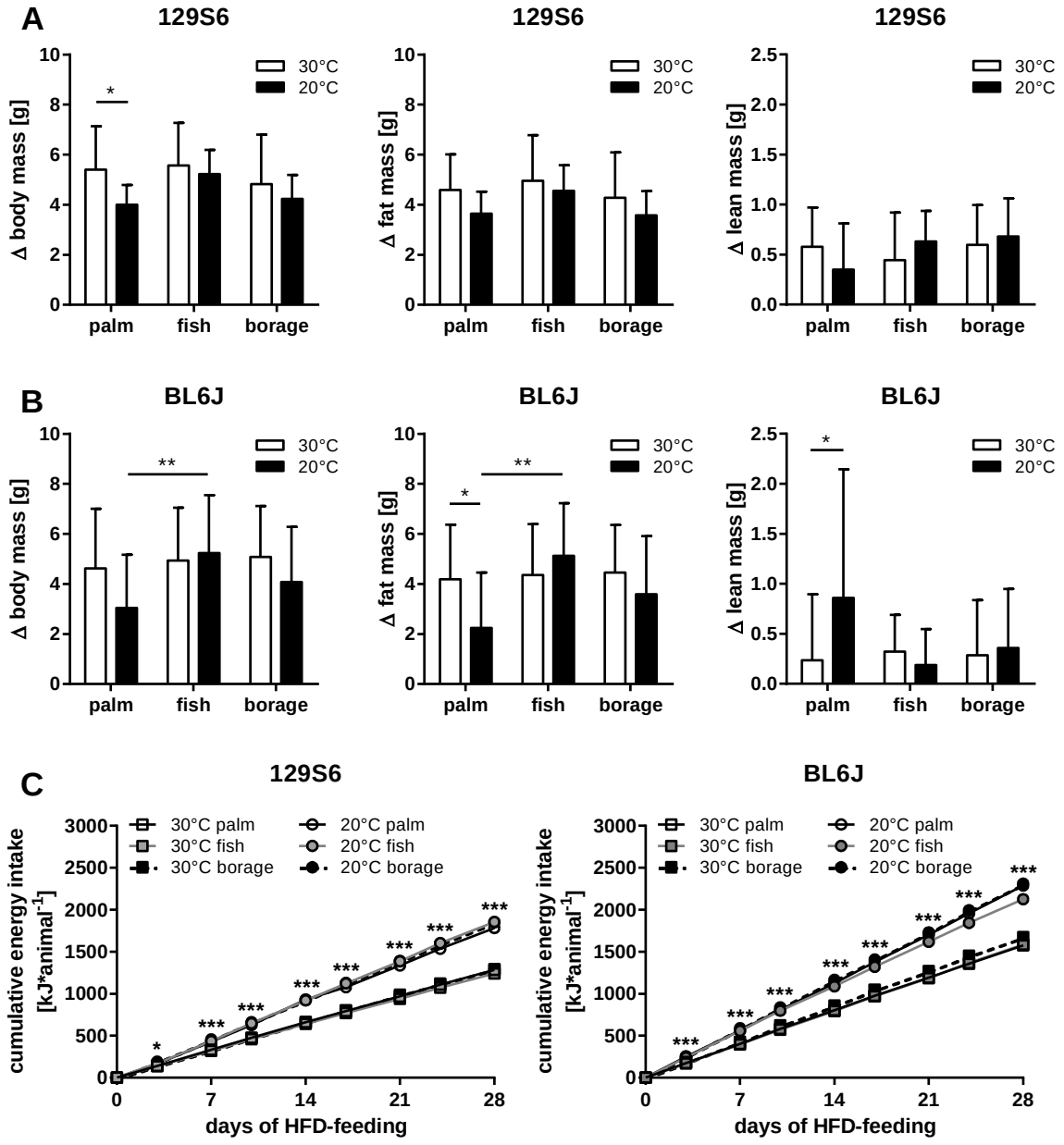

Figure 34: Body mass, body composition and energy intake in HFD-fed 129S6 and BL6J mice. At the age of 8 weeks, mice were housed at 30°C and 20°C and gradually fed with LFCD, IFD and HFD. Each type of diet was fed for 4 weeks. Palm, fish and borage oil were contained as alternative fat sources in IFD and HFD (n=12). (A) Body, fat and lean mass gain of 129S6 and (B) BL6J mice between beginning (day 56) and end (day 84) of HFD-feeding. All datasets were analyzed by Two Way ANOVA and Holm-Sidak post-test (* $p<0.05$; ** $p<0.01$). (C) Cumulative energy intake during HFD-feeding. Depicted data represent averaged values for each individual diet group at indicated time points. Standard deviations were omitted for reasons of clarity. Datasets were analyzed by Three Way ANOVA and Holm-Sidak post-test (* $p<0.05$; *** $p<0.001$). Asterisks indicate significant effect of housing temperature.

Mice of the 129S6 strain were previously shown to gain less body mass than BL6 mice when fed a HFD [203]. Body mass gain on HFD was, however, not different between the strains irrespective of dietary fat source and housing temperature (Figure 35A). Additionally, HFD-fed BL6J mice had a constantly increased energy intake over time compared to 129S6 mice, cumulating in significant differences in total energy intake after 4 weeks of HFD-feeding

(Figure 35B). Consequently, estimated energy expenditure during HFD-feeding was consistently higher in BL6J mice (Figure 35C).

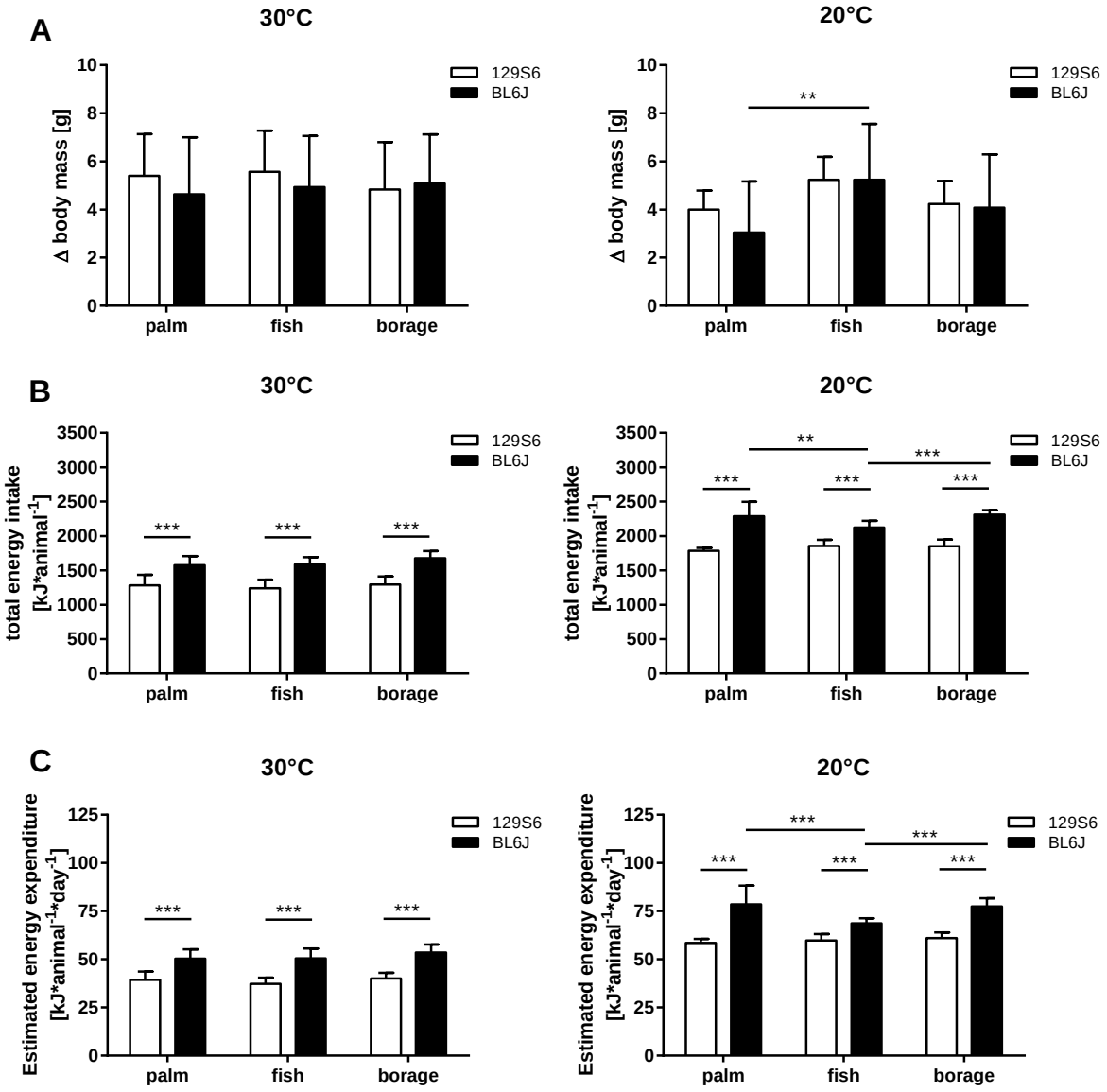

Figure 35: Strain-specific differences in the response to HFD-feeding. At the age of 8 weeks, 129S6 and BL6J mice were housed at 30°C and 20°C and gradually fed with LFCD, IFD and HFD. Each type of diet was fed for 4 weeks. Palm, fish and borage oil were contained as alternative fat sources in IFD and HFD (n=12). (A) HFD-induced changes in body mass, depicted in Figure **34**A and B, were regrouped to identify differences between mouse strains. (B) Total cumulative energy intake at the end of HFD-feeding. (C) Energy expenditure during HFD-feeding was estimated according to [204] in consideration of energy intake and changes in body composition.

Collectively, these data demonstrate that 129S6 and BL6J mice exhibit similar diet-induced body mass accumulation in response to a HFD. Interestingly, HFD-induced body mass gain of BL6J but not 129S6 mice was modifiable by the source of dietary fat when mice were mildly cold-exposed. This phenotype was not observed when mice were housed at 30°C, indicating a synergistic effect of fat source and reduced housing temperature affecting body mass development in response to HFD-feeding. Glucose tolerance was repeatedly assessed

throughout the experiment to investigate whether diet-induced characteristics in body mass development are reflected in systemic glucose homeostasis.

As demonstrated before (compare Figure 32C), fasting blood glucose under LFCD-feeding was considerably influenced by genetic background (Figure 36). After HFD-feeding, 129S6 mice still had significantly lower fasting blood glucose levels compared to BL6J mice, irrespective of dietary fat source and housing temperature (Figure 36). Fasting blood glucose was prone to changes of the dietary fat content in both strains. This diet-induced increase in fasting blood glucose tended to be more pronounced in fish and borage oil-fed animals than palm oil-fed mice, indicating an effect of extraordinary n6/n3 ratios on glucose homeostasis in the fasted state.

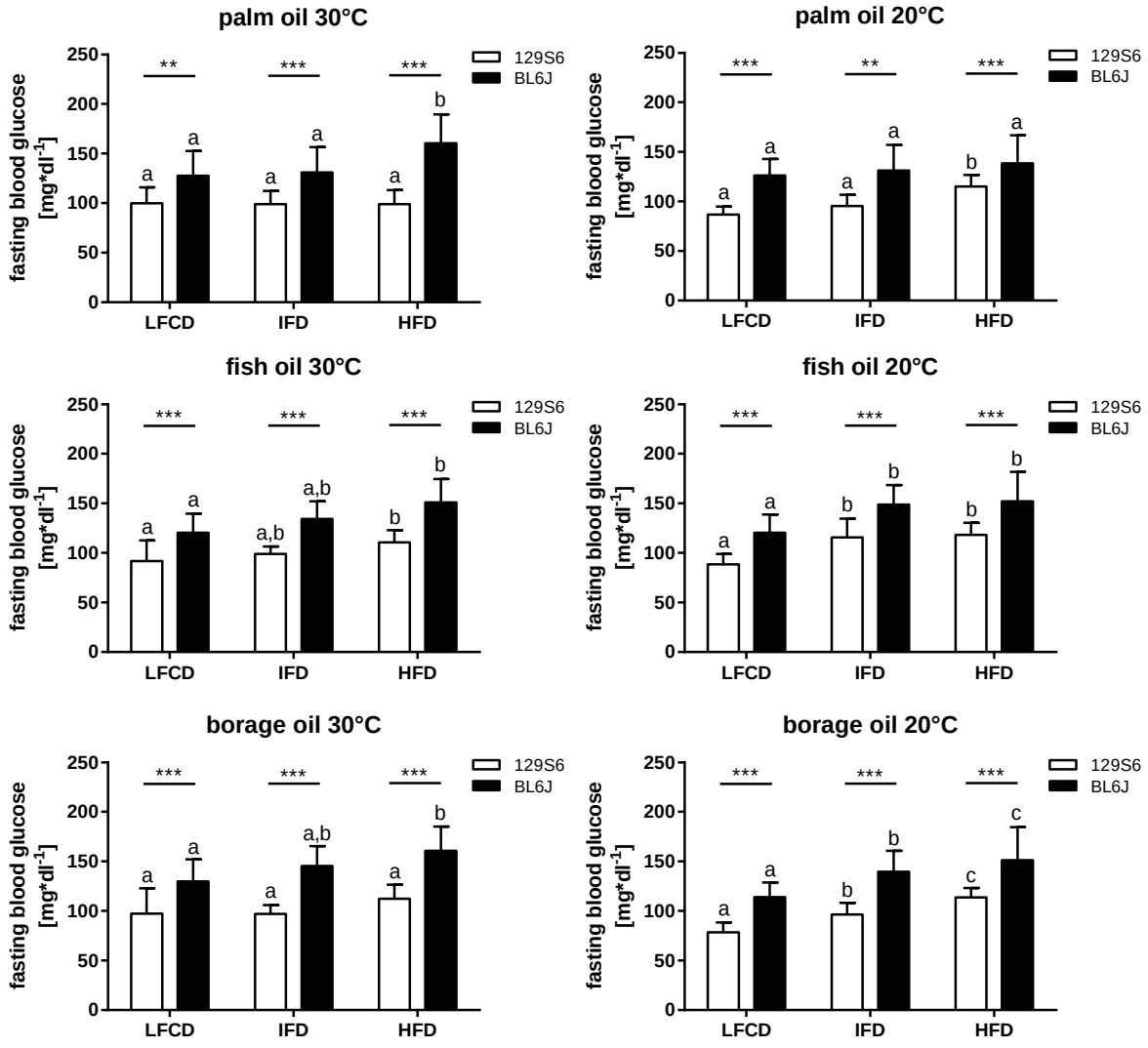

Figure 36: Fasting blood glucose in 129S6 and BL6J mice. At the age of 8 weeks, mice were housed at 30°C and 20°C and gradually fed with LFCD, IFD and HFD. Each type of diet was fed for 4 weeks. Palm, fish and borage oil were contained as alternative fat sources in IFD and HFD (n=12). Fasting blood glucose levels were measured during oGTTs at the end of each feeding interval. Each dataset was analyzed by Two Way RM ANOVA and Holm-Sidak post-test. Asterisks indicate significant effect of mouse strain (** $p<0.01$; *** $p<0.001$). Printed characters indicate significant difference ($p<0.05$) in fasting blood glucose induced by differential fat content in the respective mouse strain.

Differences in fasting blood glucose were largely reflected in glucose tolerance when mice were housed at 20°C (Figure 37). Feeding of IFD and HFD at 20°C caused a gradual impairment of glucose tolerance in both strains. Differences in glucose tolerance between 129S6 and BL6J mice under LFCD at 20°C were entirely maintained and partly amplified in response to IFD and HFD.

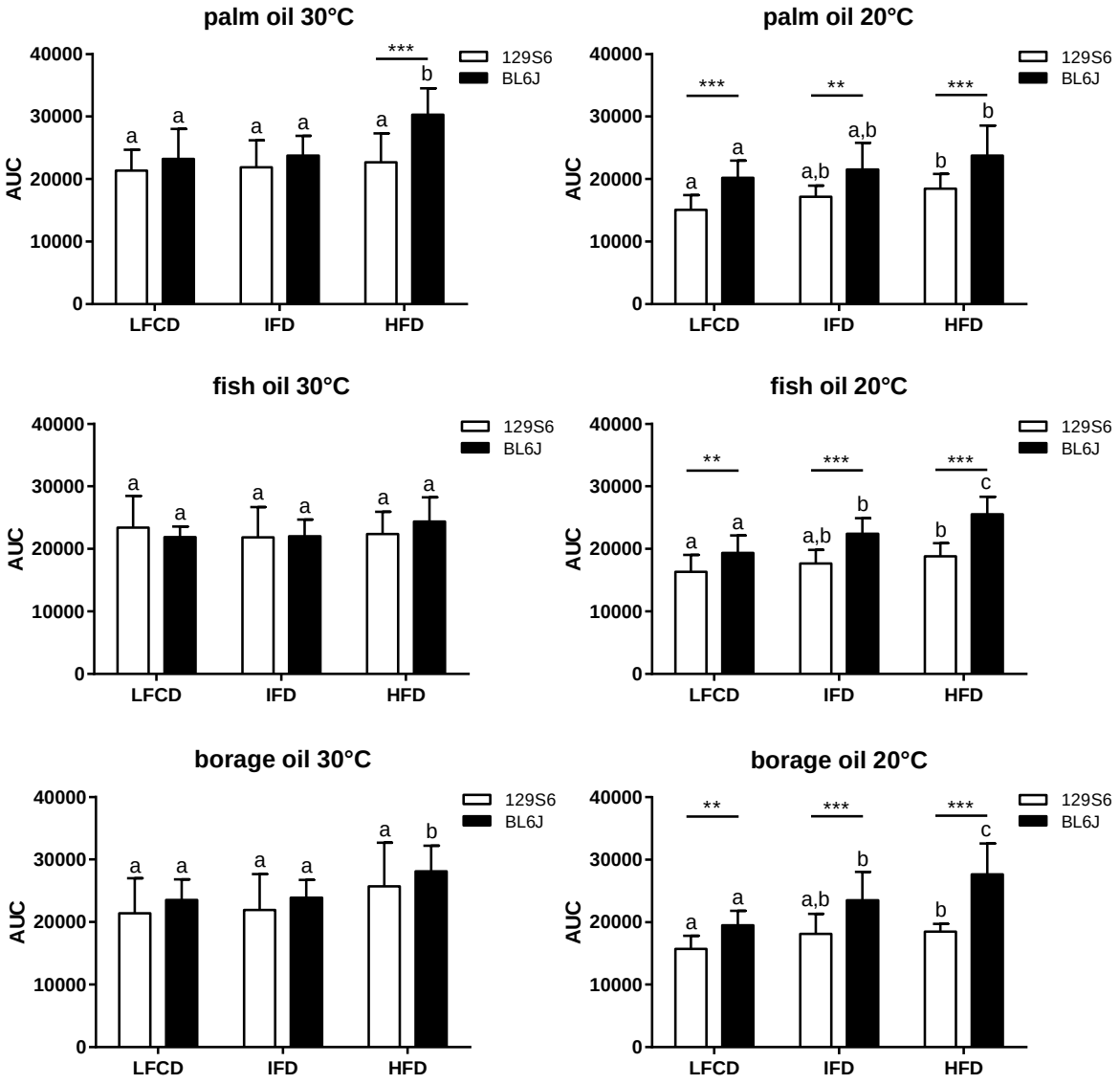

Figure 37: Glucose tolerance of 129S6 and BL6J mice. At the age of 8 weeks, mice were housed at 30°C and 20°C and gradually fed with LFCD, IFD and HFD. Each type of diet was fed for 4 weeks. Palm, fish and borage oil were contained as alternative fat sources in IFD and HFD (n=12). Glucose tolerance (AUC of blood glucose levels) was assessed at the end of each feeding interval. Each dataset was analyzed by Two Way RM ANOVA and Holm-Sidak post-test. Asterisks indicate significant difference between 129S6 and BL6J mice for the respective type of diet (** p<0.01; *** p<0.001). Printed characters indicate differences in glucose tolerance induced by dietary fat content within the respective strain (p<0.05).

At 30°C, glucose tolerance of 129S6 mice was not significantly affected by the dietary fat content, whereas glucose tolerance of BL6J mice was impaired by palm and borage oil-comprising HFD (Figure 37). Interestingly, this regulation led to a considerable

difference in glucose tolerance between palm oil-fed 129S6 and BL6J mice under HFD, indicating this fat source to affect glucose tolerance in a strain-specific manner.

Taken together, 129S6 and BL6J mice are two inbred mouse strains characterized by differential NST capacity. Elevated NST capacity of 129S6 mice may contribute to systemic energy expenditure. Consequently, elevated NST capacity may be accompanied by an increased capacity for glucose uptake into BAT and brite fat for enhanced Ucp1-mediated dissipation of energy, thus affecting blood glucose clearance and body mass accumulation. Such phenotype may be influenced by the source of dietary fat affecting Ucp1 expression in BAT and WAT. Indeed, body mass gain of BL6J mice fed a HFD at 20°C was modifiable by the source of dietary fat, indicating a strain-specific, synergistic interaction of fat source and housing temperature. Collectively, 129S6 and BL6J mice exhibited similar body mass gain in response to HFD-feeding. However, 129S6 mice were characterized by a consistently improved glucose tolerance when housed at 20°C, associating elevated NST capacity of this strain with a protective function in the regulation of systemic glucose tolerance. This putative, protective function of elevated NST capacity did not influence blood glucose clearance at 30°C under non-obesogenic conditions. As 129S6 but not BL6J mice were, however, protected from HFD-induced impairment of glucose tolerance at 30°C, elevated NST capacity of the first strain may provide a reserve capacity for the maintenance of systemic glucose homeostasis under obesogenic conditions. This effect was most pronounced when mice received a diet with intermediate n6/n3 ratio. Collectively, these results point towards a beneficial role for the thermogenic function of brown and brite adipocytes in the regulation of blood glucose clearance, which requires validation in a mouse model of impaired NST.

3.5 Glucose tolerance of Ucp1-KO mice

The capacity for NST is conferred by the presence of Ucp1. Ablation of Ucp1 in mice results in impaired BAT function, primarily characterized by the severe inability to defend body temperature in a cold environment due to the absence of NST [47]. As previous experiments have demonstrated, NST capacity differed in the WT inbred mouse strains 129S6 and BL6J and was moreover adaptively influenced by housing temperature. A similar relationship was identified for the regulation of glucose homeostasis: glucose tolerance was beneficially affected by mild cold-exposure in both strains. Moreover, 129S6 mice were less prone to an impairment of glucose tolerance in response to hypercaloric feeding. To test whether this phenotype is indeed dependent on NST, Ucp1-KO mice were employed. Among the three different mouse models used, NST capacity was highest in 129S6, intermediate in BL6J and negligible in Ucp1-KO mice. Thus, comparison of BL6J WT vs. KO mice not only mimicked the comparison of 129S6 vs. BL6J mice in terms of NST capacity (high vs. low), but also served as direct evidence for a role of BAT and brite fat function in the regulation of systemic glucose homeostasis.

At the age of 8 weeks, WT and Ucp1-KO mice bred on BL6J background were housed at 30°C and 20°C and subjected to LFCD-feeding. After 4 weeks, mice were challenged with IFD and HFD as described above (section 3.4.2). Importantly, only palm oil-comprising IFD and HFD was used

as the n6/n3 ratio in fish and borage oil-comprising IFDs and HFDs was extraordinary low and high, respectively. In palm oil-containing diets, this ratio was intermediate and most similar to the ratio of non-obesogenic LFCD, thus reducing the difference between different types of diets basically to the difference in fat content.

In the previous experiment involving 129S6 and BL6J mice, glucose tolerance of 129S6 mice was improved compared to BL6J mice when animals were housed at 20°C. This effect was consistent under both obesogenic (IFD and HFD) and non-obesogenic (LFCD) conditions (compare Figure 37). As expected, glucose tolerance in the present experiment tended to be gradually impaired by elevated dietary fat content at 20°C (Figure 38B). Differences between WT and Ucp1-KO mice were, however, not observed, indicating that glucose tolerance under mild cold-exposure is not affected by the thermogenic function of BAT and brite fat. In line with previous results (compare Figure 37), glucose tolerance of BL6J WT mice was impaired by HFD-feeding at 30°C (Figure 38B). In KO mice, glucose tolerance at 30°C was impaired by IFD and HFD, resulting in a significant difference in glucose tolerance between WT and KO mice under these conditions (Figure 38A and B).

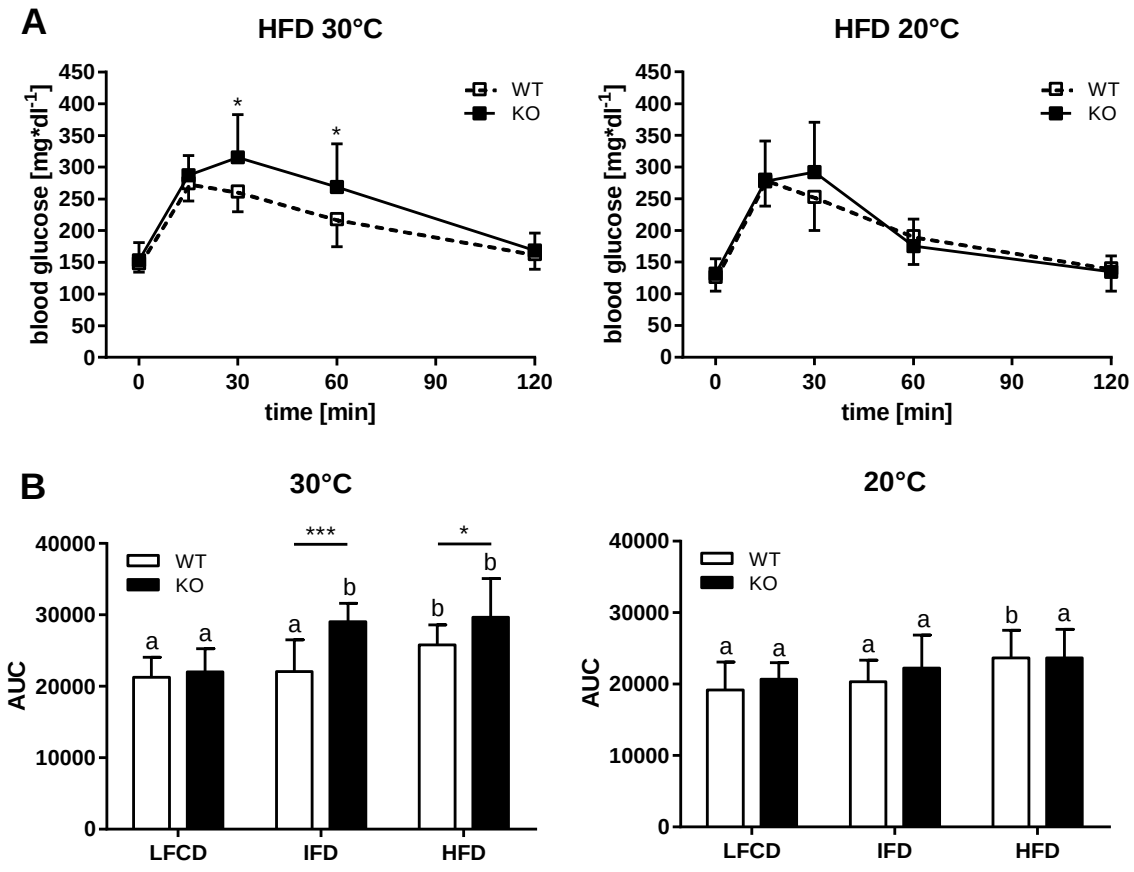

Figure 38: Glucose tolerance of WT and Ucp1-KO mice. At the age of 8 weeks, mice were housed at 30°C and 20°C and gradually fed with LFCD, IFD and HFD. Palm oil was used as fat source to increase the fat content of IFD and HFD compared to LFCD. Each type of diet was fed for 4 weeks. Glucose tolerance was assessed at the end of each feeding interval (n=8-10). (A) Blood glucose levels during oGTTs before (0 min) and after glucose gavage at the end of HFD-feeding. (B) Glucose tolerance (AUC of blood glucose levels) of WT and Ucp1-KO mice. All datasets were analyzed by Two Way RM ANOVA and Holm-Sidak post-test. Asterisks indicate significant difference between WT and KO mice (* $p<0.05$; *** $p<0.001$). Printed characters indicate significant effect of fat source within the respective genotype ($p<0.05$).

Insulin tolerance tests (ITT) were conducted during each of the three feeding intervals four days prior to oGTTs to assess differences in glucose tolerance in the context of insulin sensitivity (Figure 39). When mice were fed at 30°C, insulin sensitivity of WT mice was gradually impaired (Figure 39B), whereas this regulation was attenuated in Ucp1-KO mice. Consequently, insulin sensitivity under IFD was similar between WT and Ucp1-KO mice, whereas KO mice were more insulin sensitive than WT mice under HFD.

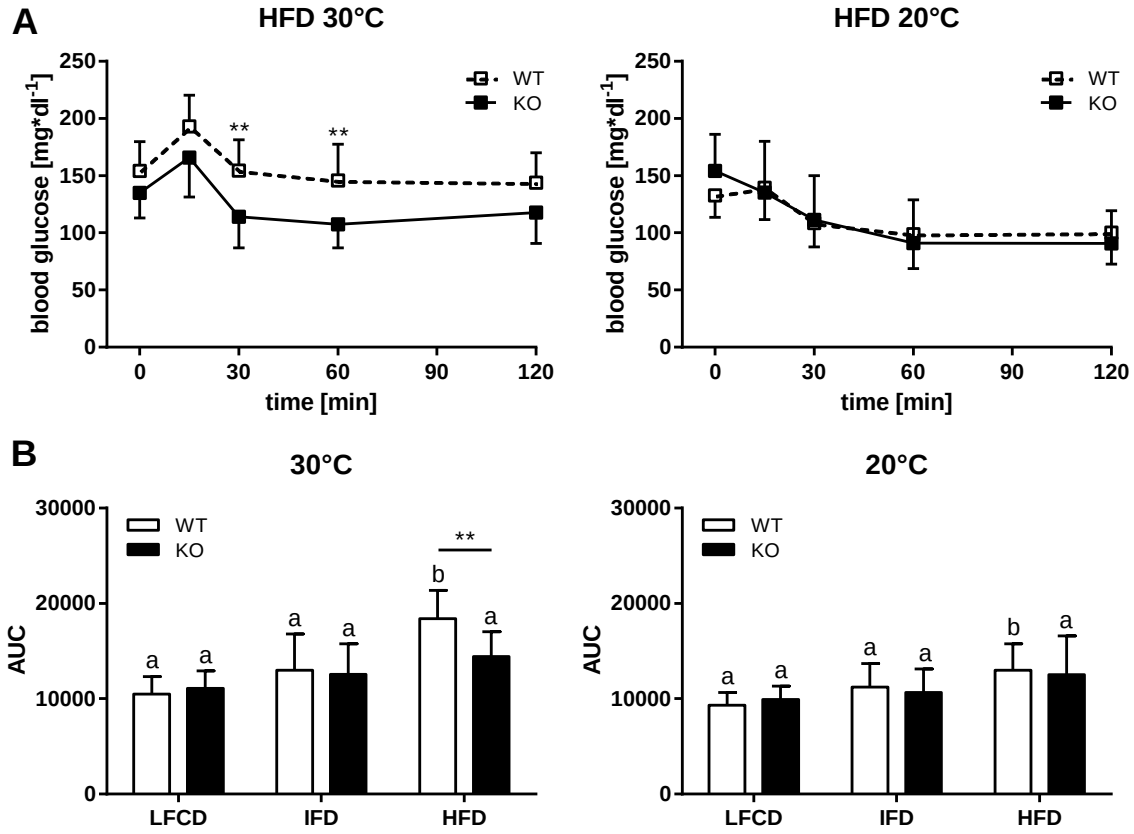

Figure 39: Insulin sensitivity of WT and Ucp1-KO mice. At the age of 8 weeks, mice were housed at 30°C and 20°C and gradually fed with LFCD, IFD and HFD. Palm oil was used as fat source to increase the fat content of IFD and HFD compared to LFCD. Each type of diet was fed for 4 weeks. Insulin sensitivity was assessed at the end of each feeding interval 4 days prior to oGTTs. (A) Blood glucose levels during ITTs of HFD-fed mice measured before (0 min) and after administration of insulin (n=8-10). Both datasets were analyzed by Two Way RM ANOVA and Holm-Sidak post-test. Asterisks (** p<0.01) indicate significant effect of genotype at the indicated time points. (B) Insulin sensitivity (AUC of blood glucose levels) of WT and Ucp1-KO mice. Single mice were not subjected to ITTs at the end of LFCD-feeding (LFCD: n=6-10; IFD and HFD: n=8-10). Data were thus analyzed by Two Way ANOVA and Holm-Sidak post-test. Asterisks indicate significant difference between WT and KO mice (** p<0.01). Printed characters indicate significant effect of fat source within the respective genotype (p<0.05).

Alterations in glucose tolerance at 30°C after transition from IFD to HFD were in WT and Ucp1-KO mice similarly regulated by alterations in insulin sensitivity (Figure 40A). Relatively improved insulin sensitivity of HFD-fed KO vs. WT mice likely prevented further exacerbation of glucose tolerance in KO mice at 30°C. This difference in insulin sensitivity may be largely explained by HFD-induced differences in adiposity (Figure 40B). However, independent from insulin sensitivity, glucose tolerance of KO vs. WT mice was impaired in response to both IFD and HFD-feeding at 30°C (Figure 40A). This indicates blood glucose clearance under hypercaloric

conditions to be affected by an insulin-independent glucose transport mechanism that requires the presence of Ucp1.

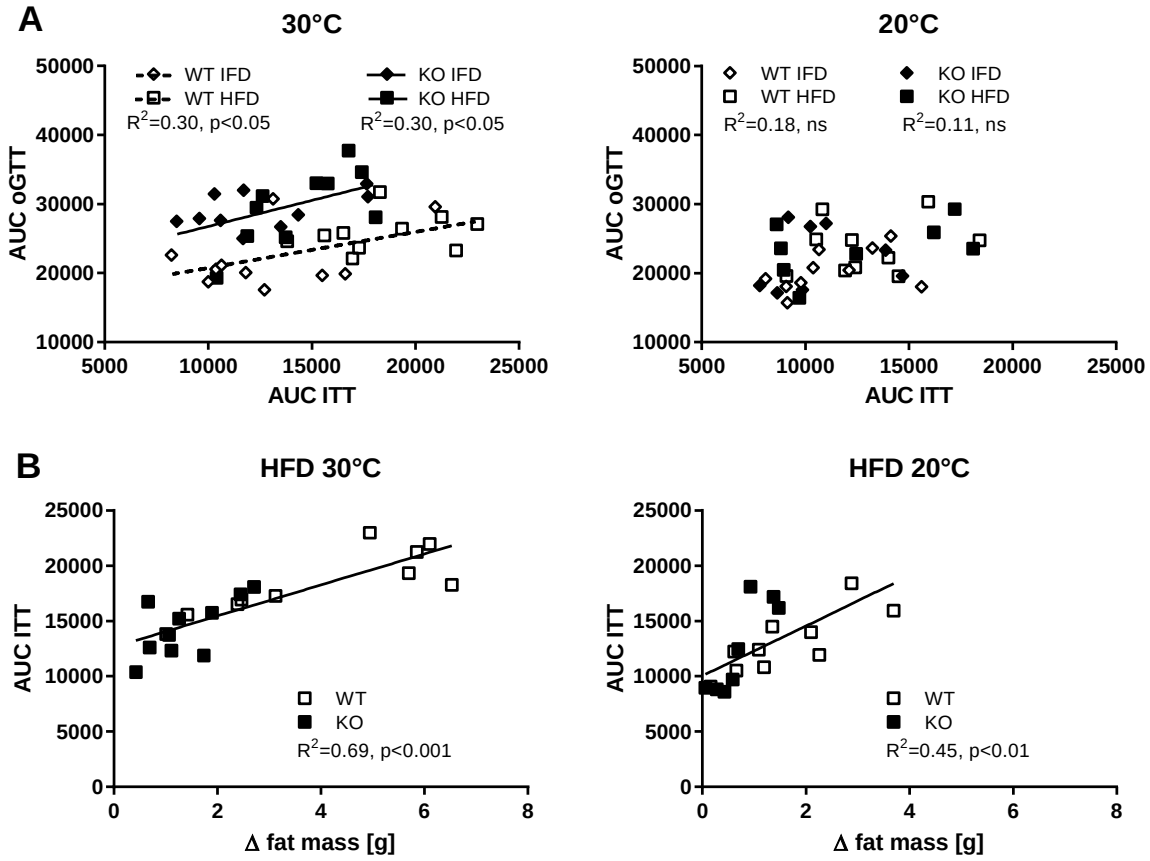

Figure 40: Relationship between glucose tolerance, insulin sensitivity and fat mass gain in WT and Ucp1-KO mice. At the age of 8 weeks, mice were housed at 30°C and 20°C and gradually fed with LFCD, IFD and HFD. Palm oil was used as fat source to increase the fat content of IFD and HFD compared to LFCD. Each type of diet was fed for 4 weeks. Insulin sensitivity and glucose tolerance were assessed within 4 days at the end of each feeding interval (n=8-10). (A) Relationship between glucose tolerance (AUC oGTT) and insulin sensitivity (AUC ITT) in WT and Ucp1-KO mice. R^2 (determined from the Pearson correlation coefficient) was calculated across IFD and HFD-fed mice of each genotype to investigate the influence of diet-induced alterations in insulin sensitivity on alterations of glucose tolerance. (B) Relationship between insulin sensitivity at the end of HFD-feeding and HFD-induced fat mass gain. In both datasets, R^2 (determined from the Pearson correlation coefficient) was calculated across all groups to investigate the influence of differential fat mass gain on insulin sensitivity.

Since BAT mediates DIT [106], ablation of Ucp1 may promote body mass gain in response to a HFD caused by an impaired ability to dissipate excess energy derived from food [107, 108]. In the present experiment, Ucp1-KO mice did not differ from WT mice in body mass development during LFCD and IFD-feeding, although KO mice tended to exhibit lower body mass at both housing temperatures (Figure 41A). In line with previous observations (compare Figure 33), feeding of palm oil-comprising HFD to BL6J mice at 20°C did not alter the rate of body mass gain compared to LFCD and IFD (Figure 41A), resulting in similar body mass development of WT and Ucp1-KO mice under mild cold-exposure. In contrast, WT mice exhibited significantly higher body mass accumulation than KO mice when the HFD was fed at 30°C. This differential body mass gain under HFD was largely influenced by differential fat mass gain (Figure 41B).

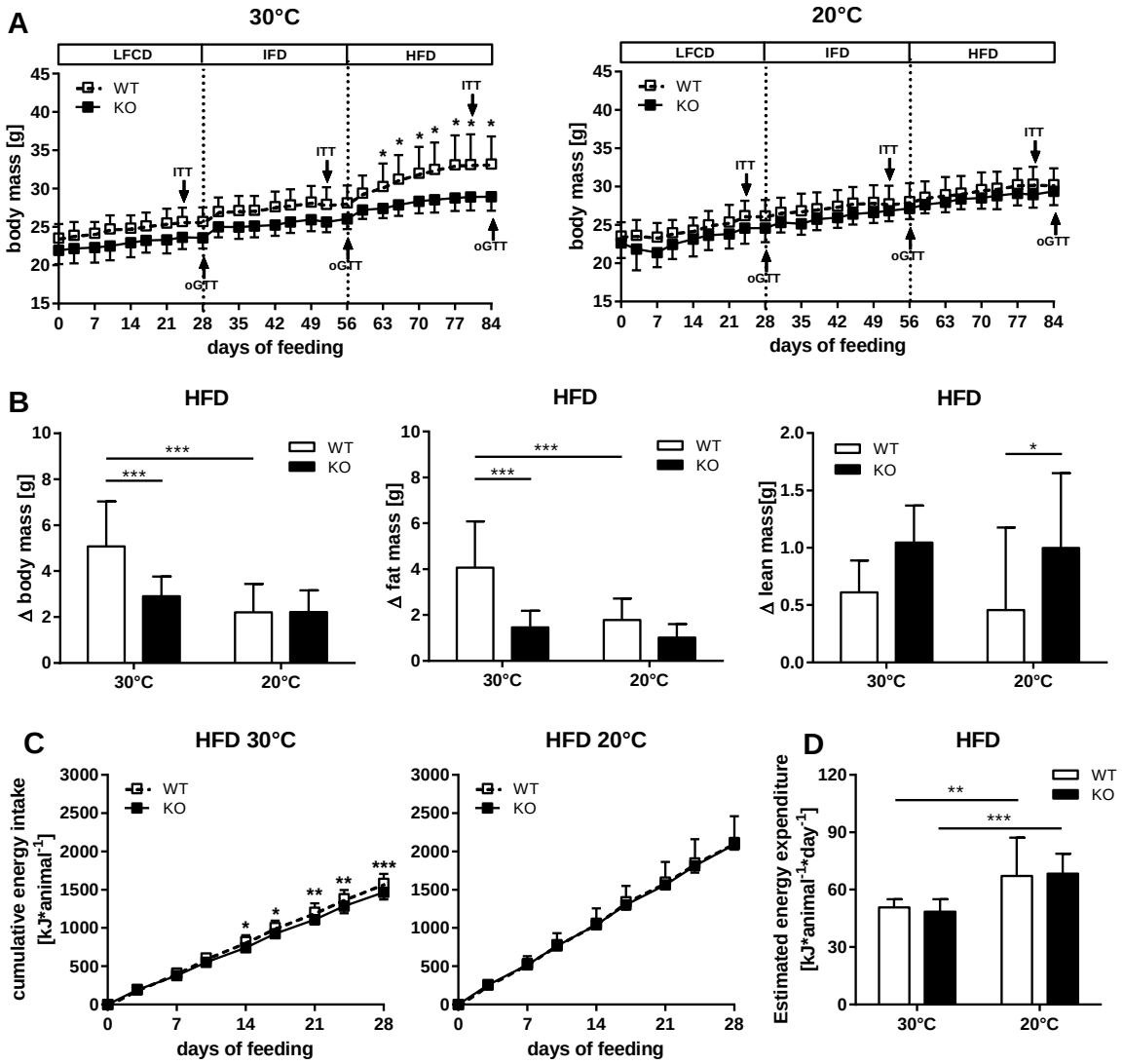

Figure 41: Effects of LFCD, IFD and HFD-feeding on body mass, body composition and food intake in WT and Ucp1-KO mice. At the age of 8 weeks, mice were housed at 30°C and 20°C and gradually fed with LFCD, IFD and HFD. Palm oil was used as fat source to increase the fat content of IFD and HFD compared to LFCD. Each type of diet was fed for 4 weeks (n=8-10). (A) Body mass development throughout the feeding period. Vertical dashed lines indicate diet change. ITTs and oGTTs were performed at indicated time points. Both datasets were analyzed by Two Way RM ANOVA and Holm-Sidak post-test. Asterisks indicate significant difference between WT and Ucp1-KO mice at indicated time points ($p<0.05$). (B) Body, fat and lean mass gain between beginning (day 56) and end (day 84) of HFD-feeding. Datasets were analyzed by Two Way ANOVA and Holm-Sidak post-test (* $p<0.05$; *** $p<0.001$). (C) Cumulative energy intake during HFD feeding. Both datasets were analyzed by Two Way RM ANOVA and Holm-Sidak post-test. Asterisks indicate significant difference between WT and KO mice at the indicated time points (* $p<0.05$; ** $p<0.01$; *** $p<0.001$). (D) Energy expenditure during HFD-feeding was estimated according to [204] in consideration of energy intake and changes in body composition. Data were analyzed by Two Way ANOVA and Holm-Sidak post-test (** $p<0.01$; *** $p<0.001$).

Ucp1-KO mice exhibited constantly reduced energy intake throughout HFD-feeding at 30°C (Figure 41C), cumulating in a total energy intake difference of 165 kJ between WT and KO mice (Table 15). As the total energetic costs for fat mass accumulation differed by 128 kJ, this difference in energy intake is sufficient to explain the observed differences in fat mass gain (Table 15). In line with published observations [108], estimated energy expenditure of HFD-fed WT and Ucp1-KO mice was increased by mild cold-exposure but similar between WT and

KO mice under both housing conditions (Figure 41D). These data indicate that differential fat mass accumulation of WT and Ucp1-KO mice in response to HFD-feeding at 30°C is predominantly influenced by differences in energy intake.

Table 15: Comparison of total energy intake and energetic costs of fat mass accumulation during HFD-feeding.

	WT 30°C	KO 30°C	WT 20°C	KO 20°C
Δ fat mass [g][1]	4.1 ± 2.0	1.5 ± 0.7	1.8 ± 0.9	1.0 ± 0.6
Energy required for fat mass deposition [kJ][2]	199.1 ± 98.3	71.1 ± 35.6	87 ± 45.9	49.4 ± 29.2
difference WT vs. KO	**128**		**37.6**	
Total energy intake [kJ]	1583 ±125	1418 ±179	1955 ±551	1957 ±300
difference WT vs. KO	**165**		**-2**	

Data represent mean ± standard deviation (n=8-10). [1]Fat mass gain between beginning (day 56) and end (day 84) of HFD-feeding. [2]Assuming portions of fat and protein of 90.8% and 0.79%, respectively, per g of adipose tissue [201], and requirements of 53.4 kJ and 52.9 kJ of metabolizable energy for deposition of 1 g fat and protein, respectively [202].

In summary, these data corroborate a distinct role for NST capacity in the regulation of systemic glucose tolerance. NST is provided by BAT, which dissipates energy as heat in response to reduced ambient temperature or hypercaloric feeding. The capacity for NST may be complemented by brite adipocytes in WAT. Since NST in BAT is supported by uptake of glucose from the blood circulation, increased NST capacity may result in enhanced glucose uptake and metabolization in BAT and brite fat, thus improving blood glucose clearance. The results presented here provide direct and indirect evidence for such relationship using mouse models of differential NST capacity. In this regard, NST capacity was found to be unaffected by monogenic ablation of Cox7a1, whereas the inbred mouse strains 129S6 and BL6J were identified as polygenic model of differential NST capacity. Under mild cold-exposure, 129S6 mice exhibited improved blood glucose clearance compared to BL6J mice. This effect was observed under obesogenic and non-obesogenic conditions, not modifiable by the source of dietary fat and associated with differences in strain-specific NST capacity. This phenotype was, however, not observed in WT and NST-deprived Ucp1-KO mice, indicating glucose tolerance under mild cold-exposure to be unaffected by NST capacity. At thermoneutral environment, glucose tolerance of 129S6 and BL6J mice was similar under non-obesogenic conditions, an effect that was as well observed when WT and Ucp1-KO mice were compared. Glucose tolerance of 129S6 mice was unaffected by hypercaloric feeding, whereas glucose tolerance of BL6J mice was conditionally impaired. This diet-induced impairment of glucose tolerance was considerably more pronounced in Ucp1-KO mice. Impaired glucose tolerance of Ucp1-KO vs. WT mice did not result from reduced insulin sensitivity of KO mice, suggesting the existence of an insulin-independent glucose transport mechanism that benefits glucose tolerance in the presence of Ucp1. This mechanism does not influence glucose tolerance under non-obesogenic conditions but attenuates the impairment of glucose tolerance in response to hypercaloric feeding. As Ucp1-KO mice exhibited lower body mass gain than WT mice at 30°C in response to HFD, these results indicate that NST capacity has a beneficial effect for systemic glucose homeostasis but not for diet-induced body mass accumulation.

4 DISCUSSION

4.1 Background of the present work

The recent rediscovery of functional brown adipose tissue (BAT) in humans [90-93] has revived the interest in its function and physiology. Facing the burden of the global prevalence of obesity and type 2 diabetes mellitus, its ability to dissipate energy by metabolization of lipids and glucose renders BAT a target for weight loss and the improvement of metabolic health. In fact, there is growing evidence that activation or recruitment of BAT in human subjects promotes energy expenditure, whole-body insulin sensitivity and glucose disposal [113, 114, 142]. Moreover, transplanted human brite adipocytes derived from capillary networks are capable of improving glucose tolerance in mice [205]. Thus, enhanced BAT function is hypothesized to prevent or even cure pathologic states of hyperglycemia, although demonstration of direct evidence for such relationship in humans has not yet been achieved. In mice, glucose uptake into BAT is of fundamental importance to maintain normothermia in a subthermoneutral environment [206]. Elevated mass of BAT and brite fat improves glucose tolerance [118, 119] whereas it is impaired in mice with reduced thermogenic BAT function [207-209]. This suggests a gradual effect of non-shivering thermogenesis (NST) capacity on glucose uptake and thus blood glucose clearance. Cold-exposure is a strong stimulant of NST capacity in rodents and so far the predominant method of choice for human interventions owing to the lack of sufficiently characterized pharmacological or effective nutritional stimulants. The identification and implementation of novel compounds for a widespread application requires characterization of molecular pathways as well as the identification and targeted manipulation of components that drive activation of BAT and brite adipogenesis. The present thesis therefore aimed to (1) clarify the role of the cold-induced protein Cox7a1 in the recruitment of NST capacity to possibly provide a novel target, (2) test the efficacy of a nutritional intervention in brite adipogenesis and (3) augment and specify the current body of evidence for a direct relationship between BAT function and glucose homeostasis by the use of mouse models with differential NST capacity.

4.2 Cox7a1 has no essential role for BAT function

Activation of BAT during cold-exposure is characterized by adaptive upregulation of proteins involved in mitochondrial respiratory thermogenesis as the key molecular pathway that discriminates white adipose tissue (WAT) and BAT [146]. The rate-limiting enzyme within this system, cytochrome *c* oxidase (CCO), is capable of adjusting its activity on the qualitative level by phosphorylation, allosteric regulation and the expression of isoforms for at least 5 of its 13 subunits [150]. The function of subunit 7a (Cox7a) can be fulfilled by Cox7a1 or Cox7a2. The latter is ubiquitously expressed whereas Cox7a1 is particularly abundant in skeletal muscle and heart. Ablation of Cox7a1 blunts CCO activity in these tissues [160, 161].

Cox7a1 is one of several genes, which are characterized by consistently enriched expression in BAT vs. WAT as well as cold-induced upregulation in WAT during browning [162]. Thus, this set of brown adipocyte marker genes serves as transcriptional fingerprint for the identification of

both brown and brite adipocytes. Among these genes, uncoupling protein 1 [47], fatty acid binding protein 3 [210], carnitine palmitoyltransferase 1b [211], type 2 iodothyronine deiodinase [212], and acyl-CoA thioesterase 11 [213] affect BAT function in knockout mice, thus extending their role from a sheer marker towards a protein with functional relevance within the thermogenic molecular machinery. The role of Cox7a1 has not been investigated so far. Interestingly, Cox7a1 is a cold-responsive protein of BAT whereas expression of its paralogue is hardly affected by ambient temperature [146]. Moreover, the levels of Cox7a1 and Cox7a2 mRNA expression in BAT resembled those in heart (Figure 8A), indicating these isoforms to be of similar importance for these two tissues characterized by exceptional oxidative capacity. Upregulation of Cox7a1 in cold-activated BAT may thus contribute to NST by replacing Cox7a2 to adjust CCO activity to increased uncoupling protein 1 (Ucp1) mediated proton conductance. Wildtype (WT) and Cox7a1 knockout (KO) mice were employed to test this hypothesis.

Mice were subjected to different temperature regimens and BAT function was characterized on the molecular level focusing on CCO activity and Ucp1 protein levels in tissue homogenates. As expected, Ucp1 expression was lowest under thermoneutral conditions and followed a gradual upregulation in response to decreased housing temperature (Figure 9C). The activity of CCO was regulated in an identical manner (Figure 10), likely to compensate for increased Ucp1-mediated proton leak. Upregulation of CCO activity during cold-acclimation may principally be achieved by different physiological mechanisms: an increased abundance of mitochondria per cell (mitochondrial biogenesis), an increased abundance of assembled CCO per mitochondrial mass or regulatory features affecting CCO activity such as the expression of subunit isoforms. Cox4i2 represents the lung-specific isoform of subunit 4, whereas Cox6a2 and Cox7a1 represent the heart-type isoforms of subunits 6a and 7a, respectively, with enriched expression in heart and skeletal muscle. Single ablation of these isoforms reduces CCO activity in the mentioned tissues [160, 161, 214-216]. Despite its strong induction in cold-activated BAT, ablation of Cox7a1, however, did not affect CCO activity at any temperature acclimation state. In heart, Cox7a2 protein is 5-fold upregulated to compensate for deletion of Cox7a1 despite unaffected Cox7a2 mRNA levels, but this response fails to restore CCO activity [160]. Similarly, Cox7a2 mRNA levels were not affected by Cox7a1-KO in BAT (Figure 8B). Protein levels of Cox7a1 and Cox7a2 were not measured due to a high sequence identity (about 65%) within the mature peptides excluding the discrimination of both isoforms by standard analysis methods such as Western Blot. A possible upregulation of Cox7a2 protein may thus be capable of replacing Cox7a1 function in BAT but not in heart.

To investigate the effect of Cox7a1 ablation on the organismic level, NST capacity was determined in WT and KO mice in response to a single high-dose injection of norepinephrine (NE). Male and female mice were subjected to two consecutive measurements, which were conducted in room temperature-acclimated state and after acute (4 days) or chronic (28 days) housing at 4°C. In line with previous observations [188], both basal metabolic rate and NST capacity were stepwise increased during cold acclimation (Figure 11B) to maintain body temperature (Figure 11C). Since murine brite adipocytes represent an additional pool of

thermogenic cells [20, 21], one may speculate whether increased NST capacity was the result of Ucp1 expression in both BAT (Figure 9C) and WAT (Figure 14). None of the tested parameters was, however, affected by the presence or absence of Cox7a1, suggesting that Cox7a1 is not required for the thermogenic function of brown and brite adipocytes.

Thermogenic BAT function was studied in adult mice of a constitutive knockout mouse model and putative defects in NST may thus be compensated by counterregulatory mechanisms. In mouse models with characterized BAT defect, increased browning of WAT may partially restore thermogenesis [188, 217, 218]. Brite fat appeared, however, normal in Cox7a1-KO mice (Figure 13) and NE-stimulatable NST capacity did not differ between WT and KO mice, thus questioning the need for compensatory thermogenesis. Newborn mice, devoid of any adaptively acquired counteractive function in other tissues, were subjected to a thermal imaging approach to test this hypothesis. The method was validated using pups of a Ucp1-KO mouse line characterized by complete absence of NST during adult life [47]. Skin surface temperature in the interscapular region (iSST) was employed as measure for BAT-derived heat production. In line with imaging experiments in adult Ucp1-KO mice [219], low iSST was confirmed in KO pups compared to WT and heterozygous (HET) littermates (Figure 12C), indicating the capability of this method to detect defective NST in an early stage of life. Cox7a1 is first detectable on embryonic day 17 [159] and its ablation may thus similarly affect thermogenesis. There were, however, no differences in iSST between WT, HET and KO animals of neonate Cox7a1 litters (Figure 12E), indicating that Cox7a1 influences adaptive thermogenesis neither in adult nor in newborn mice. Thus, Cox7a1 is dispensable for NST and its ablation does not require the counteracting function of other tissues.

Beyond its classical role in the maintenance of body temperature, BAT is involved in diet-induced thermogenesis (DIT) [106]. Irrespective of any thermoregulatory requirement, BAT is stimulated by increased sympathetic activity in response to hypercaloric feeding to dissipate excess energy from food [220]. Conversely, impaired BAT function is hypothesized to result in excessive body mass accumulation. Such phenotype may be masked at room temperature when adaptive thermogenesis is obligatory required irrespective of its origin. Indeed, Ucp1-KO mice with impaired BAT function are lean at room temperature [108] but may become obese when fed a high-fat diet (HFD) under thermoneutral conditions [107, 108]. To further investigate BAT function in Cox7a1-KO mice, animals were housed under thermoneutral conditions and subjected to a feeding regimen known to promote diet-induced obesity (DIO) and impaired glucose tolerance when fed at room temperature [199]. As expected, HFD-fed mice gained more body mass than mice on low-fat control diet (LFCD) throughout the feeding period (Figure 16B). Neither total body mass gain (Figure 16D) nor glucose tolerance (Figure 17) at the end of HFD-feeding was, however, influenced by the presence or absence of Cox7a1. These results demonstrate that Cox7a1 is not required for the metabolic response to HFD-feeding.

WT and Cox7a1-KO mice were bred on C57BL/6J background. Mice of this strain are typically prone to HFD-induced impairment of glucose tolerance when housed at room temperature

[199, 221]. Thus unexpectedly, glucose tolerance was similar between LFCD and HFD-fed mice housed at thermoneutrality (Figure 17B). As will be discussed below (section 4.5), glucose tolerance in LFCD-fed state is reduced by thermoneutral housing temperature, possibly as consequence of minimized NST capacity and thus BAT-mediated glucose uptake. Accordingly, this phenotype probably resulted from impaired glucose tolerance in LFCD-fed mice rather than an improved one in HFD-fed mice.

Taken together, Cox7a1 is a widely used brown and brite adipocyte marker gene and a cold-responsive protein of BAT. Maximal CCO activity in heart and skeletal muscle requires high Cox7a1 abundance in these tissues. However, Cox7a1 was not required for CCO activity in BAT, for BAT-derived heat production in neonate and adult animals, for brite adipogenesis and for the response to hypercaloric feeding. Thus, Cox7a1 is dispensable for BAT function. The function of subunit 7a for CCO activity in BAT is likely exerted by Cox7a2 only, which in many tissues throughout the body is the sole isoform for this subunit. Conditional knockout of either one or the other isoform may help to clarify the role of this subunit for tissue-specific CCO activity and its physiological consequences.

4.3 The capacity for NST differs between 129S6/SvEvTac and C57BL/6J mice

The function of BAT is widely hypothesized to influence systemic glucose homeostasis in mice and men [113, 119, 222]. BAT provides NST, which is supported by the oxidation of glucose taken up from the blood circulation. An increased potential for heat production in BAT may augment glucose uptake into the tissue thus enhancing blood glucose clearance. Moreover, this effect may be complemented by brite adipocytes representing an additional pool of thermogenic cells. Two mouse strains, C57BL/6J (BL6J) and 129S6/SvEvTac (129S6), were characterized with respect to their NST capacity constituting a polygenic approach to test this hypothesis.

BL6J and 129S6 are two common inbred mouse strains widely used for a variety of scientific purposes. The first is bred by the Jackson Laboratory since decades and represents one among several substrains of the C57BL parent strain generated in 1921 by Clarence Cook Little [223]. The latter, 129S6, is one among various 129 substrains that is distinctly bred by Taconic since 1992 originating from a cross of two substrains of the 129/SvEv stock of Martin Evans, which is itself derived from the stock of Leroy Stevens [224]. 129 strains differ from BL6 strains on the whole-genome-level by exhibiting more than 800,000 indels and more than 4 million single nucleotide polymorphisms resulting in at least 25,000 structural variants [225]. This genetic diversity causes mice of the 129S6 strain to display an improved ability for brite adipogenesis during postnatal development [226]. Brite adipocytes are functionally thermogenic [20, 21] and their abundance may thus modulate adaptive heat production. Mice of the 129S6 and BL6J strains were employed to study the nature of this browning phenomenon during adult life and to investigate its relationship to NST capacity.

The capacity for NST was determined by means of a NE-test. Mice were acclimated to 30°C to eliminate ambient temperature as important factor in the recruitment of NST. Mice of the

129S6 strain exhibited an approximately 40% increased NST capacity (Figure 22). NE is the physiological activator of NST and its administration in high dose results in a general activation of adrenoreceptors throughout the body. As evident in Ucp1-KO mice, the general pharmacological response evoked by NE is negligible [227, 228] and NE-induced oxygen consumption can be interpreted as almost entirely Ucp1-dependent. Given that the capacity for BAT-derived heat production at 30°C was likely similar in both strains as indicated by Ucp1 protein levels and CCO activity (Figure 21), this strain difference in NST capacity may originate from other Ucp1-competent tissues. In fact, 129S6 mice display considerably higher Ucp1 expression in skeletal muscle resulting from intermuscular fat [229]. Moreover, the abundance of multilocular cells in subcutaneous inguinal WAT was higher in 129S6 than BL6J mice (Figure 19), indicating the higher postnatal predisposition for brite adipogenesis in 129S6 mice [226] to persist in adult life. This strain difference is even maintained *in vitro* in differentiated primary inguinal adipocytes along with a higher Ucp1-dependent oxygen consumption in cells derived from 129S6 vs. BL6J mice [230]. Compensatory browning of WAT in mouse models of specific BAT ablation is capable of restoring NST capacity [218]. Thus, the higher NST capacity in 129S6 mice was likely caused by a higher abundance of brite adipocytes and/or ectopic Ucp1 expression in muscle. This phenotype renders the comparison of both mouse strains at thermoneutral housing temperature a polygenic alternative to monogenic gain- or loss-of-function models to distinctly investigate whether a differential predisposition for brite adipogenesis is capable of modulating energy expenditure to affect body mass development or glucose tolerance.

Housing at subthermoneutral ambient temperature physiologically recruits NST capacity in mice. Mild cold-exposure consequently increases the capacity for NE-stimulatable heat production in BL6J mice [188]. Mice of the 129S6 and BL6J strains were acclimated to 20°C representing a mild cold-challenge to investigate whether differences in NST capacity, which were observed at 30°C, are influenceable by means of environmental stimulation. The capacity for NST was not determined by NE-test when mice were housed at 20°C. Gene expression of Ucp1 (Figure 20) and the abundance of multilocular cells (Figure 19) in WAT as well as Ucp1 protein levels in BAT (Figure 21B) were, however, higher in 129S6 than BL6J mice. Given the higher NST capacity of 129S6 mice at 30°C, the observed strain differences in BAT and WAT at 20°C were likely sufficient to maintain or even amplify this magnitude of difference in NST capacity.

Environmental effects on NST capacity can be mimicked by targeted activation of the β_3-adrenergic receptor predominantly expressed by brown and white adipocytes [231, 232]. To pharmacologically recapitulate the effect of mild cold-exposure, 129S6 and BL6J mice were subjected to CL-316243 (CL) treatment thus receiving a highly specific β_3-adrenergic agonist [233]. Mice were acclimated to 30°C prior to treatment to minimize endogenous NST capacity. CL was repeatedly administered over 7 days in four different doses to characterize the strain-specific responsivity. As expected [19, 234], Ucp1 expression was stimulated in BAT and WAT by repeated CL-administration reaching maximal levels at 0.2 mg/kg/day in both tissues

and both mouse strains (Figure 24A and Figure 25B). Higher Ucp1 expression was observed in 129S6 mice under all conditions, supporting previous observations on their higher potential to adaptively recruit NST. Of note, high-dose CL-administration (5 mg/kg) was detrimental to 129S6 but not BL6J mice within 24 hours after the first injection. As evident from experiments with 2,4-dinitrophenol, overly acute stimulation of mitochondrial uncoupled respiration is capable of inducing hyperthermia and death [235, 236]. In fact, a single CL-administration acutely activates Ucp1-mediated thermogenesis [47, 237, 238]. Detrimental effects in 129S6 mice thus likely originated from acute hyperthermia that was promoted by hindered heat loss at 30°C housing temperature in response to a single, high dose of CL, which stimulated heat production by high basal levels of Ucp1 in BAT and WAT. This phenotype underlines the physiological significance of differential NST capacity.

In summary, 129S6 and BL6J are two inbred mouse strains characterized by differential NST capacity. Mice of the 129S6 strain had a higher NST capacity when acclimated to 30°C, which may originate from their higher abundance of brite adipocytes in WAT. Moreover, this strain had the ability to express Ucp1 at a higher level in BAT and WAT when these tissues were environmentally or pharmacologically stimulated, indicating a higher potential for the adaptive recruitment of NST. Thus, comparison of 129S6 and BL6J mice constitutes a polygenic model to investigate the systemic effect of differential BAT and brite fat function.

4.4 The dietary fatty acid composition affects the production of browning-associated oxylipins in WAT of BL6J mice

Brite adipocytes are functionally thermogenic [20, 21] and their abundance in thermoneutral environment likely caused 129S6 mice to exhibit a higher NST capacity than BL6J mice. This phenotype may confer 129S6 mice an improved capacity for blood glucose uptake, which may in turn affect glucose homeostasis. Browning of WAT is dependent on the presence of cyclooxygenase (COX) and associated with the COX-mediated production of prostaglandin E_2 (PGE_2) and prostaglandin I_2 (PGI_2), two arachidonic acid (AA) derived prostaglandins of the n6 series secreted by mature adipocytes to stimulate brite differentiation of precursor cells [165, 166, 174-176]. Fatty acids of the n6 and n3 series compete to serve as substrate for COX [179, 180], resulting in the production of different eicosanoid subtypes depending on the particular precursor fatty acid (compare Figure 6). Mice of the 129S6 and BL6J strains were fed with diets characterized by differential fatty acid composition to investigate whether strain-specific differences in brite adipocyte abundance are further modifiable by means of a nutritional intervention thus affecting NST capacity.

Mice of both strains were housed under thermoneutral conditions and fed with LFCD or an intermediate-fat diet (IFD) characterized by moderately elevated fat content via the addition of an experimental oil. A diet rich in the AA-precursor γ-linolenic acid (GLA) reduces body fat accumulation in rats [239, 240], possibly promoted by increased Ucp1-mediated energy expenditure in BAT [240]. Borage oil, a rich source of GLA [241], was used as one experimental fat source to study the effects of an n6-enriched diet on Ucp1 expression in WAT,

hypothesizing the increased formation of AA from GLA, which may favor the formation AA-derived oxylipins to drive browning. Fish oil serves as rich source of the n3 fatty acids eicosapentaenoic (EPA) and docosahexaenoic acid (DHA) [241]. Fish oil consistently attenuates body and fat mass accumulation when administered to rodents, an effect that is discussed to involve Ucp1-dependent [242] or independent mechanisms [243-245] in WAT. Fish oil was used as alternative experimental fat source to directly compare and evaluate the efficacy of n3 vs. n6 fatty acids in the recruitment of brite adipocytes. These effects were compared to an IFD comprising palm oil, characterized by the complete absence of GLA, EPA and DHA (see Table 4).
All IFDs were fed for 4 weeks. Effects on Ucp1 expression in BAT and WAT were faint and subject to large variation. Although IFD-feeding consistently blunted Ucp1 expression in WAT of both mouse strains, borage-containing IFD was capable of attenuating this phenotype in BL6J but not 129S6 mice (Figure 27), indicating a strain-specific effect of dietary GLA supplementation. Samples of WAT of IFD-fed mice were subjected to oxylipin analysis to see whether this phenotype is related to differential eicosanoid production. In line with previous observations [245, 246], supplementation of mice with n3 fatty acids via a fish oil-comprising diet considerably increased the portion of n3-derived metabolites in WAT compared to other diets (Figure 30). The percentage of n6 and n3-derived metabolites was comparable between palm and borage oil-fed mice. Several individual oxylipins were, however, particularly enriched in response to borage oil administration (Table 13). As these metabolites were almost exclusively derived from AA, GLA supplementation via borage oil appears to efficiently trigger the formation of AA and its downstream metabolites, and to selectively affect brite adipocyte abundance in BL6J mice.
The potential of oxylipins in WAT browning is virtually unexplored. To date, PGE_2 and PGI_2 are the best described candidates with putative browning potential in murine models [165, 166, 174, 176, 247]. Ambivalent results were obtained in a human cellular model of brite adipogenesis where browning is inhibited by PGE_2 [194] and promoted by a PGI_2-analogue [248]. In the present study, Ucp1 expression in WAT of BL6J mice was related to the abundance of both PGE_2 and 6-keto-$PGF_{1\alpha}$ (Table 14), representing a stable, inactive metabolite of PGI_2 [168], supporting both compounds as putative, endogenous browning agents. Further candidate compounds associated with Ucp1 expression in BL6J mice were prostaglandin A_1 (PGA_1), thromboxane B_2 (TXB_2), lipoxin A_4 (LxA_4) and 8-iso prostaglandin A_2 (8isoPGA$_2$) (Table 14). Interestingly, all these compounds almost exclusively represent COX-derived metabolites (compare Figure 6) partially enriched in WAT of borage-fed mice (Table 13), none of which associated with Ucp1 expression in WAT of 129S6 mice. Brite adipogenesis is promoted by COX, which is induced in WAT in a cold environment or upon β_3-adrenergic stimulation [165, 166]. One may speculate whether dietary GLA specifically fuels this COX-pathway in BL6J mice thus promoting brite adipocyte formation via AA-derived oxylipins.
In 129S6 mice, Ucp1 expression was associated with the abundance of 5-hydroxyeicosatetraenoic acid (5-HETE), 15-HETE, 5-oxo-eicosatetraenoic acid (5-oxo-ETE), 5,6-dihydroxy-eicosatetraenoic acid (5,6-DiHETE) as well as epoxyeicosatrienoic acids (EETs)

(Table 14). Except for 5,6-DiHETE, all these compounds were not specifically enriched in a certain diet-group (Table 13) and exclusively obtained from COX-independent metabolization (compare Figure 6). Given that Ucp1 expression was also higher in IFD-fed 129S6 mice than in BL6J mice (Figure 27), these respective compounds may contribute to the development and maintenance of elevated basal levels of brite adipocytes in 129S6 versus BL6J mice.

Mechanistically, PGA_1, 5-oxo-ETE, 15-HETE as well as EETs have been shown to interact with peroxisome proliferator-activated receptor (PPAR) γ [249-252]. Activation of PPARγ in WAT stimulates the expression of Ucp1 [10, 253, 254]. Consequently, these oxylipins may influence brite adipocyte abundance in a PPARγ-dependent mechanism thus complementing PGE_2 and PGI_2 as oxylipin candidate compounds with possible browning effect. Additionally, browning of WAT under cold-exposure was recently shown to depend on catecholamines secreted by alternatively activated macrophages attracted to WAT via interleukin-4 (IL-4) secreted by resident eosinophils [255, 256]. Moreover, IL-4-recruited macrophages promote browning of WAT by secretion of 9-hydroxyoctadecadienoic acid (9-HODE) and 13-HODE, both of which are oxylipin species serving as ligands for PPARγ [257]. Since 5-oxo-ETE functions as very potent eosinophil chemoattractant and activator [258, 259], one may speculate whether this compound is capable of initiating a coordinated browning process via such eosinophil-IL-4-macrophage-dependent pathway that may be potentiated by other compounds in a PPARγ-dependent manner.

Taken together, the oxylipin profile produced in WAT of mice is modifiable by dietary fatty acid composition. A borage oil-comprising diet rich in GLA favored the production of AA-derived compounds, some of which may contribute to browning of WAT in BL6J mice. In contrast, brite adipocyte abundance in 129S6 mice was not modifiable by the source of dietary fat and associated with other AA-derived oxylipin species that may discriminate the browning potential of these mouse strains. The present study supports the suggested roles of PGE_2 and PGI_2 in murine WAT browning and reveals several new candidate compounds that may drive Ucp1 expression. Their particular mechanism of action as well as their source (mature adipocytes, endothelial cells or immune cells) and their actual browning potential remain to be clarified in future studies. As 129S6 and BL6J mice represent mouse strains of differential NST capacity, the modification of dietary fatty acid composition may influence their capability for Ucp1-dependent heat production and thus metabolic effects related to energy expenditure.

4.5 129S6 mice have a better glucose tolerance than BL6J mice

Elevated mass of BAT and brite fat beneficially affects body mass development and glucose tolerance in mice [118, 119, 260-262]. This effect may originate from enhanced energy expenditure in these tissues, causing an increased uptake of glucose from the bloodstream to support Ucp1-dependent heat production. Mice of the 129S6 strain were shown to exhibit a higher NST capacity than BL6J mice, a phenotype that may consequently result in an improved ability for glucose uptake into BAT and brite fat, which may in turn affect glucose homeostasis.

Mice of the 129S6 and BL6J strains were subjected to a feeding experiment to investigate the systemic effect of differential NST capacity on body mass development and glucose tolerance.
Mice of both strains were initially fed with LFCD at 30°C or 20°C housing temperature. LFCD-feeding was followed by the administration of IFDs characterized by differences in the dietary fatty acid composition aiming at the modulation of brite adipocyte abundance via fatty acid-derived oxylipins. Mice were challenged with HFDs to elucidate the effect on diet-induced body mass accumulation. Mice of all diet-groups gained body mass at a similar rate when HFDs were administered at 30°C. Interestingly, body mass accumulation of BL6J but not 129S6 mice was influenceable by the source of dietary fat when HFDs were administered at 20°C (Figure 33). This effect may originate from the uncommon experimental setup of the present study, owing to the period of IFD-feeding. Indeed, the same type of palm oil-comprising HFD induces a marked alteration in the rate of body mass gain in the same stock of BL6J animals when LFCD-feeding directly precedes HFD-feeding at 23°C [199]. In the present study, however, the rate of body mass gain of palm oil-fed BL6J mice housed at 20°C was quite similar during LFCD, IFD and HFD-feeding. Similarly, fish oil administration is generally considered to attenuate body and/or fat mass gain in rodents in a variety of settings [263]. Such protective effect was not observed in the present study. Thus, differential body mass development of BL6J mice may originate from a strain-specific 'priming effect' of IFDs that is synergized by mild cold-exposure and preconditions the organism for body mass gain under HFD-feeding.
Mice of the 129S6 strain were previously shown to gain less body mass than BL6 mice when fed a HFD [203]. In the present study, body mass gain under HFD was, however, largely comparable between 129S6 and BL6J mice at either housing temperature irrespective of the dietary fat source (Figure 35A). In fact, the susceptibility of 129S6 mice to DIO was recently shown to be influenced by compositional changes of the gut microbiota evoked by accommodation in the respective local environment [264]. Indeed, breeding of mice in different locations is capable of generating striking differences in microbiota composition of the same mouse strain [265, 266]. Thus, similar body mass gain of mice in the present study may arise from a local environment that abrogates differences between 129S6 and BL6J mice previously observed in other facilities.
BAT mediates DIT [106] and elevated NST capacity may therefore attenuate diet-induced body mass accumulation [107]. Mice of the 129S6 strain are characterized by elevated NST capacity compared to BL6J mice, but mice of both strains exhibited similar body mass gain in response to HFD (Figure 35A). Total energy intake and estimated total energy expenditure was even reduced in 129S6 mice (Figure 35B and C). In a hypothetical pair-feeding experiment, in which mice of both strains receive the identical amount of energy from a HFD, BL6J mice are expected to gain less body mass than 129S6 mice. Thus, elevated NST capacity of 129S6 mice may either not contribute to a limitation of body mass accumulation, or reduced NST capacity of BL6J mice may be compensated by means of other mechanisms such as increased activity.
The varying susceptibility of different mouse strains to the effects of hypercaloric feeding represents a useful tool to investigate the underlying mechanisms. In this respect, 129S6 and

BL6J mice were previously shown to differ in glucose tolerance and insulin sensitivity [203, 267]. To further investigate putative differences in glucose tolerance in the context of differential NST capacity, mice of both strains were periodically subjected to oral glucose tolerance tests (oGTT) in the course of this feeding experiment.

Fasting blood glucose levels were consistently higher in BL6J mice, irrespective of diet or housing temperature (Figure 36). This phenotype has been observed earlier in chow-fed mice and was accompanied by comparable fasting insulin levels [267], indicative of increased hepatic glucose output in BL6J mice contributing to elevated fasting glycaemia. A considerable impact of housing temperature on glucose tolerance was observed during oGTTs performed at the end of LFCD-feeding. Housing of mice at 20°C promoted glucose tolerance in mice of both strains (Figure 32A and B), suggesting acclimation to a thermoneutral environment per se to reduce blood glucose clearance. In fact, cold-exposure of rodents results in a notable upregulation of glucose uptake into BAT in line with the need to fuel adaptive heat production [116, 268-271]. Moreover, the maintenance of body temperature in mice exposed to cold essentially relies on glucose uptake and utilization in BAT [206]. This tissue is capable of absorbing glucose at a much higher rate than other tissues in mice [116, 119, 247], indicating a considerable uptake capacity despite its low mass. Accordingly, this effect of housing temperature on glucose tolerance probably originated from a remodeling process as result of acclimation that conferred mildly cold-exposed (20°C) mice the sustained ability for increased glucose uptake into BAT during oGTTs performed at 23°C. In fact, the need for adaptive heat production at 23°C was identical for all animals although mice of different acclimation state (30°C vs. 20°C) differed in NST capacity. In mice acclimated to 30°C, NST capacity is estimated to suffice for the maintenance of body temperature without shivering even when these are exposed to environmental temperatures below 20°C [188]. Thus, differences in glucose tolerance between mice of different acclimation state likely originated from a differential glucose uptake capacity into BAT and brite fat as result of NST capacity rather from than acute effects of ambient temperature.

In addition to this general protective effect of mild cold-exposure, glucose tolerance of LFCD-fed 129S6 mice was more promoted by housing at 20°C (Figure 32A and B) concomitant with higher Ucp1 levels in BAT and WAT under this condition (Figure 20 and Figure 21). Moreover, this strain-specific difference in glucose tolerance was entirely maintained in the further course of the experiment although glucose tolerance was gradually impaired by IFD and HFD in both strains (Figure 37). This effect may originate from the chronic, β-adrenergic stimulation during mild cold-acclimation since this phenotype was almost absent in mice housed at 30°C. In fact, not the insulin-stimulated but the adrenergically-stimulated glucose uptake into BAT is *in vivo* dependent on Ucp1 [272]. Adrenergically-stimulated glucose uptake into brown adipocytes is mediated in cyclic adenosine monophosphate (cAMP) and protein kinase A (PKA) dependent manner via the insulin-independent glucose transporter Glut1, which is expressed and translocated at higher levels in response to a β-adrenergic stimulus [273-276]. Similarly, a recent study shows that even browning of WAT is capable of

ameliorating blood glucose clearance in an insulin-independent manner influenced by Glut1 abundance [247]. Considering the common cAMP/PKA-dependent pathway in the recruitment of Glut1 and Ucp1, 129S6 mice kept at 20°C may not only be more responsive than BL6J mice on the level of adaptive Ucp1 induction but also on the level of Glut1. This effect may support thermogenesis during adrenergic stimulation thus benefitting blood glucose clearance independent from potential differences in insulin sensitivity. This hypothesized mechanism remains to be addressed in future experiments, comparing Ucp1 and Glut1 mRNA and/or protein levels in BAT and WAT of mildly cold-exposed 129S6 and BL6J mice, for instance.

Glucose tolerance of LFCD and IFD-fed 129S6 and BL6J mice was similar when animals were housed at 30°C. Among the three different HFDs, administration of palm oil and borage oil resulted in a significant impairment of glucose tolerance in BL6J mice, whereas this phenotype was not observed in fish oil-fed BL6J mice (Figure 37). This indicates a beneficial effect of the very low dietary n6/n3 ratio of the fish oil-comprising diets. In line with these results, impairment of glucose tolerance tends to be attenuated in BL6J mice after 12 weeks of HFD-feeding at 23°C when the HFD comprises fish oil instead of palm oil [277]. Concomitantly, Ucp1 mRNA levels are upregulated in BAT of fish oil-fed mice [277], indicating glucose tolerance to be affected by an interaction of the fat source with NST capacity. In the present study, fish oil-comprising IFD fed at 30°C did not increase Ucp1 levels in BAT and WAT of BL6J mice compared to other fat sources (Figure 27D and Figure 29A). Thus, fish oil-comprising HFD likely maintained glucose tolerance in BL6J mice by means of other mechanisms, although neither Ucp1 levels nor NST capacity were assessed in HFD-fed state.

Interestingly, 129S6 mice were completely protected from significant HFD-induced alterations of glucose tolerance at 30°C (Figure 37). This strain-specific regulation resulted in a significant difference in blood glucose clearance between 129S6 and BL6J mice when the animals received palm oil-comprising HFD. The n6/n3 ratio in this diet was intermediate compared to fish and borage-comprising HFDs and similar to LFCD. Diet-induced alterations in glucose tolerance were thus predominantly influenced by the difference in dietary fat content. Accordingly, strain-specific differences in glucose tolerance in response to HFD were thus likely affected either by differential insulin sensitivity, or an insulin-independent mechanism linked to differential NST capacity providing circulating glucose as fuel for Ucp1-mediated heat production. Elevated NST capacity of 129S6 mice thus appears not to influence glucose tolerance under non-obesogenic conditions (LFCD), but to protect from the diabetogenic influence of hypercaloric feeding when mice are not challenged with extraordinary n6/n3 ratios. Such a hypothetical mechanism can be tested by assessment of glucose tolerance in a model devoid of NST capacity such as Ucp1 ablated mice.

Taken together, body mass accumulation and the development of impaired glucose tolerance are diet-induced, phenotypic alterations dissentingly affected by differential NST capacity. Mice of the 129S6 and BL6J strains exhibited similar body mass gain in response to HFD, whereas blood glucose clearance was improved in 129S6 mice, which are characterized by elevated NST capacity. Improved glucose tolerance of this strain may originate from an Ucp1-dependent

mechanism promoting glucose uptake into BAT and brite fat. This mechanism is hypothesized to account for strain-specific differences in glucose tolerance under mild cold-exposure and may also protect 129S6 mice from the diabetogenic effect of a HFD fed at 30°C. These effects require validation in Ucp1-ablated mice, characterized by impaired NST capacity, to elucidate the distinct role for BAT and/or brite fat in the regulation of glucose tolerance.

4.6 Diet-induced impairment of glucose tolerance is attenuated in the presence of Ucp1

The capability of elevated NST capacity to prevent and improve genetic and diet-induced impairment of glucose tolerance is evident from mouse models with ectopic overexpression of Ucp1 [278-280]. The investigation of blood glucose clearance in 129S6 and BL6J mice in the previous experiment suggested BAT and brite fat as the physiological origin of this effect. In turn, Ucp1-KO mice, devoid of intact thermogenic function in these tissues, are hypothesized to exhibit a dysregulation of this system. WT and Ucp1-KO mice were used to validate previous findings in 129S6 and BL6J mice and to corroborate a functional role for Ucp1 in brown and brite adipocytes in the regulation of systemic glucose tolerance.

Mice of both genotypes were subjected to a feeding experiment as previously described for 129S6 and BL6J mice, which was conducted at 30°C and 20°C and characterized by three consecutive feeding periods to administer LFCD, IFD and HFD. The latter diets were increased in fat content solely by supplementation of palm oil. Thus, the influence of extraordinary dietary n6/n3 ratios was eliminated and differences between these three types of diets were basically reduced to the difference in fat content. As discussed above (section 4.5), this fat source appeared to particularly influence blood glucose clearance in the context of differential NST capacity. Glucose tolerance was periodically assessed via oGTTs.

The preceding experiment with 129S6 and BL6J mice suggested blood glucose clearance in LFCD-fed state to be beneficially affected by mild cold-exposure in both strains. Housing at 20°C had a stronger effect on blood glucose clearance in 129S6 mice, corroborating the notion that Ucp1 in BAT and brite fat may be responsible for this difference. Glucose tolerance was, however, similar in LFCD-fed WT and Ucp1-KO mice acclimated to 20°C. This phenotype remained unaltered throughout the entire experiment (Figure 38B). Thus, these results are in line with observations in primary brown adipocytes, indicating that adrenergically-mediated glucose uptake does not require the presence of Ucp1 [281]. *In vivo*, WT and Ucp1-KO mice exhibit differential glucose uptake into BAT in unstimulated state (in the absence of exogenous NE or insulin) when acclimated to 26°C [272]. However, WT but not Ucp1-KO mice are capable of increasing their lower BAT glucose uptake in response to NE [272]. Moreover, *in vivo* cold-stimulated glucose uptake of BAT is impaired in male Ucp1-KO vs. WT mice [282]. Accordingly, there are several possible mechanisms that may explain similar glucose tolerance of WT and Ucp1-KO mice in the present experiment: (1) the presence or absence of NST capacity causes putative differences in glucose uptake capacity of BAT and /or brite fat that are insufficient to influence blood glucose clearance; (2) adrenergically-mediated glucose

uptake into BAT is *in vivo* not dependent on Ucp1; (3) housing of mice at 20°C represents a condition of adrenergic stimulation that adjusts BAT/brite fat glucose uptake in WT mice to the elevated basal level of Ucp1-KO mice; (4) WT mice exhibit higher glucose uptake into BAT/brite fat affecting glucose tolerance, an effect that is compensated in KO mice by glucose uptake into other tissues. From the physiological perspective, the latter mechanism may play an important role since WT and Ucp1-KO mice were reared and housed in subthermoneutral environment. This housing condition requires the recruitment and constant supply of alternative heat-producing mechanisms for the maintenance of body temperature in KO mice. NE-stimulatable HP in Ucp1-KO mice acclimated to 18°C is sufficient to maintain body temperature up until 20°C [188], indicating marginal shivering during acclimation. Maximal shivering enables these mice to survive an ambient temperature as low as -0.9°C [188]. Accordingly, shivering thermogenesis of mildly cold-exposed (20°C) Ucp1-KO mice of the present study is likely insignificant and evokes increased glucose turnover in skeletal muscle probably to a minor extent. Instead, thermogenic futile cycles have repeatedly been hypothesized to exist in skeletal muscle and WAT to partially restore NST in the absence of Ucp1 [188, 217, 227, 283-285]. Moreover, mildly cold-exposed Ucp1-KO mice exhibit increased serum levels of BAT-derived fibroblast growth factor 21 [286], an endocrine factor that stimulates glucose uptake into adipocytes [287, 288] thus lowering blood glucose levels [289]. Given these alternative sites of increased glucose uptake in Ucp1-KO mice, the actual significance of Ucp1-dependent NST capacity for glucose tolerance under mild cold-exposure remains currently unresolved. Additionally, the phenotype observed in this experiment represents a clear discrepancy to a previous study reporting impaired blood glucose clearance in Ucp1-KO mice fed a HFD for 3 months at 23°C [207]. Differences in study design may contribute to this contrasting observation. Thus, blood glucose clearance at subthermoneutral environment requires further clarification on the molecular and physiological level that could be complemented by the use of a conditional Ucp1-KO model.

Housing of mice at 30°C eliminates the need for thermoregulation and excludes compensatory glucose consumption of other tissues. Thus, the effect of NST capacity on the regulation of glucose tolerance is more specifically assessable in mice acclimated to thermoneutral environment. In the previous experiment involving 129S6 and BL6J mice, glucose tolerance at 30°C was similar in LFCD-fed state. In the further progress, 129S6 but not BL6J mice were protected from a significant impairment of glucose tolerance under HFD, an effect that is hypothesized to originate from a differential glucose uptake capacity into BAT and/or brite fat related to NST. Equivalently, WT and Ucp1-KO mice had similar glucose tolerance in LFCD-fed state, indicating that Ucp1 does not contribute to blood glucose clearance under non-obesogenic conditions. As observed earlier in BL6J mice, glucose tolerance of WT mice was impaired by HFD but not IFD. In line with the hypothesized function of Ucp1 in the regulation of glycaemia, glucose tolerance was significantly impaired in KO mice at the end of IFD-feeding (Figure 38B) despite comparable insulin sensitivity (Figure 39). This result indicates that a moderate elevation of the dietary fat content is sufficient to affect blood glucose clearance in

the absence of NST. Moreover, these results complement evidence from a recent study in thermoneutral environment demonstrating a marked difference in glucose tolerance between WT and Ucp1-KO mice in response to 9 weeks of HFD-feeding [208].

In the present study, the IFD-induced impairment of glucose tolerance in Ucp1-KO mice was not further exacerbated by the HFD (Figure 38B). This effect likely originated from a relatively improved insulin sensitivity of KO vs. WT mice under HFD-feeding (Figure 39 and Figure 40A), which was probably the result of reduced adiposity in Ucp1-KO mice (Figure 40B). Irrespective of this improved insulin sensitivity, glucose tolerance of KO mice was consistently impaired under conditions of hypercaloric feeding, indicating the existence of an insulin-insensitive component that enhances glucose disposal in the presence of Ucp1. Considering its function for glucose uptake upon adrenergic stimulation of BAT [273-275], one may speculate whether this component is Glut1, induced by the adrenergic effect of IFD and HFD [220] to deliver excessive circulating glucose for Ucp1-mediated dissipation. Thus, these results strongly suggest that the thermogenic function of BAT renders this tissue a sink for excessive circulating glucose, attenuating diet-induced impairment of glucose tolerance. Moreover, BAT is an endocrine tissue, secreting factors ('batokines') that affect glucose uptake in autocrine/paracrine manner [290], or act in endocrine manner on other tissues mediating the beneficial effect of BAT transplantation on glucose homeostasis [119, 291]. Further molecular analyses are thus required to clarify whether differences in glucose tolerance between WT and Ucp1-KO mice are solely due to differences in NST capacity, or whether this phenotype is influenced by putative differences in the endocrine function of BAT. Similarly, putative differences in insulin secretion in response to a glucose challenge must be excluded. Collectively, these data substantiate and complement results of the previous experiment involving 129S6 and BL6J mice (section 4.5), thus providing direct evidence for BAT function to influence systemic glucose homeostasis.

BAT mediates DIT [106] and its thermogenic function is therefore hypothesized to limit excessive body mass gain in response to hypercaloric feeding by dissipating excess energy. In line with this concept, Ucp1 ablation was found to promote DIO development particularly in thermoneutral environment, an effect ascribed to the abrogated need to recruit and fuel alternative mechanisms of heat production [107]. In the present study, Ucp1-KO mice housed at 30°C gained less body mass than WT mice when fed a HFD (Figure 41B), which was fully explainable by reduced energy intake. The origin of this reduced energy intake remains elusive, but may be related to the period of IFD-feeding causing an organismic adaption to attenuate the adverse metabolic effects of HFD-feeding. A similar effect can be observed in the response to changes in ambient temperature, where pre-acclimation to mild cold (18°C) enables Ucp1-KO mice to survive a longer period of severe cold-exposure (4°C) [188, 228], whereas acute exposure to 4°C has a lethal effect for Ucp1-KO mice within hours without pre-acclimation [47]. Thus, the results of the present experiment do not support earlier observations that ablation of Ucp1 results in increased body mass accumulation. Furthermore, such a relationship was as well not identified by other studies demonstrating similar body mass gain of HFD-fed WT and KO mice under thermoneutral housing conditions [108, 208].

Ucp1-mediated thermogenesis therefore appears to attenuate diet-induced impairment of glucose tolerance but not body mass gain.

Taken together, thermogenesis as the key function of BAT and brite fat influences blood glucose clearance and thus affects systemic glucose homeostasis in mice. Unexpectedly, constitutive ablation of Ucp1 did not influence blood glucose clearance in mice housed at 20°C representing an environment that enforces adaptive heat production supported by the turnover of glucose. As Ucp1-KO mice are devoid of BAT-derived NST, mild cold-exposure likely recruited alternative thermogenic mechanisms thus compensating reduced dissipation of energy from glucose in BAT. This need is abrogated in thermoneutral environment where Ucp1-KO mice became glucose intolerant in response to hypercaloric feeding, an effect that was prevented from further exacerbation by a relatively improved insulin sensitivity. This phenotype strongly suggests the interaction of Ucp1 with an insulin-independent glucose transport mechanism, which is hypothesized to mediate a beneficial metabolic effect in the context of DIT uncoupled from an influence on body mass development.

4.7 Conclusion

The extensive study of BAT physiology and function during the past decades led to a gradual shift from its original notion as ‘heater organ’ of small mammals towards a tissue with considerable potential to improve metabolic health. The rediscovery of functional BAT in humans and the identification of brite adipocytes as additional, inducible pool of thermogenic cells therefore boosted the interest in the function of this tissue as a potential target to combat obesity and associated disorders. This concept constituted the formation of the European DIABAT consortium thus promoting basic research on brown and brite adipocytes as basis to develop targeted treatment strategies for human subjects focusing on the prevention and treatment of type 2 diabetes mellitus.

There is accumulating evidence in mice and humans that an increase in the abundance of BAT and brite fat beneficially affects blood glucose clearance. The characterization of NST capacity in different mouse models proved to be a useful tool to investigate this relationship in more detail. Using a monogenic and a polygenic approach in two independent experiments, the present thesis provides both direct and indirect evidence consistently supporting the thermogenic function of BAT and brite fat to contribute to systemic blood glucose clearance. The present study expands current knowledge by demonstrating that under thermoneutral housing conditions (1) minimized NST capacity in BAT and brite fat does not affect glycaemia under non-obesogenic conditions, (2) a moderate increase in dietary fat content is sufficient to dysregulate blood glucose clearance in the absence of NST capacity, and (3) diet-induced impairment of glucose tolerance in the absence of NST capacity occurs independent from insulin sensitivity. Collectively, these data suggest that the regulation of glucose tolerance involves an Ucp1-dependent glucose transport mechanism that uncouples blood glucose clearance from insulin signaling and likely renders BAT and/or brite fat a sink for excessive circulating glucose. The present thesis corroborates a distinct role for NST to serve as reserve

capacity against metabolic impairment under hypercaloric conditions, which is hypothesized to represent the actual benefit of DIT rather than the control of body mass gain. The detailed characterization of this phenotype on the molecular level as well as its manipulability by targeted nutritional or pharmacological approaches remains an issue for future experiments. Given the considerable prevalence of obesity-associated diabetes, these findings are of particular importance in a translational context and will encourage future research on the recruitment and metabolic role of BAT and brite fat for the prevention and treatment of human disease.

LITERATURE

1. Unger RH, Scherer PE: Gluttony, sloth and the metabolic syndrome: a roadmap to lipotoxicity. *Trends Endocrinol Metab* 2010, 21:345-352.
2. Cinti S: *The Adipose Organ.* Kurtis, Milan; 1999.
3. Gesner K: *Conradi Gesneri medici Tigurini historiae animalium lib. I. de quadrupedibus viviparis.*: Tiguri, apud Christ. Froschoverum; 1551.
4. Klingenspor M, Herzig S, Pfeifer A: Brown fat develops a brite future. *Obes Facts* 2012, 5:890-896.
5. Heldmaier G, Neuweiler G: *Vergleichende Tierphysiologie: Band 2 Vegetative Physiologie.* Springer; 2004.
6. Rauch JC, Hayward JS: Topography and vascularization of brown fat in a small nonhibernator (deer mouse, Peromyscus maniculatus). *Can J Zool* 1969, 47:1301-1314.
7. Cinti S: The Adipose Organ. In *Adipose Tissue and Adipokines in Health and Disease.* Edited by Giamila Fantuzzi and Theodore Mazzone: Humana Press Inc.; 2007: 3-19
8. Moore H-PH, Silver RB, Mottillo EP, Bernlohr DA, Granneman JG: Perilipin targets a novel pool of lipid droplets for lipolytic attack by hormone-sensitive lipase. *J Biol Chem* 2005, 280:43109-43120.
9. Young P, Arch JR, Ashwell M: Brown adipose tissue in the parametrial fat pad of the mouse. *FEBS Lett* 1984, 167:10-14.
10. Petrovic N, Walden TB, Shabalina IG, Timmons JA, Cannon B, Nedergaard J: Chronic peroxisome proliferator-activated receptor gamma (PPARgamma) activation of epididymally derived white adipocyte cultures reveals a population of thermogenically competent, UCP1-containing adipocytes molecularly distinct from classic brown adipocytes. *J Biol Chem* 2010, 285:7153-7164.
11. Ishibashi J, Seale P: Medicine. Beige can be slimming. *Science* 2010, 328:1113-1114.
12. Waldén TB, Hansen IR, Timmons JA, Cannon B, Nedergaard J: Recruited vs. nonrecruited molecular signatures of brown, "brite," and white adipose tissues. *Am J Physiol Endocrinol Metab* 2012, 302:E19-31.
13. Wang QA, Tao C, Gupta RK, Scherer PE: Tracking adipogenesis during white adipose tissue development, expansion and regeneration. *Nat Med* 2013, 19:1338-1344.
14. Rosenwald M, Perdikari A, Rülicke T, Wolfrum C: Bi-directional interconversion of brite and white adipocytes. *Nat Cell Biol* 2013, 15:659-667.
15. Vitali A, Murano I, Zingaretti MC, Frontini A, Ricquier D, Cinti S: The adipose organ of obesity-prone C57BL/6J mice is composed of mixed white and brown adipocytes. *J Lipid Res* 2012, 53:619-629.
16. Barbatelli G, Murano I, Madsen L, Hao Q, Jimenez M, Kristiansen K, Giacobino JP, De Matteis R, Cinti S: The emergence of cold-induced brown adipocytes in mouse white fat depots is determined predominantly by white to brown adipocyte transdifferentiation. *Am J Physiol Endocrinol Metab* 2010, 298:E1244-1253.
17. Himms-Hagen J, Melnyk A, Zingaretti MC, Ceresi E, Barbatelli G, Cinti S: Multilocular fat cells in WAT of CL-316243-treated rats derive directly from white adipocytes. *Am J Physiol Cell Physiol* 2000, 279:C670-681.
18. Li Y, Lasar D, Fromme T, Klingenspor M: White, brite, and brown adipocytes: the evolution and function of a heater organ in mammals. *Canadian Journal of Zoology* 2013, 92:615-626.

19. Nagase I, Yoshida T, Kumamoto K, Umekawa T, Sakane N, Nikami H, Kawada T, Saito M: Expression of uncoupling protein in skeletal muscle and white fat of obese mice treated with thermogenic beta 3-adrenergic agonist. *J Clin Invest* 1996, 97:2898-2904.

20. Li Y, Fromme T, Schweizer S, Schottl T, Klingenspor M: Taking control over intracellular fatty acid levels is essential for the analysis of thermogenic function in cultured primary brown and brite/beige adipocytes. *EMBO Rep* 2014, 15:1069-1076.

21. Shabalina IG, Petrovic N, de Jong JM, Kalinovich AV, Cannon B, Nedergaard J: UCP1 in brite/beige adipose tissue mitochondria is functionally thermogenic. *Cell Rep* 2013, 5:1196-1203.

22. Seale P, Bjork B, Yang W, Kajimura S, Chin S, Kuang S, Scimè A, Devarakonda S, Conroe HM, Erdjument-Bromage H, et al: PRDM16 controls a brown fat/skeletal muscle switch. *Nature* 2008, 454:961-967.

23. Shan T, Liang X, Bi P, Zhang P, Liu W, Kuang S: Distinct populations of adipogenic and myogenic Myf5-lineage progenitors in white adipose tissues. *J Lipid Res* 2013, 54:2214-2224.

24. Sanchez-Gurmaches J, Hung CM, Sparks CA, Tang Y, Li H, Guertin DA: PTEN loss in the Myf5 lineage redistributes body fat and reveals subsets of white adipocytes that arise from Myf5 precursors. *Cell Metab* 2012, 16:348-362.

25. Long JZ, Svensson KJ, Tsai L, Zeng X, Roh HC, Kong X, Rao RR, Lou J, Lokurkar I, Baur W, et al: A smooth muscle-like origin for beige adipocytes. *Cell Metab* 2014, 19:810-820.

26. Gordon CJ: Thermal physiology of laboratory mice: Defining thermoneutrality. *Journal of Thermal Biology* 2012, 37:654-685.

27. Kingma B, Frijns A, van Marken Lichtenbelt W: The thermoneutral zone: implications for metabolic studies. *Front Biosci (Elite Ed)* 2012, 4:1975-1985.

28. Cannon B, Nedergaard J: Brown adipose tissue: function and physiological significance. *Physiol Rev* 2004, 84:277-359.

29. Bautista DM, Siemens J, Glazer JM, Tsuruda PR, Basbaum AI, Stucky CL, Jordt S-E, Julius D: The menthol receptor TRPM8 is the principal detector of environmental cold. *Nature* 2007, 448:204-208.

30. Colburn RW, Lubin ML, Stone DJ, Wang Y, Lawrence D, D'Andrea MR, Brandt MR, Liu Y, Flores CM, Qin N: Attenuated cold sensitivity in TRPM8 null mice. *Neuron* 2007, 54:379-386.

31. Dhaka A, Murray AN, Mathur J, Earley TJ, Petrus MJ, Patapoutian A: TRPM8 is required for cold sensation in mice. *Neuron* 2007, 54:371-378.

32. Morrison SF, Madden CJ: Central nervous system regulation of brown adipose tissue. *Compr Physiol* 2014, 4:1677-1713.

33. Desautels M, Dulos RA, Mozaffari B: Selective loss of uncoupling protein from mitochondria of surgically denervated brown adipose tissue of cold-acclimated mice. *Biochem Cell Biol* 1986, 64:1125-1134.

34. Klingenspor M, Meywirth A, Stöhr S, Heldmaier G: Effect of unilateral surgical denervation of brown adipose tissue on uncoupling protein mRNA level and cytochrom-c-oxidase activity in the Djungarian hamster. *J Comp Physiol B* 1994, 163:664-670.

35. Wirsen C: Adrenergic innervation of adipose tissue examined by fluorescence microscopy. *Nature* 1964, 202:913.

36. Bargmann W, von Hehn G, Lindner E: On the cells of the brown fatty tissue and their innervation. *Z Zellforsch Mikrosk Anat* 1968, 85:601-613.

37. Zhao J, Unelius L, Bengtsson T, Cannon B, Nedergaard J: Coexisting beta-adrenoceptor subtypes: significance for thermogenic process in brown fat cells. *Am J Physiol* 1994, 267:C969-979.

38. Susulic VS, Frederich RC, Lawitts J, Tozzo E, Kahn BB, Harper ME, Himms-Hagen J, Flier JS, Lowell BB: Targeted disruption of the beta 3-adrenergic receptor gene. *J Biol Chem* 1995, 270:29483-29492.

39. Grujic D, Susulic VS, Harper ME, Himms-Hagen J, Cunningham BA, Corkey BE, Lowell BB: Beta3-adrenergic receptors on white and brown adipocytes mediate beta3-selective agonist-induced effects on energy expenditure, insulin secretion, and food intake. A study using transgenic and gene knockout mice. *J Biol Chem* 1997, 272:17686-17693.

40. Collins S: β-Adrenoceptor Signaling Networks in Adipocytes for Recruiting Stored Fat and Energy Expenditure. *Front Endocrinol (Lausanne)* 2011, 2:102.

41. Zechner R, Zimmermann R, Eichmann TO, Kohlwein SD, Haemmerle G, Lass A, Madeo F: FAT SIGNALS--lipases and lipolysis in lipid metabolism and signaling. *Cell Metab* 2012, 15:279-291.

42. Zimmermann R, Strauss JG, Haemmerle G, Schoiswohl G, Birner-Gruenberger R, Riederer M, Lass A, Neuberger G, Eisenhaber F, Hermetter A, Zechner R: Fat mobilization in adipose tissue is promoted by adipose triglyceride lipase. *Science* 2004, 306:1383-1386.

43. Robidoux J, Kumar N, Daniel KW, Moukdar F, Cyr M, Medvedev AV, Collins S: Maximal beta3-adrenergic regulation of lipolysis involves Src and epidermal growth factor receptor-dependent ERK1/2 activation. *J Biol Chem* 2006, 281:37794-37802.

44. Klingenspor M, Fromme T: Brown Adipose Tissue. In *Adipose Tissue Biology.* Edited by Symonds ME: Springer New York; 2011: 39-69

45. Locke RM, Rial E, Nicholls DG: The acute regulation of mitochondrial proton conductance in cells and mitochondria from the brown fat of cold-adapted and warm-adapted guinea pigs. *Eur J Biochem* 1982, 129:381-387.

46. Heaton GM, Wagenvoord RJ, Kemp A, Nicholls DG: Brown-adipose-tissue mitochondria: photoaffinity labelling of the regulatory site of energy dissipation. *Eur J Biochem* 1978, 82:515-521.

47. Enerbäck S, Jacobsson A, Simpson EM, Guerra C, Yamashita H, Harper ME, Kozak LP: Mice lacking mitochondrial uncoupling protein are cold-sensitive but not obese. *Nature* 1997, 387:90-94.

48. Ricquier D, Mory G, Bouillaud F, Thibault J, Weissenbach J: Rapid increase of mitochondrial uncoupling protein and its mRNA in stimulated brown adipose tissue. Use of a cDNA probe. *FEBS Lett* 1984, 178:240-244.

49. Ricquier D, Bouillaud F, Toumelin P, Mory G, Bazin R, Arch J, Pénicaud L: Expression of uncoupling protein mRNA in thermogenic or weakly thermogenic brown adipose tissue. Evidence for a rapid beta-adrenoreceptor-mediated and transcriptionally regulated step during activation of thermogenesis. *J Biol Chem* 1986, 261:13905-13910.

50. Jacobsson A, Stadler U, Glotzer MA, Kozak LP: Mitochondrial uncoupling protein from mouse brown fat. Molecular cloning, genetic mapping, and mRNA expression. *J Biol Chem* 1985, 260:16250-16254.

51. Bonet ML, Oliver P, Palou A: Pharmacological and nutritional agents promoting browning of white adipose tissue. *Biochim Biophys Acta* 2013, 1831:969-985.

52. Villarroya F, Iglesias R, Giralt M: PPARs in the Control of Uncoupling Proteins Gene Expression. *PPAR Res* 2007, 2007:74364.

53. Carroll AM, Haines LR, Pearson TW, Brennan C, Breen EP, Porter RK: Immunodetection of UCP1 in rat thymocytes. *Biochem Soc Trans* 2004, 32:1066-1067.

54. Aquila H, Link TA, Klingenberg M: The uncoupling protein from brown fat mitochondria is related to the mitochondrial ADP/ATP carrier. Analysis of sequence homologies and of folding of the protein in the membrane. *EMBO J* 1985, 4:2369-2376.

55. Berardi MJ, Shih WM, Harrison SC, Chou JJ: Mitochondrial uncoupling protein 2 structure determined by NMR molecular fragment searching. *Nature* 2011, 476:109-113.

56. Boss O, Samec S, Paoloni-Giacobino A, Rossier C, Dulloo A, Seydoux J, Muzzin P, Giacobino JP: Uncoupling protein-3: a new member of the mitochondrial carrier family with tissue-specific expression. *FEBS Lett* 1997, 408:39-42.

57. Vidal-Puig A, Solanes G, Grujic D, Flier JS, Lowell BB: UCP3: an uncoupling protein homologue expressed preferentially and abundantly in skeletal muscle and brown adipose tissue. *Biochem Biophys Res Commun* 1997, 235:79-82.

58. Fleury C, Neverova M, Collins S, Raimbault S, Champigny O, Levi-Meyrueis C, Bouillaud F, Seldin MF, Surwit RS, Ricquier D, Warden CH: Uncoupling protein-2: a novel gene linked to obesity and hyperinsulinemia. *Nat Genet* 1997, 15:269-272.

59. Gimeno RE, Dembski M, Weng X, Deng N, Shyjan AW, Gimeno CJ, Iris F, Ellis SJ, Woolf EA, Tartaglia LA: Cloning and characterization of an uncoupling protein homolog: a potential molecular mediator of human thermogenesis. *Diabetes* 1997, 46:900-906.

60. Arsenijevic D, Onuma H, Pecqueur C, Raimbault S, Manning BS, Miroux B, Couplan E, Alves-Guerra MC, Goubern M, Surwit R, et al: Disruption of the uncoupling protein-2 gene in mice reveals a role in immunity and reactive oxygen species production. *Nat Genet* 2000, 26:435-439.

61. Gong DW, Monemdjou S, Gavrilova O, Leon LR, Marcus-Samuels B, Chou CJ, Everett C, Kozak LP, Li C, Deng C, et al: Lack of obesity and normal response to fasting and thyroid hormone in mice lacking uncoupling protein-3. *J Biol Chem* 2000, 275:16251-16257.

62. Vidal-Puig AJ, Grujic D, Zhang CY, Hagen T, Boss O, Ido Y, Szczepanik A, Wade J, Mootha V, Cortright R, et al: Energy metabolism in uncoupling protein 3 gene knockout mice. *J Biol Chem* 2000, 275:16258-16266.

63. Zhang CY, Baffy G, Perret P, Krauss S, Peroni O, Grujic D, Hagen T, Vidal-Puig AJ, Boss O, Kim YB, et al: Uncoupling protein-2 negatively regulates insulin secretion and is a major link between obesity, beta cell dysfunction, and type 2 diabetes. *Cell* 2001, 105:745-755.

64. Mitchell P: Coupling of phosphorylation to electron and hydrogen transfer by a chemi-osmotic type of mechanism. *Nature* 1961, 191:144-148.

65. Mitchell P: Chemiosmotic coupling in oxidative and photosynthetic phosphorylation. *Biol Rev Camb Philos Soc* 1966, 41:445-502.

66. Vinothkumar KR, Zhu J, Hirst J: Architecture of mammalian respiratory complex I. *Nature* 2014, 515:80-84.

67. Sun F, Huo X, Zhai Y, Wang A, Xu J, Su D, Bartlam M, Rao Z: Crystal structure of mitochondrial respiratory membrane protein complex II. *Cell* 2005, 121:1043-1057.

68. Iwata S, Lee JW, Okada K, Lee JK, Iwata M, Rasmussen B, Link TA, Ramaswamy S, Jap BK: Complete structure of the 11-subunit bovine mitochondrial cytochrome bc1 complex. *Science* 1998, 281:64-71.

69. Yoshikawa S, Shinzawa-Itoh K, Nakashima R, Yaono R, Yamashita E, Inoue N, Yao M, Fei MJ, Libeu CP, Mizushima T, et al: Redox-coupled crystal structural changes in bovine heart cytochrome c oxidase. *Science* 1998, 280:1723-1729.

70. Zhou A, Rohou A, Schep DG, Bason JV, Montgomery MG, Walker JE, Grigorieff N, Rubinstein JL: Structure and conformational states of the bovine mitochondrial ATP synthase by cryo-EM. *Elife* 2015, 4.

71. Pebay-Peyroula E, Dahout-Gonzalez C, Kahn R, Trézéguet V, Lauquin GJ-M, Brandolin G: Structure of mitochondrial ADP/ATP carrier in complex with carboxyatractyloside. *Nature* 2003, 426:39-44.

72. Acin-Perez R: An intragenic suppressor in the cytochrome c oxidase I gene of mouse mitochondrial DNA. *Human Molecular Genetics* 2003, 12:329-339.

73. Villani G, Attardi G: In vivo control of respiration by cytochrome c oxidase in human cells. *Free Radic Biol Med* 2000, 29:202-210.

74. Villani G, Greco M, Papa S, Attardi G: Low reserve of cytochrome c oxidase capacity in vivo in the respiratory chain of a variety of human cell types. *J Biol Chem* 1998, 273:31829-31836.

75. Chance B, Williams G: Respiratory enzymes in oxidative phosphorylation. III. The steady state. *J Biol Chem* 1955, 217:409-427.

76. Lardy HA WH: Oxidative phosphorylation: role of inorganic phosphate and acceptor systems in control of metabolic rates. *J Biol Chem* 1952, 195:215-224.

77. Smith RE, Roberts JC, Hittelman KJ: Nonphosphorylating respiration of mitochondria from brown adipose tissue of rats. *Science* 1966, 154:653-654.

78. Cannon B, Vogel G: The mitochondrial ATPase of brown adipose tissue. Purification and comparison with the mitochondrial ATPase from beef heart. *FEBS Lett* 1977, 76:284-289.

79. Houstěk J, Drahota Z: Purification and properties of mitochondrial adenosine triphosphatase of hamster brown adipose tissue. *Biochim Biophys Acta* 1977, 484:127-139.

80. Lin CS, Klingenberg M: Isolation of the uncoupling protein from brown adipose tissue mitochondria. *FEBS Lett* 1980, 113:299-303.

81. Divakaruni AS, Brand MD: The regulation and physiology of mitochondrial proton leak. *Physiology (Bethesda)* 2011, 26:192-205.

82. Heaton GM, Nicholls DG: The structural specificity of the nucleotide-binding site and the reversible nature of the inhibition of proton conductance induced by bound nucleotides in brown-adipose-tissue mitochondria. *Biochem Soc Trans* 1977, 5:210-212.

83. Nicholls DG: Hamster brown-adipose-tissue mitochondria. Purine nucleotide control of the ion conductance of the inner membrane, the nature of the nucleotide binding site. *Eur J Biochem* 1976, 62:223-228.

84. Nicholls DG: Hamster brown-adipose-tissue mitochondria. The control of respiration and the proton electrochemical potential gradient by possible physiological effectors of the proton conductance of the inner membrane. *Eur J Biochem* 1974, 49:573-583.

85. Shabalina IG, Ost M, Petrovic N, Vrbacky M, Nedergaard J, Cannon B: Uncoupling protein-1 is not leaky. *Biochim Biophys Acta* 2010, 1797:773-784.

86. Parker N, Crichton PG, Vidal-Puig AJ, Brand MD: Uncoupling protein-1 (UCP1) contributes to the basal proton conductance of brown adipose tissue mitochondria. *J Bioenerg Biomembr* 2009, 41:335-342.

87. Azzu V, Brand MD: The on-off switches of the mitochondrial uncoupling proteins. *Trends Biochem Sci* 2010, 35:298-307.

88. Heaton JM: The distribution of brown adipose tissue in the human. *J Anat* 1972, 112:35-39.

89. Nedergaard J, Bengtsson T, Cannon B: Unexpected evidence for active brown adipose tissue in adult humans. *Am J Physiol Endocrinol Metab* 2007, 293:E444-452.

90. Virtanen KA, Lidell ME, Orava J, Heglind M, Westergren R, Niemi T, Taittonen M, Laine J, Savisto N-J, Enerbäck S, Nuutila P: Functional brown adipose tissue in healthy adults. *N Engl J Med* 2009, 360:1518-1525.

91. Cypess AM, Lehman S, Williams G, Tal I, Rodman D, Goldfine AB, Kuo FC, Palmer EL, Tseng Y-H, Doria A, et al: Identification and importance of brown adipose tissue in adult humans. *N Engl J Med* 2009, 360:1509-1517.

92. van Marken Lichtenbelt WD, Vanhommerig JW, Smulders NM, Drossaerts JMAFL, Kemerink GJ, Bouvy ND, Schrauwen P, Teule GJJ: Cold-activated brown adipose tissue in healthy men. *N Engl J Med* 2009, 360:1500-1508.

93. Saito M, Okamatsu-Ogura Y, Matsushita M, Watanabe K, Yoneshiro T, Nio-Kobayashi J, Iwanaga T, Miyagawa M, Kameya T, Nakada K, et al: High incidence of metabolically active brown adipose tissue in healthy adult humans: effects of cold exposure and adiposity. *Diabetes* 2009, 58:1526-1531.

94. Orava J, Nuutila P, Lidell ME, Oikonen V, Noponen T, Viljanen T, Scheinin M, Taittonen M, Niemi T, Enerbäck S, Virtanen KA: Different metabolic responses of human brown adipose tissue to activation by cold and insulin. *Cell Metab* 2011, 14:272-279.

95. Ouellet V, Labbé SM, Blondin DP, Phoenix S, Guérin B, Haman F, Turcotte EE, Richard D, Carpentier AC: Brown adipose tissue oxidative metabolism contributes to energy expenditure during acute cold exposure in humans. *J Clin Invest* 2012, 122:545-552.

96. Muzik O, Mangner TJ, Leonard WR, Kumar A, Janisse J, Granneman JG: 15O PET measurement of blood flow and oxygen consumption in cold-activated human brown fat. *J Nucl Med* 2013, 54:523-531.

97. Lidell ME, Betz MJ, Leinhard OD, Heglind M, Elander L, Slawik M, Mussack T, Nilsson D, Romu T, Nuutila P, et al: Evidence for two types of brown adipose tissue in humans. *Nat Med* 2013.

98. Sharp LZ, Shinoda K, Ohno H, Scheel DW, Tomoda E, Ruiz L, Hu H, Wang L, Pavlova Z, Gilsanz V, Kajimura S: Human BAT possesses molecular signatures that resemble beige/brite cells. *PLoS One* 2012, 7:e49452.

99. Shinoda K, Luijten IHN, Hasegawa Y, Hong H, Sonne SB, Kim M, Xue R, Chondronikola M, Cypess AM, Tseng Y-H, et al: Genetic and functional characterization of clonally derived adult human brown adipocytes. *Nat Med* 2015, 21:389-394.

100. Wu J, Boström P, Sparks LM, Ye L, Choi JH, Giang A-H, Khandekar M, Virtanen KA, Nuutila P, Schaart G, et al: Beige adipocytes are a distinct type of thermogenic fat cell in mouse and human. *Cell* 2012, 150:366-376.

101. Cypess AM, White AP, Vernochet C, Schulz TJ, Xue R, Sass CA, Huang TL, Roberts-Toler C, Weiner LS, Sze C, et al: Anatomical localization, gene expression profiling and functional characterization of adult human neck brown fat. *Nat Med* 2013, 19:635-639.

102. Jespersen NZ, Larsen TJ, Peijs L, Daugaard S, Homøe P, Loft A, de Jong J, Mathur N, Cannon B, Nedergaard J, et al: A classical brown adipose tissue mRNA signature partly overlaps with brite in the supraclavicular region of adult humans. *Cell Metab* 2013, 17:798-805.

103. Frontini A, Vitali A, Perugini J, Murano I, Romiti C, Ricquier D, Guerrieri M, Cinti S: White-to-brown transdifferentiation of omental adipocytes in patients affected by pheochromocytoma. *Biochim Biophys Acta* 2013, 1831:950-959.

104. Sidossis LS, Porter C, Saraf MK, Børsheim E, Radhakrishnan RS, Chao T, Ali A, Chondronikola M, Mlcak R, Finnerty CC, et al: Browning of Subcutaneous White Adipose Tissue in Humans after Severe Adrenergic Stress. *Cell Metab* 2015, 22:219-227.

105. Vijgen GHEJ, Bouvy ND, Teule GJJ, Brans B, Schrauwen P, van Marken Lichtenbelt WD: Brown adipose tissue in morbidly obese subjects. *PLoS One* 2011, 6:e17247.

106. Rothwell NJ, Stock MJ: A role for brown adipose tissue in diet-induced thermogenesis. *Nature* 1979, 281:31-35.

107. Feldmann HM, Golozoubova V, Cannon B, Nedergaard J: UCP1 ablation induces obesity and abolishes diet-induced thermogenesis in mice exempt from thermal stress by living at thermoneutrality. *Cell Metab* 2009, 9:203-209.

108. Liu X, Rossmeisl M, McClaine J, Kozak LP: Paradoxical resistance to diet-induced obesity in UCP1-deficient mice. *Journal of Clinical Investigation* 2003, 111:399-407.

109. Guo T, Marmol P, Moliner A, Björnholm M, Zhang C, Shokat KM, Ibanez CF: Adipocyte ALK7 links nutrient overload to catecholamine resistance in obesity. *Elife* 2014, 3:e03245.

110. Mowers J, Uhm M, Reilly SM, Simon J, Leto D, Chiang S-H, Chang L, Saltiel AR: Inflammation produces catecholamine resistance in obesity via activation of PDE3B by the protein kinases IKKε and TBK1. *Elife* 2013, 2:e01119.

111. Vijgen GHEJ, Bouvy ND, Teule GJJ, Brans B, Hoeks J, Schrauwen P, van Marken Lichtenbelt WD: Increase in brown adipose tissue activity after weight loss in morbidly obese subjects. *J Clin Endocrinol Metab* 2012, 97:E1229-1233.

112. Yoneshiro T, Aita S, Matsushita M, Kameya T, Nakada K, Kawai Y, Saito M: Brown adipose tissue, whole-body energy expenditure, and thermogenesis in healthy adult men. *Obesity (Silver Spring)* 2011, 19:13-16.

113. Chondronikola M, Volpi E, Børsheim E, Porter C, Annamalai P, Enerbäck S, Lidell ME, Saraf MK, Labbe SM, Hurren NM, et al: Brown adipose tissue improves whole-body glucose homeostasis and insulin sensitivity in humans. *Diabetes* 2014, 63:4089-4099.

114. Cypess AM, Weiner LS, Roberts-Toler C, Elia EF, Kessler SH, Kahn PA, English J, Chatman K, Trauger SA, Doria A, Kolodny GM: Activation of human brown adipose tissue by a beta3-adrenergic receptor agonist. *Cell Metab* 2015, 21:33-38.

115. Ma SW, Foster DO: Uptake of glucose and release of fatty acids and glycerol by rat brown adipose tissue in vivo. *Can J Physiol Pharmacol* 1986, 64:609-614.

116. Bartelt A, Bruns OT, Reimer R, Hohenberg H, Ittrich H, Peldschus K, Kaul MG, Tromsdorf UI, Weller H, Waurisch C, et al: Brown adipose tissue activity controls triglyceride clearance. *Nat Med* 2011, 17:200-205.

117. Wu C, Cheng W, Xing H, Dang Y, Li F, Zhu Z: Brown Adipose Tissue Can Be Activated or Inhibited within an Hour before 18F-FDG Injection: A Preliminary Study with MicroPET. *Journal of Biomedicine and Biotechnology* 2011, 2011:5.

118. Tharp KM, Jha AK, Kraiczy J, Yesian A, Karateev G, Sinisi R, Dubikovskaya EA, Healy KE, Stahl A: Matrix-Assisted Transplantation of Functional Beige Adipose Tissue. *Diabetes* 2015, 64:3713-3724.

119. Stanford KI, Middelbeek RJW, Townsend KL, An D, Nygaard EB, Hitchcox KM, Markan KR, Nakano K, Hirshman MF, Tseng Y-H, Goodyear LJ: Brown adipose tissue regulates glucose homeostasis and insulin sensitivity. *J Clin Invest* 2013, 123:215-223.

120. Ng M, Fleming T, Robinson M, Thomson B, Graetz N, Margono C, Mullany EC, Biryukov S, Abbafati C, Abera SF, et al: Global, regional, and national prevalence of overweight and obesity in children and adults during 1980-2013: a systematic analysis for the Global Burden of Disease Study 2013. *Lancet* 2014, 384:766-781.

121. WHO: Obesity and overweight Fact sheet No. 311, 2015. Access date: 06.02.2016. [http://www.who.int/mediacentre/factsheets/fs311/en/]

122. Guh DP, Zhang W, Bansback N, Amarsi Z, Birmingham CL, Anis AH: The incidence of co-morbidities related to obesity and overweight: a systematic review and meta-analysis. *BMC Public Health* 2009, 9:88.

123. Prospective Studies Collaboration, Whitlock G, Lewington S, Sherliker P, Clarke R, Emberson J, Halsey J, Qizilbash N, Collins R, Peto R: Body-mass index and cause-specific mortality in 900 000 adults: collaborative analyses of 57 prospective studies. *Lancet* 2009, 373:1083-1096.

124. Lenz M, Richter T, Mühlhauser I: The morbidity and mortality associated with overweight and obesity in adulthood: a systematic review. *Dtsch Arztebl Int* 2009, 106:641-648.

125. Klinke R, Baumann R: *Physiologie.* Thieme; 2010.

126. Janikiewicz J, Hanzelka K, Kozinski K, Kolczynska K, Dobrzyn A: Islet β-cell failure in type 2 diabetes--Within the network of toxic lipids. *Biochem Biophys Res Commun* 2015, 460:491-496.

127. Samuel VT, Petersen KF, Shulman GI: Lipid-induced insulin resistance: unravelling the mechanism. *Lancet* 2010, 375:2267-2277.

128. Samuel VT, Shulman GI: Mechanisms for insulin resistance: common threads and missing links. *Cell* 2012, 148:852-871.

129. Item F, Konrad D: Visceral fat and metabolic inflammation: the portal theory revisited. *Obes Rev* 2012, 13 Suppl 2:30-39.

130. WHO: Diabetes Fact sheet No. 312, 2015. Access date: 06.02.2016. [http://www.who.int/mediacentre/factsheets/fs312/en/]

131. Global Burden of Disease Study Collaborators: Global, regional, and national incidence, prevalence, and years lived with disability for 301 acute and chronic diseases and injuries in 188 countries, 1990-2013: a systematic analysis for the Global Burden of Disease Study 2013. *Lancet* 2015, 386:743-800.

132. Mathers CD, Loncar D: Projections of global mortality and burden of disease from 2002 to 2030. *PLoS Med* 2006, 3:e442.

133. Pfeiffer AFH, Klein HH: The treatment of type 2 diabetes. *Dtsch Arztebl Int* 2014, 111:69-81; quiz 82.

134. Ribaric G, Buchwald JN, McGlennon TW: Diabetes and weight in comparative studies of bariatric surgery vs conventional medical therapy: a systematic review and meta-analysis. *Obes Surg* 2014, 24:437-455.

135. Buchwald H, Estok R, Fahrbach K, Banel D, Jensen MD, Pories WJ, Bantle JP, Sledge I: Weight and type 2 diabetes after bariatric surgery: systematic review and meta-analysis. *Am J Med* 2009, 122:248-256.e245.

136. Runkel N, Colombo-Benkmann M, Hüttl TP, Tigges H, Mann O, Flade-Kuthe R, Shang E, Susewind M, Wolff S, Wunder R, et al: Evidence-based German guidelines for surgery for obesity. *Int J Colorectal Dis* 2011, 26:397-404.

137. Daousi C, Casson IF, Gill GV, MacFarlane IA, Wilding JPH, Pinkney JH: Prevalence of obesity in type 2 diabetes in secondary care: association with cardiovascular risk factors. *Postgrad Med J* 2006, 82:280-284.

138. Nguyen NT, Nguyen X-MT, Lane J, Wang P: Relationship between obesity and diabetes in a US adult population: findings from the National Health and Nutrition Examination Survey, 1999-2006. *Obes Surg* 2011, 21:351-355.

139. Mugharbel KM, Al-Mansouri MA: Prevalence of obesity among type 2 diabetic patients in Al-khobar primary health care centers. *J Family Community Med* 2003, 10:49-53.

140. Hart CL, Hole DJ, Lawlor DA, Davey Smith G: How many cases of Type 2 diabetes mellitus are due to being overweight in middle age? Evidence from the Midspan prospective cohort studies using mention of diabetes mellitus on hospital discharge or death records. *Diabet Med* 2007, 24:73-80.

141. Wild S, Roglic G, Green A, Sicree R, King H: Global prevalence of diabetes: estimates for the year 2000 and projections for 2030. *Diabetes Care* 2004, 27:1047-1053.

142. Yoneshiro T, Aita S, Matsushita M, Kayahara T, Kameya T, Kawai Y, Iwanaga T, Saito M: Recruited brown adipose tissue as an antiobesity agent in humans. *J Clin Invest* 2013, 123:3404-3408.

143. Lee P, Smith S, Linderman J, Courville AB, Brychta RJ, Dieckmann W, Werner CD, Chen KY, Celi FS: Temperature-acclimated brown adipose tissue modulates insulin sensitivity in humans. *Diabetes* 2014, 63:3686-3698.

144. van der Lans AA, Hoeks J, Brans B, Vijgen GH, Visser MG, Vosselman MJ, Hansen J, Jorgensen JA, Wu J, Mottaghy FM, et al: Cold acclimation recruits human brown fat and increases nonshivering thermogenesis. *J Clin Invest* 2013, 123:3395-3403.

145. Blondin DP, Labbé SM, Tingelstad HC, Noll C, Kunach M, Phoenix S, Guérin B, Turcotte EE, Carpentier AC, Richard D, Haman F: Increased brown adipose tissue oxidative capacity in cold-acclimated humans. *J Clin Endocrinol Metab* 2014, 99:E438-446.

146. Forner F, Kumar C, Luber CA, Fromme T, Klingenspor M, Mann M: Proteome differences between brown and white fat mitochondria reveal specialized metabolic functions. *Cell Metab* 2009, 10:324-335.

147. Pierron D, Wildman DE, Huttemann M, Letellier T, Grossman LI: Evolution of the couple cytochrome c and cytochrome c oxidase in primates. *Adv Exp Med Biol* 2012, 748:185-213.

148. Tsukihara T, Aoyama H, Yamashita E, Tomizaki T, Yamaguchi H, Shinzawa-Itoh K, Nakashima R, Yaono R, Yoshikawa S: The whole structure of the 13-subunit oxidized cytochrome c oxidase at 2.8 A. *Science* 1996, 272:1136-1144.

149. Kadenbach B, Jarausch J, Hartmann R, Merle P: Separation of mammalian cytochrome c oxidase into 13 polypeptides by a sodium dodecyl sulfate-gel electrophoretic procedure. *Anal Biochem* 1983, 129:517-521.

150. Kadenbach B, Hüttemann M: The subunit composition and function of mammalian cytochrome c oxidase. *Mitochondrion* 2015, 24:64-76.

151. Hüttemann M, Jaradat S, Grossman LI: Cytochrome c oxidase of mammals contains a testes-specific isoform of subunit VIb--the counterpart to testes-specific cytochrome c? *Mol Reprod Dev* 2003, 66:8-16.

152. Hüttemann M, Schmidt TR, Grossman LI: A third isoform of cytochrome c oxidase subunit VIII is present in mammals. *Gene* 2003, 312:95-102.

153. Hüttemann M, Kadenbach B, Grossman LI: Mammalian subunit IV isoforms of cytochrome c oxidase. *Gene* 2001, 267:111-123.

154. Schlerf A, Droste M, Winter M, Kadenbach B: Characterization of two different genes (cDNA) for cytochrome c oxidase subunit VIa from heart and liver of the rat. *EMBO J* 1988, 7:2387-2391.

155. Lightowlers R, Ewart G, Aggeler R, Zhang YZ, Calavetta L, Capaldi RA: Isolation and characterization of the cDNAs encoding two isoforms of subunit CIX of bovine cytochrome c oxidase. *J Biol Chem* 1990, 265:2677-2681.

156. Seelan RS, Grossman LI: Cytochrome c oxidase subunit VIIa isoforms. Characterization and expression of bovine cDNAs. *J Biol Chem* 1991, 266:19752-19757.

157. Wolz W, Kress W, Mueller CR: Genomic sequence and organization of the human gene for cytochrome c oxidase subunit (COX7A1) VIIa-M. *Genomics* 1997, 45:438-442.

158. Lazarou M, Smith SM, Thorburn DR, Ryan MT, McKenzie M: Assembly of nuclear DNA-encoded subunits into mitochondrial complex IV, and their preferential integration into supercomplex forms in patient mitochondria. *FEBS J* 2009, 276:6701-6713.

159. Jaradat SA, Ko MS, Grossman LI: Tissue-specific expression and mapping of the Cox7ah gene in mouse. *Genomics* 1998, 49:363-370.

160. Huttemann M, Klewer S, Lee I, Pecinova A, Pecina P, Liu J, Lee M, Doan JW, Larson D, Slack E, et al: Mice deleted for heart-type cytochrome c oxidase subunit 7a1 develop dilated cardiomyopathy. *Mitochondrion* 2012, 12:294-304.

161. Lee I, Hüttemann M, Liu J, Grossman LI, Malek MH: Deletion of heart-type cytochrome c oxidase subunit 7a1 impairs skeletal muscle angiogenesis and oxidative phosphorylation. *J Physiol* 2012, 590:5231-5243.

162. Christian M: Transcriptional fingerprinting of "browning" white fat identifies NRG4 as a novel adipokine. *Adipocyte* 2014, 4:50-54.

163. Seale P, Kajimura S, Yang W, Chin S, Rohas LM, Uldry M, Tavernier G, Langin D, Spiegelman BM: Transcriptional control of brown fat determination by PRDM16. *Cell Metab* 2007, 6:38-54.

164. Maurer SF, Fromme T, Grossman LI, Hüttemann M, Klingenspor M: The brown and brite adipocyte marker Cox7a1 is not required for non-shivering thermogenesis in mice. *Sci Rep* 2015, 5:17704.

165. Vegiopoulos A, Muller-Decker K, Strzoda D, Schmitt I, Chichelnitskiy E, Ostertag A, Berriel Diaz M, Rozman J, Hrabe de Angelis M, Nusing RM, et al: Cyclooxygenase-2 controls energy homeostasis in mice by de novo recruitment of brown adipocytes. *Science* 2010, 328:1158-1161.

166. Madsen L, Pedersen LM, Lillefosse HH, Fjaere E, Bronstad I, Hao Q, Petersen RK, Hallenborg P, Ma T, De Matteis R, et al: UCP1 induction during recruitment of brown adipocytes in white adipose tissue is dependent on cyclooxygenase activity. *PLoS One* 2010, 5:e11391.

167. Stipanuk MH, Caudill MA: *Biochemical, Physiological, and Molecular Aspects of Human Nutrition.* Elsevier Health Sciences; 2013.

168. Le Faouder P, Baillif V, Spreadbury I, Motta J-P, Rousset P, Chêne G, Guigné C, Tercé F, Vanner S, Vergnolle N, et al: LC-MS/MS method for rapid and concomitant quantification of pro-inflammatory and pro-resolving polyunsaturated fatty acid metabolites. *J Chromatogr B Analyt Technol Biomed Life Sci* 2013, 932:123-133.

169. Strassburg K, Huijbrechts AM, Kortekaas KA, Lindeman JH, Pedersen TL, Dane A, Berger R, Brenkman A, Hankemeier T, van Duynhoven J, et al: Quantitative profiling of oxylipins through comprehensive LC-MS/MS analysis: application in cardiac surgery. *Anal Bioanal Chem* 2012, 404:1413-1426.

170. Dyall SC: Long-chain omega-3 fatty acids and the brain: a review of the independent and shared effects of EPA, DPA and DHA. *Front Aging Neurosci* 2015, 7:52.

171. KEGG Pathway Database: Pathway Map 00590, Arachidonic acid metabolism, Mus musculus (mouse), 2016. Access date: 06.02.2016. [http://www.genome.jp/dbget-bin/www_bget?pathway:mmu00590]

172. Medina JF, Haeggström J, Kumlin M, Rådmark O: Leukotriene A4: metabolism in different rat tissues. *Biochimica et Biophysica Acta (BBA) - Lipids and Lipid Metabolism* 1988, 961:203-212.

173. Chen Y, Zackert WE, Roberts LJ, Morrow JD: Evidence for the formation of a novel cyclopentenone isoprostane, 15-A2t-isoprostane (8-iso-prostaglandin A2) in vivo. *Biochim Biophys Acta* 1999, 1436:550-556.

174. Garcia-Alonso V, Lopez-Vicario C, Titos E, Moran-Salvador E, Gonzalez-Periz A, Rius B, Parrizas M, Werz O, Arroyo V, Claria J: Coordinate functional regulation between microsomal prostaglandin E synthase-1 (mPGES-1) and peroxisome proliferator-activated receptor gamma (PPARgamma) in the conversion of white-to-brown adipocytes. *J Biol Chem* 2013, 288:28230-28242.

175. García-Alonso V, Clària J: Prostaglandin E2 signals white-to-brown adipogenic differentiation. *Adipocyte* 2014, 3:290-296.

176. Bayindir I, Babaeikelishomi R, Kocanova S, Sousa IS, Lerch S, Hardt O, Wild S, Bosio A, Bystricky K, Herzig S, Vegiopoulos A: Transcriptional Pathways in cPGI2-Induced Adipocyte Progenitor Activation for Browning. *Front Endocrinol (Lausanne)* 2015, 6:129.

177. Pisani DF, Amri E-Z, Ailhaud G: Disequilibrium of polyunsaturated fatty acids status and its dual effect in modulating adipose tissue development and functions. *Ocl* 2015, 22:D405.

178. Sjövall P, Rossmeisl M, Hanrieder J, Kuda O, Kopecky J, Bryhn M: Dietary uptake of omega-3 fatty acids in mouse tissue studied by time-of-flight secondary ion mass spectrometry (TOF-SIMS). *Anal Bioanal Chem* 2015, 407:5101-5111.

179. Wada M, DeLong CJ, Hong YH, Rieke CJ, Song I, Sidhu RS, Yuan C, Warnock M, Schmaier AH, Yokoyama C, et al: Enzymes and receptors of prostaglandin pathways with arachidonic acid-derived versus eicosapentaenoic acid-derived substrates and products. *J Biol Chem* 2007, 282:22254-22266.

180. Culp BR, Titus BG, Lands WE: Inhibition of prostaglandin biosynthesis by eicosapentaenoic acid. *Prostaglandins Med* 1979, 3:269-278.

181. Hofmann WE, Liu X, Bearden CM, Harper ME, Kozak LP: Effects of genetic background on thermoregulation and fatty acid-induced uncoupling of mitochondria in UCP1-deficient mice. *J Biol Chem* 2001, 276:12460-12465.

182. Purves RD: Optimum numerical integration methods for estimation of area-under-the-curve (AUC) and area-under-the-moment-curve (AUMC). *J Pharmacokinet Biopharm* 1992, 20:211-226.

183. Virtue S, Vidal-Puig A: Assessment of brown adipose tissue function. *Front Physiol* 2013, 4:128.

184. Heldmaier G: Metabolic and thermoregulatory responses to heat and cold in the Djungarian hamster,Phodopus sungorus. *Journal of comparative physiology* 1975, 102:115-122.

185. Scholander PF, Walters V, Hock R, Irving L: Body insulation of some arctic and tropical mammals and birds. *Biol Bull* 1950, 99:225-236.

186. Scholander PF, Hock R, Walters V, Irving L: Adaptation to cold in arctic and tropical mammals and birds in relation to body temperature, insulation, and basal metabolic rate. *Biol Bull* 1950, 99:259-271.

187. Scholander PF, Hock R, Walters V, Johnson F, Irving L: Heat regulation in some arctic and tropical mammals and birds. *Biol Bull* 1950, 99:237-258.

188. Meyer CW, Willershäuser M, Jastroch M, Rourke BC, Fromme T, Oelkrug R, Heldmaier G, Klingenspor M: Adaptive thermogenesis and thermal conductance in wild-type and UCP1-KO mice. *Am J Physiol Regul Integr Comp Physiol* 2010, 299:R1396-1406.

189. Golozoubova V, Cannon B, Nedergaard J: UCP1 is essential for adaptive adrenergic nonshivering thermogenesis. *Am J Physiol Endocrinol Metab* 2006, 291:E350-357.

190. Andersen CL, Jensen JL, Ørntoft TF: Normalization of real-time quantitative reverse transcription-PCR data: a model-based variance estimation approach to identify genes suited for normalization, applied to bladder and colon cancer data sets. *Cancer Res* 2004, 64:5245-5250.

191. Klingenspor M, Ebbinghaus C, Hülshorst G, Stöhr S, Spiegelhalter F, Haas K, Heldmaier G: Multiple regulatory steps are involved in the control of lipoprotein lipase activity in brown adipose tissue. *J Lipid Res* 1996, 37:1685-1695.

192. Meyer CW, Korthaus D, Jagla W, Cornali E, Grosse J, Fuchs H, Klingenspor M, Roemheld S, Tschop M, Heldmaier G, et al: A novel missense mutation in the mouse growth hormone gene causes semidominant dwarfism, hyperghrelinemia, and obesity. *Endocrinology* 2004, 145:2531-2541.

193. Welsch U, Deller T, Elsberger S: *Sobotta Lehrbuch Histologie: Unter Mitarbeit von Thomas Deller.* Elsevier Health Sciences Germany; 2011.

194. Pisani DF, Ghandour RA, Beranger GE, Le Faouder P, Chambard J-C, Giroud M, Vegiopoulos A, Djedaini M, Bertrand-Michel J, Tauc M, et al: The ω6-fatty acid, arachidonic acid, regulates the conversion of white to brite adipocyte through a prostaglandin/calcium mediated pathway. *Mol Metab* 2014, 3:834-847.

195. Hüther FJ, Kadenbach B: Specific effects of ATP on the kinetics of reconstituted bovine heart cytochrome-c oxidase. *FEBS Lett* 1986, 207:89-94.

196. Hüther FJ, Kadenbach B: ADP increases the affinity for cytochrome c by interaction with the matrix side of bovine heart cytochrome c oxidase. *Biochem Biophys Res Commun* 1987, 147:1268-1275.

197. Obregón MJ, Jacobsson A, Kirchgessner T, Schotz MC, Cannon B, Nedergaard J: Postnatal recruitment of brown adipose tissue is induced by the cold stress experienced by the pups. An analysis of mRNA levels for thermogenin and lipoprotein lipase. *Biochem J* 1989, 259:341-346.

198. Sundin U, Cannon B: GDP-binding to the brown fat mitochondria of developing and cold-adapted rats. *Comparative Biochemistry and Physiology B-Biochemistry & Molecular Biology* 1980, 65:463-471.

199. Kless C, Muller VM, Schuppel VL, Lichtenegger M, Rychlik M, Daniel H, Klingenspor M, Haller D: Diet-induced obesity causes metabolic impairment independent of alterations in gut barrier integrity. *Mol Nutr Food Res* 2015, 59:968-978.

200. Galmozzi A, Sonne SB, Altshuler-Keylin S, Hasegawa Y, Shinoda K, Luijten IHN, Chang JW, Sharp LZ, Cravatt BF, Saez E, Kajimura S: ThermoMouse: an in vivo model to identify modulators of UCP1 expression in brown adipose tissue. *Cell Rep* 2014, 9:1584-1593.

201. Thomas LW: The chemical composition of adipose tissue of man and mice. *Q J Exp Physiol Cogn Med Sci* 1962, 47:179-188.

202. Pullar JD, Webster AJ: The energy cost of fat and protein deposition in the rat. *Br J Nutr* 1977, 37:355-363.

203. Almind K, Kahn CR: Genetic determinants of energy expenditure and insulin resistance in diet-induced obesity in mice. *Diabetes* 2004, 53:3274-3285.

204. Ravussin Y, Gutman R, LeDuc CA, Leibel RL: Estimating energy expenditure in mice using an energy balance technique. *Int J Obes (Lond)* 2013, 37:399-403.

205. Min SY, Kady J, Nam M, Rojas-Rodriguez R, Berkenwald A, Kim JH, Noh H-L, Kim JK, Cooper MP, Fitzgibbons T, et al: Human 'brite/beige' adipocytes develop from capillary networks, and their implantation improves metabolic homeostasis in mice. *Nat Med* 2016.

206. Albert V, Svensson K, Shimobayashi M, Colombi M, Muñoz S, Jimenez V, Handschin C, Bosch F, Hall MN: mTORC2 sustains thermogenesis via Akt-induced glucose uptake and glycolysis in brown adipose tissue. *EMBO Mol Med* 2016.

207. Kontani Y, Wang Y, Kimura K, Inokuma K-I, Saito M, Suzuki-Miura T, Wang Z, Sato Y, Mori N, Yamashita H: UCP1 deficiency increases susceptibility to diet-induced obesity with age. *Aging Cell* 2005, 4:147-155.

208. Zietak M, Kozak LP: Bile acids induce uncoupling protein 1-dependent thermogenesis and stimulate energy expenditure at thermoneutrality in mice. *Am J Physiol Endocrinol Metab* 2015:ajpendo.00485.02015.

209. Zhang X, Lam KSL, Ye H, Chung SK, Zhou M, Wang Y, Xu A: Adipose tissue-specific inhibition of hypoxia-inducible factor 1{alpha} induces obesity and glucose intolerance by impeding energy expenditure in mice. *J Biol Chem* 2010, 285:32869-32877.

210. Vergnes L, Chin R, Young SG, Reue K: Heart-type fatty acid-binding protein is essential for efficient brown adipose tissue fatty acid oxidation and cold tolerance. *J Biol Chem* 2011, 286:380-390.

211. Ji S, You Y, Kerner J, Hoppel CL, Schoeb TR, Chick WS, Hamm DA, Sharer JD, Wood PA: Homozygous carnitine palmitoyltransferase 1b (muscle isoform) deficiency is lethal in the mouse. *Mol Genet Metab* 2008, 93:314-322.

212. de Jesus LA, Carvalho SD, Ribeiro MO, Schneider M, Kim SW, Harney JW, Larsen PR, Bianco AC: The type 2 iodothyronine deiodinase is essential for adaptive thermogenesis in brown adipose tissue. *J Clin Invest* 2001, 108:1379-1385.

213. Zhang Y, Li Y, Niepel MW, Kawano Y, Han S, Liu S, Marsili A, Larsen PR, Lee CH, Cohen DE: Targeted deletion of thioesterase superfamily member 1 promotes energy expenditure and protects against obesity and insulin resistance. *Proc Natl Acad Sci U S A* 2012, 109:5417-5422.

214. Huttemann M, Lee I, Gao X, Pecina P, Pecinova A, Liu J, Aras S, Sommer N, Sanderson TH, Tost M, et al: Cytochrome c oxidase subunit 4 isoform 2-knockout mice show reduced enzyme activity, airway hyporeactivity, and lung pathology. *FASEB J* 2012, 26:3916-3930.

215. Radford NB, Wan B, Richman A, Szczepaniak LS, Li JL, Li K, Pfeiffer K, Schagger H, Garry DJ, Moreadith RW: Cardiac dysfunction in mice lacking cytochrome-c oxidase subunit VIaH. *Am J Physiol Heart Circ Physiol* 2002, 282:H726-733.

216. Quintens R, Singh S, Lemaire K, De Bock K, Granvik M, Schraenen A, Vroegrijk IO, Costa V, Van Noten P, Lambrechts D, et al: Mice deficient in the respiratory chain gene Cox6a2 are protected against high-fat diet-induced obesity and insulin resistance. *PLoS One* 2013, 8:e56719.

217. Ukropec J, Anunciado RP, Ravussin Y, Hulver MW, Kozak LP: UCP1-independent Thermogenesis in White Adipose Tissue of Cold-acclimated Ucp1-/- Mice. *Journal of Biological Chemistry* 2006, 281:31894-31908.

218. Schulz TJ, Huang P, Huang TL, Xue R, McDougall LE, Townsend KL, Cypess AM, Mishina Y, Gussoni E, Tseng Y-H: Brown-fat paucity due to impaired BMP signalling induces compensatory browning of white fat. *Nature* 2013, 495:379-383.

219. Crane JD, Mottillo EP, Farncombe TH, Morrison KM, Steinberg GR: A standardized infrared imaging technique that specifically detects UCP1-mediated thermogenesis in vivo. *Mol Metab* 2014, 3:490-494.

220. Young JB, Saville E, Rothwell NJ, Stock MJ, Landsberg L: Effect of diet and cold exposure on norepinephrine turnover in brown adipose tissue of the rat. *J Clin Invest* 1982, 69:1061-1071.

221. Montgomery MK, Hallahan NL, Brown SH, Liu M, Mitchell TW, Cooney GJ, Turner N: Mouse strain-dependent variation in obesity and glucose homeostasis in response to high-fat feeding. *Diabetologia* 2013, 56:1129-1139.

222. Wang T-Y, Liu C, Wang A, Sun Q: Intermittent cold exposure improves glucose homeostasis associated with brown and white adipose tissues in mice. *Life Sci* 2015.

223. The Jackson Laboratory, Bar Harbor, ME 04609, USA: The Jackson Laboratory Handbook on Genetically Standardized Mice. Sixth Edition, October 2009.

224. Simpson EM, Linder CC, Sargent EE, Davisson MT, Mobraaten LE, Sharp JJ: Genetic variation among 129 substrains and its importance for targeted mutagenesis in mice. *Nat Genet* 1997, 16:19-27.

225. Keane TM, Goodstadt L, Danecek P, White MA, Wong K, Yalcin B, Heger A, Agam A, Slater G, Goodson M, et al: Mouse genomic variation and its effect on phenotypes and gene regulation. *Nature* 2011, 477:289-294.

226. Lasar D, Julius A, Fromme T, Klingenspor M: Browning attenuates murine white adipose tissue expansion during postnatal development. *Biochim Biophys Acta* 2013, 1831:960-968.

227. Granneman JG, Burnazi M, Zhu Z, Schwamb LA: White adipose tissue contributes to UCP1-independent thermogenesis. *Am J Physiol Endocrinol Metab* 2003, 285:E1230-1236.

228. Golozoubova V, Hohtola E, Matthias A, Jacobsson A, Cannon B, Nedergaard J: Only UCP1 can mediate adaptive nonshivering thermogenesis in the cold. *FASEB J* 2001, 15:2048-2050.

229. Almind K, Manieri M, Sivitz WI, Cinti S, Kahn CR: Ectopic brown adipose tissue in muscle provides a mechanism for differences in risk of metabolic syndrome in mice. *Proc Natl Acad Sci U S A* 2007, 104:2366-2371.

230. Li Y, Bolze F, Fromme T, Klingenspor M: Intrinsic differences in BRITE adipogenesis of primary adipocytes from two different mouse strains. *Biochim Biophys Acta* 2014, 1841:1345-1352.

231. Muzzin P, Revelli JP, Kuhne F, Gocayne JD, McCombie WR, Venter JC, Giacobino JP, Fraser CM: An adipose tissue-specific beta-adrenergic receptor. Molecular cloning and down-regulation in obesity. *J Biol Chem* 1991, 266:24053-24058.

232. Nahmias C, Blin N, Elalouf JM, Mattei MG, Strosberg AD, Emorine LJ: Molecular characterization of the mouse beta 3-adrenergic receptor: relationship with the atypical receptor of adipocytes. *EMBO J* 1991, 10:3721-3727.

233. Bloom JD, Dutia MD, Johnson BD, Wissner A, Burns MG, Largis EE, Dolan JA, Claus TH: Disodium (R,R)-5-[2-[[2-(3-chlorophenyl)-2-hydroxyethyl]-amino] propyl]-1,3-benzodioxole-2,2-dicarboxylate (CL 316,243). A potent beta-adrenergic agonist virtually specific for beta 3 receptors. A promising antidiabetic and antiobesity agent. *J Med Chem* 1992, 35:3081-3084.

234. Himms-Hagen J, Cui J, Danforth E, Taatjes DJ, Lang SS, Waters BL, Claus TH: Effect of CL-316,243, a thermogenic beta 3-agonist, on energy balance and brown and white adipose tissues in rats. *Am J Physiol* 1994, 266:R1371-1382.

235. Hoch FLaH, Frances P.: Hyperthermia, muscle rigidity, and uncoupling in skeletal muscle mitochondria in rats treated with halothane and 2,4-dinitrophenol. *Anesthesiology* 1973, 38:237-243.

236. Kaiser JA: Studies on the toxicity of disophenol (2,6-diiodo-4-nitrophenol) to dogs and rodents plus some comparisons with 2,4-dinitrophenol. *Ther Ggw* 1964, 103:232-244.

237. Inokuma K-i, Okamatsu-Ogura Y, Omachi A, Matsushita Y, Kimura K, Yamashita H, Saito M: Indispensable role of mitochondrial UCP1 for antiobesity effect of beta3-adrenergic stimulation. *Am J Physiol Endocrinol Metab* 2006, 290:E1014-1021.

238. Lowell BB, S-Susulic V, Hamann A, Lawitts JA, Himms-Hagen J, Boyer BB, Kozak LP, Flier JS: Development of obesity in transgenic mice after genetic ablation of brown adipose tissue. *Nature* 1993, 366:740-742.

239. Takada R, Saitoh M, Mori T: Dietary gamma-linolenic acid-enriched oil reduces body fat content and induces liver enzyme activities relating to fatty acid beta-oxidation in rats. *J Nutr* 1994, 124:469-474.

240. Takahashi Y, Ide T, Fujita H: Dietary gamma-linolenic acid in the form of borage oil causes less body fat accumulation accompanying an increase in uncoupling protein 1 mRNA level in brown adipose tissue. *Comp Biochem Physiol B Biochem Mol Biol* 2000, 127:213-222.

241. Ebermann R, Elmadfa I: *Lehrbuch Lebensmittelchemie und Ernährung.* Springer Vienna; 2011.

242. Kim M, Goto T, Yu R, Uchida K, Tominaga M, Kano Y, Takahashi N, Kawada T: Fish oil intake induces UCP1 upregulation in brown and white adipose tissue via the sympathetic nervous system. *Sci Rep* 2015, 5:18013.

243. Janovská P, Flachs P, Kazdová L, Kopecký J: Anti-obesity effect of n-3 polyunsaturated fatty acids in mice fed high-fat diet is independent of cold-induced thermogenesis. *Physiol Res* 2013, 62:153-161.

244. Flachs P, Horakova O, Brauner P, Rossmeisl M, Pecina P, Franssen-van Hal N, Ruzickova J, Sponarova J, Drahota Z, Vlcek C, et al: Polyunsaturated fatty acids of marine origin upregulate mitochondrial biogenesis and induce beta-oxidation in white fat. *Diabetologia* 2005, 48:2365-2375.

245. Flachs P, Ruhl R, Hensler M, Janovska P, Zouhar P, Kus V, Macek Jilkova Z, Papp E, Kuda O, Svobodova M, et al: Synergistic induction of lipid catabolism and anti-inflammatory lipids in white fat of dietary obese mice in response to calorie restriction and n-3 fatty acids. *Diabetologia* 2011, 54:2626-2638.

246. González-Périz A, Horrillo R, Ferré N, Gronert K, Dong B, Morán-Salvador E, Titos E, Martínez-Clemente M, López-Parra M, Arroyo V, Clària J: Obesity-induced insulin resistance and hepatic steatosis are alleviated by omega-3 fatty acids: a role for resolvins and protectins. *FASEB J* 2009, 23:1946-1957.

247. Mössenböck K, Vegiopoulos A, Rose AJ, Sijmonsma TP, Herzig S, Schafmeier T: Browning of White Adipose Tissue Uncouples Glucose Uptake from Insulin Signaling. *PLoS ONE* 2014, 9:e110428.

248. Ghandour RA, Giroud M, Vegiopoulos A, Herzig S, Ailhaud G, Amri E-Z, Pisani DF: IP-receptor and PPARs trigger the conversion of human white to brite adipocyte induced by carbaprostacyclin. *Biochim Biophys Acta* 2016.

249. Naruhn S, Meissner W, Adhikary T, Kaddatz K, Klein T, Watzer B, Müller-Brüsselbach S, Müller R: 15-hydroxyeicosatetraenoic acid is a preferential peroxisome proliferator-activated receptor beta/delta agonist. *Mol Pharmacol* 2010, 77:171-184.

250. Ng VY, Huang Y, Reddy LM, Falck JR, Lin ET, Kroetz DL: Cytochrome P450 eicosanoids are activators of peroxisome proliferator-activated receptor alpha. *Drug Metab Dispos* 2007, 35:1126-1134.

251. O'Flaherty JT, Rogers LC, Paumi CM, Hantgan RR, Thomas LR, Clay CE, High K, Chen YQ, Willingham MC, Smitherman PK, et al: 5-Oxo-ETE analogs and the proliferation of cancer cells. *Biochimica et Biophysica Acta (BBA) - Molecular and Cell Biology of Lipids* 2005, 1736:228-236.

252. Yu K, Bayona W, Kallen CB, Harding HP, Ravera CP, McMahon G, Brown M, Lazar MA: Differential activation of peroxisome proliferator-activated receptors by eicosanoids. *J Biol Chem* 1995, 270:23975-23983.

253. Carmona MC, Louche K, Lefebvre B, Pilon A, Hennuyer N, Audinot-Bouchez V, Fievet C, Torpier G, Formstecher P, Renard P, et al: S 26948: a new specific peroxisome proliferator activated receptor gamma modulator with potent antidiabetes and antiatherogenic effects. *Diabetes* 2007, 56:2797-2808.

254. Vernochet C, Peres SB, Davis KE, McDonald ME, Qiang L, Wang H, Scherer PE, Farmer SR: C/EBPalpha and the corepressors CtBP1 and CtBP2 regulate repression of select visceral white adipose genes during induction of the brown phenotype in white adipocytes by peroxisome proliferator-activated receptor gamma agonists. *Mol Cell Biol* 2009, 29:4714-4728.

255. Qiu Y, Nguyen KD, Odegaard JI, Cui X, Tian X, Locksley RM, Palmiter RD, Chawla A: Eosinophils and type 2 cytokine signaling in macrophages orchestrate development of functional beige fat. *Cell* 2014, 157:1292-1308.

256. Rao RR, Long JZ, White JP, Svensson KJ, Lou J, Lokurkar I, Jedrychowski MP, Ruas JL, Wrann CD, Lo JC, et al: Meteorin-like Is a Hormone that Regulates Immune-Adipose Interactions to Increase Beige Fat Thermogenesis. *Cell* 2014, 157:1279-1291.

257. Lee Y-H, Kim S-N, Kwon H-J, Maddipati KR, Granneman JG: Adipogenic role of alternatively activated macrophages in β-adrenergic remodeling of white adipose tissue. *Am J Physiol Regul Integr Comp Physiol* 2016, 310:R55-65.

258. Powell WS, Chung D, Gravel S: 5-Oxo-6,8,11,14-eicosatetraenoic acid is a potent stimulator of human eosinophil migration. *J Immunol* 1995, 154:4123-4132.

259. Schwenk U, Schröder JM: 5-Oxo-eicosanoids are potent eosinophil chemotactic factors. Functional characterization and structural requirements. *J Biol Chem* 1995, 270:15029-15036.

260. Liu X, Zheng Z, Zhu X, Meng M, Li L, Shen Y, Chi Q, Wang D, Zhang Z, Li C, et al: Brown adipose tissue transplantation improves whole-body energy metabolism. *Cell Res* 2013, 23:851-854.

261. Zhu Z, Spicer EG, Gavini CK, Goudjo-Ako AJ, Novak CM, Shi H: Enhanced sympathetic activity in mice with brown adipose tissue transplantation (transBATation). *Physiol Behav* 2014, 125:21-29.

262. Liu X, Wang S, You Y, Meng M, Zheng Z, Dong M, Lin J, Zhao Q, Zhang C, Yuan X, et al: Brown Adipose Tissue Transplantation Reverses Obesity in Ob/Ob Mice. *Endocrinology* 2015, 156:2461-2469.

263. Buckley JD, Howe PRC: Long-chain omega-3 polyunsaturated fatty acids may be beneficial for reducing obesity-a review. *Nutrients* 2010, 2:1212-1230.

264. Ussar S, Griffin NW, Bezy O, Fujisaka S, Vienberg S, Softic S, Deng L, Bry L, Gordon JI, Kahn CR: Interactions between Gut Microbiota, Host Genetics and Diet Modulate the Predisposition to Obesity and Metabolic Syndrome. *Cell Metab* 2015, 22:516-530.

265. Yang I, Eibach D, Kops F, Brenneke B, Woltemate S, Schulze J, Bleich A, Gruber AD, Muthupalani S, Fox JG, et al: Intestinal microbiota composition of interleukin-10 deficient C57BL/6J mice and susceptibility to Helicobacter hepaticus-induced colitis. *PLoS One* 2013, 8:e70783.

266. Jakobsson HE, Rodríguez-Piñeiro AM, Schütte A, Ermund A, Boysen P, Bemark M, Sommer F, Bäckhed F, Hansson GC, Johansson MEV: The composition of the gut microbiota shapes the colon mucus barrier. *EMBO Rep* 2015, 16:164-177.

267. Kulkarni RN, Almind K, Goren HJ, Winnay JN, Ueki K, Okada T, Kahn CR: Impact of genetic background on development of hyperinsulinemia and diabetes in insulin receptor/insulin receptor substrate-1 double heterozygous mice. *Diabetes* 2003, 52:1528-1534.

268. Yu XX, Lewin DA, Forrest W, Adams SH: Cold elicits the simultaneous induction of fatty acid synthesis and beta-oxidation in murine brown adipose tissue: prediction from differential gene expression and confirmation in vivo. *FASEB J* 2002, 16:155-168.

269. Shimizu Y, Nikami H, Saito M: Sympathetic activation of glucose utilization in brown adipose tissue in rats. *J Biochem* 1991, 110:688-692.

270. Takahashi A, Shimazu T, Maruyama Y: Importance of sympathetic nerves for the stimulatory effect of cold exposure on glucose utilization in brown adipose tissue. *Jpn J Physiol* 1992, 42:653-664.

271. Olichon-Berthe C, Van Obberghen E, Le Marchand-Brustel Y: Effect of cold acclimation on the expression of glucose transporter Glut 4. *Mol Cell Endocrinol* 1992, 89:11-18.

272. Inokuma K-i, Ogura-Okamatsu Y, Toda C, Kimura K, Yamashita H, Saito M: Uncoupling protein 1 is necessary for norepinephrine-induced glucose utilization in brown adipose tissue. *Diabetes* 2005, 54:1385-1391.

273. Olsen JM, Sato M, Dallner OS, Sandström AL, Pisani DF, Chambard J-C, Amri E-Z, Hutchinson DS, Bengtsson T: Glucose uptake in brown fat cells is dependent on mTOR complex 2-promoted GLUT1 translocation. *J Cell Biol* 2014, 207:365-374.

274. Dallner OS, Chernogubova E, Brolinson KA, Bengtsson T: Beta3-adrenergic receptors stimulate glucose uptake in brown adipocytes by two mechanisms independently of glucose transporter 4 translocation. *Endocrinology* 2006, 147:5730-5739.

275. Shimizu Y, Satoh S, Yano H, Minokoshi Y, Cushman SW, Shimazu T: Effects of noradrenaline on the cell-surface glucose transporters in cultured brown adipocytes: novel mechanism for selective activation of GLUT1 glucose transporters. *Biochem J* 1998, 330 (Pt 1):397-403.

276. Chernogubova E, Cannon B, Bengtsson T: Norepinephrine increases glucose transport in brown adipocytes via beta3-adrenoceptors through a cAMP, PKA, and PI3-kinase-dependent pathway stimulating conventional and novel PKCs. *Endocrinology* 2004, 145:269-280.

277. Ludwig T, Worsch S, Heikenwalder M, Daniel H, Hauner H, Bader BL: Metabolic and immunomodulatory effects of n-3 fatty acids are different in mesenteric and epididymal adipose tissue of diet-induced obese mice. *Am J Physiol Endocrinol Metab* 2013, 304:E1140-1156.

278. Li B, Nolte LA, Ju JS, Han DH, Coleman T, Holloszy JO, Semenkovich CF: Skeletal muscle respiratory uncoupling prevents diet-induced obesity and insulin resistance in mice. *Nat Med* 2000, 6:1115-1120.

279. Voigt A, Katterle Y, Kahle M, Kluge R, Schürmann A, Joost H-G, Klaus S: Skeletal muscle mitochondrial uncoupling prevents diabetes but not obesity in NZO mice, a model for polygenic diabesity. *Genes Nutr* 2015, 10:57.

280. Bernal-Mizrachi C, Weng S, Li B, Nolte LA, Feng C, Coleman T, Holloszy JO, Semenkovich CF: Respiratory uncoupling lowers blood pressure through a leptin-dependent mechanism in genetically obese mice. *Arterioscler Thromb Vasc Biol* 2002, 22:961-968.

281. Hutchinson DS, Chernogubova E, Dallner OS, Cannon B, Bengtsson T: Beta-adrenoceptors, but not alpha-adrenoceptors, stimulate AMP-activated protein kinase in brown adipocytes independently of uncoupling protein-1. *Diabetologia* 2005, 48:2386-2395.

282. Jeanguillaume C, Metrard G, Ricquier D, Legras P, Bouchet F, Lacoeuille F, Hindre F, Morel O, Rakotonirina H: Visualization of Activated BAT in Mice, with FDG-PET and Its Relation to UCP1. *Advances in Molecular Imaging* 2013, 03:19-22.

283. Bal NC, Maurya SK, Sopariwala DH, Sahoo SK, Gupta SC, Shaikh SA, Pant M, Rowland LA, Bombardier E, Goonasekera SA, et al: Sarcolipin is a newly identified regulator of muscle-based thermogenesis in mammals. *Nat Med* 2012, 18:1575-1579.

284. Rowland LA, Bal NC, Kozak LP, Periasamy M: Uncoupling Protein 1 and Sarcolipin Are Required to Maintain Optimal Thermogenesis, and Loss of Both Systems Compromises Survival of Mice under Cold Stress. *J Biol Chem* 2015, 290:12282-12289.

285. Kazak L, Chouchani ET, Jedrychowski MP, Erickson BK, Shinoda K, Cohen P, Vetrivelan R, Lu GZ, Laznik-Bogoslavski D, Hasenfuss SC, et al: A creatine-driven substrate cycle enhances energy expenditure and thermogenesis in beige fat. *Cell* 2015, 163:643-655.

286. Keipert S, Kutschke M, Lamp D, Brachthäuser L, Neff F, Meyer CW, Oelkrug R, Kharitonenkov A, Jastroch M: Genetic disruption of uncoupling protein 1 in mice renders brown adipose tissue a significant source of FGF21 secretion. *Mol Metab* 2015, 4:537-542.

287. Kharitonenkov A, Shiyanova TL, Koester A, Ford AM, Micanovic R, Galbreath EJ, Sandusky GE, Hammond LJ, Moyers JS, Owens RA, et al: FGF-21 as a novel metabolic regulator. *J Clin Invest* 2005, 115:1627-1635.

288. Moyers JS, Shiyanova TL, Mehrbod F, Dunbar JD, Noblitt TW, Otto KA, Reifel-Miller A, Kharitonenkov A: Molecular determinants of FGF-21 activity-synergy and cross-talk with PPARgamma signaling. *J Cell Physiol* 2007, 210:1-6.

289. Adams AC, Yang C, Coskun T, Cheng CC, Gimeno RE, Luo Y, Kharitonenkov A: The breadth of FGF21's metabolic actions are governed by FGFR1 in adipose tissue. *Mol Metab* 2012, 2:31-37.

290. Peirce V, Vidal-Puig A: Regulation of glucose homoeostasis by brown adipose tissue. *Lancet Diabetes Endocrinol* 2013, 1:353-360.

291. Gunawardana SC, Piston DW: Reversal of type 1 diabetes in mice by brown adipose tissue transplant. *Diabetes* 2012, 61:674-682.

ACKNOWLEDGEMENTS

An dieser Stelle möchte ich mich bei allen bedanken, die auf wissenschaftlicher und persönlicher Ebene die Durchführung und den Abschluss dieser Arbeit ermöglicht haben.

Mein Dank gilt an erster Stelle Martin für die Möglichkeit diese Arbeit im Rahmen des DIABAT-Projekts absolvieren zu dürfen. Ich danke Dir für Dein Vertrauen, Deine Unterstützung und Deine zahlreichen Ideen, konstruktiven Vorschläge und Denkanstöße, die zum Gelingen dieser Arbeit beigetragen haben.

Ein großes Dankeschön geht an Tobi für seine Betreuung, seine unermüdliche Geduld, seine fortwährende Unterstützung und seinen Zuspruch, für seine guten Ideen, für unsere Büro-WG sowie für unzählige Grill-, Kino- und Lagerfeuerevents. Nicht zuletzt bedanke ich mich für das Korrekturlesen dieser Arbeit. Gleichermaßen sei auch Flo für zusätzliche Denkanstöße gedankt.

Allen Kolleginnen und Kollegen, mit denen ich im Laufe der Jahre zusammenarbeiten durfte, danke ich für die angenehme Arbeitsatmosphäre, für die große Hilfsbereitschaft, dass mir jeder einzelne stets mit Rat und Tat zur Seite stand sowie für die zahlreichen und vielfältigen privaten Events, die den Arbeitsalltag erleichtert haben.

Besonderer Dank gilt Nadine für ihre unermüdliche Hilfe und Geduld in Tierhausangelegenheiten, für ihren Einsatz und ihre Expertise in Sachen Computer, für wertvolle Ratschläge und dafür dass sie stets ein offenes Ohr hat. Gleichermaßen gilt mein Dank auch Anika und Sabine für deren hervorragende Unterstützung, Hilfsbereitschaft und Verlässlichkeit.

Ich bedanke mich bei Maik Hüttemann für die Zusammenarbeit und die Überlassung der Cox7a1-Maus.

Zu guter Letzt möchte ich mich bei meiner Familie und guten Freunden bedanken, allen voran Thomas, ohne deren bedingungsloses Zutun diese Arbeit niemals möglich gewesen wäre.

EIDESSTATTLICHE ERKLÄRUNG

Ich erkläre an Eides statt, dass ich die bei der Fakultät Wissenschaftszentrum Weihenstephan für Ernährung, Landnutzung und Umwelt der TUM zur Promotionsprüfung vorgelegte Arbeit mit dem Titel:

Molecular functions in brown adipose tissue and their physiological significance in the context of systemic glucose homeostasis in mice

am Lehrstuhl für Molekulare Ernährungsmedizin unter der Anleitung und Betreuung durch Univ.-Prof. Dr. Martin Klingenspor ohne sonstige Hilfe erstellt und bei der Abfassung nur die gemäß § 6 Abs. 6 und 7 Satz 2 angegebenen Hilfsmittel benutzt habe.

Ich habe keine Organisation eingeschaltet, die gegen Entgelt Betreuerinnen und Betreuer für die Anfertigung von Dissertationen sucht, oder die mir obliegenden Pflichten hinsichtlich der Prüfungsleistungen für mich ganz oder teilweise erledigt.

Ich habe die Dissertation in dieser oder ähnlicher Form in keinem anderen Prüfungsverfahren als Prüfungsleistung vorgelegt.

Die vollständige Dissertation wurde noch nicht veröffentlicht.

Ich habe den angestrebten Doktorgrad noch nicht erworben und bin nicht in einem früheren Promotionsverfahren für den angestrebten Doktorgrad endgültig gescheitert.

Die öffentlich zugängliche Promotionsordnung der TUM ist mir bekannt, insbesondere habe ich die Bedeutung von § 28 (Nichtigkeit der Promotion) und § 29 (Entzug des Doktorgrades) zur Kenntnis genommen. Ich bin mir der Konsequenzen einer falschen Eidesstattlichen Erklärung bewusst.

Mit der Aufnahme meiner personenbezogenen Daten in die Alumni-Datei bei der TUM bin ich einverstanden.

Freising, den_____ _____

Stefanie Maurer

LISTE DER VORVERÖFFENTLICHUNGEN

Teile dieser Arbeit wurden im Rahmen der folgenden Publikation bereits veröffentlicht:

Stefanie F. Maurer, Tobias Fromme, Lawrence I. Grossman, Maik Hüttemann and Martin Klingenspor. The brown and brite adipocyte marker Cox7a1 is not required for non-shivering thermogenesis in mice. *Scientific Reports* 5:17704, 2015.

Teile dieser Arbeit wurden im Rahmen internationaler Konferenzen in Form von Postern oder mündlichen Präsentation vor wissenschaftlichem Publikum vorgestellt:

Stefanie Maurer and Martin Klingenspor.
A role for brown adipose tissue in the regulation of glucose tolerance in mice.
Posterpräsentation im Rahmen des 4. jährlichen DIABAT Meetings vom 28.-29. September in Prag (Tschechische Republik).

Stefanie Maurer, Tobias Fromme, Maik Hüttemann and Martin Klingenspor.
The role of Cox7a1 in brown fat thermogenesis.
Vortrag im Rahmen des 3. jährlichen DIABAT Meetings vom 09.-10. Oktober 2014 in Nizza (Frankreich).

Stefanie Maurer, Tobias Fromme and Martin Klingenspor.
Exploring the interactive effects of dietary fatty acid composition and housing temperature on glucose tolerance in different mouse strains.
Posterpräsentation im Rahmen des 3. jährlichen DIABAT Meetings vom 09.-10. Oktober 2014 in Nizza (Frankreich).

Stefanie Maurer, Tobias Fromme and Martin Klingenspor.
Effect of dietary fatty acid composition on brown adipocyte recruitment in different mouse strains.
Posterpräsentation im Rahmen des 2. jährlichen DIABAT Meetings vom 18.-20. Oktober 2013 in Zürich (Schweiz).

Stefanie Maurer, Tobias Fromme and Martin Klingenspor.
Validation of dietary fatty acid composition effects on brown adipocyte recruitment in mice.
Posterpräsentation im Rahmen des 1. jährlichen DIABAT Meetings vom 05.-07. Oktober 2012 in Berlin.

Stefanie Maurer, Tobias Fromme and Martin Klingenspor.
The function of Cox7a1 for brown fat thermogenesis.
Posterpräsentation im Rahmen der 17th European Bioenergetics Conference (EBEC) vom 15.-20. September 2012 in Freiburg. Eine zugehörige Zusammenfassung wurde veröffentlicht (*Biochimica et Biophysica Acta (BBA) - Bioenergetics* 10/2012; 1817:S110).